ION TRANSPORT THROUGH MULTILAYER POLYELECTROLYTE MEMBRANES AND CONDUCTIVE MEMBRANES

By

Chao Cheng

A DISSERTATION

Submitted to
Michigan State University
in partial fulfillment of the requirements
for the degree of

Chemistry – Doctor of Philosophy

2013

ABSTRACT

ION TRANSPORT THROUGH MULTILAYER POLYELECTROLYTE MEMBRANES AND CONDUCTIVE MEMBRANES
By

Chao Cheng

Ion separations are essential in applications such as water softening, salt purification and waste-water treatment. Membrane-based processes are attractive for such applications because of their low energy and capital costs, but success in these processes requires selective, ultrathin membrane skins. The minimal skin thickness affords high flux along with selectivity.

Alternating adsorption of polycations and polyanions is a promising approach to form highly charged skins on porous membranes. Remarkably, as few as four bilayers of adsorbed poly(styrenesulfonate)/poly(allylamine hydrochloride) (PSS/PAH) on alumina membranes provide K^+/Mg^{2+} selectivities >350 in diffusion dialysis. The same modified membranes show K^+/Mg^{2+} selectivities of only 16 in nanofiltration (NF), however, suggesting that coupled transport of water and ions in small membrane defects reduces ion-transport selectivities. Transmembrane potential measurements show that PSS/PAH films are much more permeable to Cl^- than Mg^{2+}, and this leads to -200% rejection of trace K^+ during NF of $MgCl_2$ solutions in NF (the K^+ concentration in the membrane permeate is three times that in the feed).

The high diffusion dialysis selectivities of $(PSS/PAH)_5$-coated membranes translate to electrodialysis with an accompanying increase in ion fluxes due to electromigration. Specifically, $(PSS/PAH)_5$-coated commercial NF membranes show K^+/Mg^{2+} selectivities around 100, and the K^+ flux in electrodialysis is 45 times the flux in diffusion dialysis. However, the K^+ transference number is at most ~0.35, because protons and anions carry most of the current. Electrodialysis with chloride salts damages membranes, presumably because of electrically generated chlorine.

Controlling the membrane surface charge by application of an electric potential via a conductive membrane skin layer may greatly increase ion rejections and ion-transport selectivities. Dilute polymerization of polyaniline leads to a film of conducting polyaniline nanofibers on the membrane surface, and the resistance across the surface of such coated membranes is in the kΩ range. Unfortunately, initial experiments did not show a significant change in ion fluxes with an applied potential and conductive membranes, but this area requires further work.

Overall, generating a highly charged and dense polymer film on a porous membrane provides remarkably selective ion transport in electrodialysis and diffusion dialysis. Whether electrical potentials applied to conductive membranes can enhance this selectivity is an open question.

To My Parents

ACKNOWLEDGEMENTS

There are so many people I need to thank for the completion of this degree. First of all, I would like to thank my advisor, Merlin Bruening, for his 5 years' guide. He is a dedicate researcher and passionate instructor. I enjoyed the time that we sat together working on equations in his office. Without his understanding and support, I don't think I would survive the graduate school.

I also pay my gratitude to my fellow group members, both past and present. I like inspiring discussions on science and sharing opinions on topics covering culture, history, geography, politics, etc. I enjoyed working with everybody in the lab and I feel fortunate to have you guys through my graduate school.

I am grateful to my friends and families. Thank you all for the patience, encouragement, and smiling faces to keep me going. It is your love that supported me through the graduate school.

Graduate school is not just about a degree but a journey. During this journey, I met great mentors, made friends, and became a better me. Thank you all for being with me through this journey.

TABLE OF CONTENTS

LIST OF TABLES

LIST OF FIGURES

LIST OF SCHEMES

KEY TO ABBREVIATIONS

ATRP	Atom Transfer Radical Polymerization
CH	Chitosan
CVD	Chemical Vapor Deposition
FIBSEM	Focused ion beam–secondary electron microscopy
HA	Hyaluronic acid
iCVD	Initiated Chemical Vapor Deposition
IP	Interfacial Polymerization
LBL	Layer-by-Layer
MPD	m-phenylenediamine
NF	Nanofiltration
oCVD	oxidative Chemical Vapor Deposition
PAA	Poly(acrylic acid)
PAH	Poly(allylamine hydrochloride)
PAMPS	Poly(sodium 2-acrylamido-2-methylpropanesulfonate)
PAN	Polyaniline
PBS	Phosphate buffer solution
PEDOT	Poly(3,4-ethylenedioxythiophene)
PEI	Polyethylenimine
PEM	Polyelectrolyte Multilayer

PES	Poly(ethersulfone)
PDADMAC	Poly(diallyl dimethyl ammonium chloride)
PDMAEMA	Poly[2-(dimethylamino) ethyl methacrylate]
PGA	Poly(L-glutamic acid sodium salt)
PMMA	Poly(methyl methacrylate)
PHEMA-*g*-PAA	Poly(2-hydroxyethyl methacrylate)-*graft*-poly-(acrylic acid)
PLL	Poly(L-lysine hydrochloride)
PPD	p-phenylenediamine
PSS	Poly(4-sodium styrene sulfonate)
PVD	Physical Vapor Deposition
PVDF	Polyvinylidene difluoride
QCM	Quartz crystal microbalance
RO	Reverse Osmosis
SEM	Scanning Electron Microscopy
TMC	Trimesoyl Chloride

Chapter 1 Introduction and Background

This dissertation investigates selective ion transport through membranes modified with layer-by-layer (LBL) polyelectrolyte multilayers (PEMs) or conductive polymer nanofibers. In some cases, differences in ion sizes and charges lead to selectivities >350 in the transport of monovalent over multivalent ions.[1] Adsorption of PEMs generates a relatively dense film on top of a porous support to create a membrane skin that exhibits size-based selectivity. Moreover, the surface charge on the thin film excludes ions with the same charge sign, especially multivalent ions. Increasing the charge on the membrane surface through application of an external potential might enhance selectivity, and to this end we are developing membranes with conducting polymer skins.

To provide background for the work, this chapter first reviews methods to generate polymer thin films, including spin coating, dip coating, physical/chemical vapor deposition, polymer grafting, interfacial polymerization and LBL deposition. I emphasize the two main techniques employed in my work, LBL polyelectrolyte adsorption and dilute polymerization to form conductive polymers. Subsequent sections discuss membrane-based ion separations, conductive polymers, and the outline of this dissertation.

1.1 Applications of Thin Polymer Films

Polymer thin films can serve as conductive layers in electronic devices,[2-7] optical absorption coatings in solar cells,[8-11] active interfaces for chemical and biochemical sensors,[12-15] and anti-corrosion coatings for metals.[16-18] Consequently, optimization of the fabrication and properties of functional polymer films is essential for reducing production costs and improving performance. Moreover, understanding the mechanism of film formation and the factors that control film interfacial properties is crucial for future applications. This dissertation explores polymer-coated membranes for ion separations where the polymer thin film serves as a selective skin. Thus, film deposition is a vital part of this work.

1.2 Fabrication of Thin Polymer Films

A partial list of methods to fabricate thin polymer films includes spin coating, dip coating, physical/chemical vapor deposition, polymer grafting, interfacial polymerization and LBL adsorption. This section reviews these techniques with emphasis on LBL adsorption and dilute polymerization of conducting polymers.

1.2.1 Spin coating

In this method, an excess amount of polymer solution is placed on a flat substrate, usually in the center, which is rotated so that the polymer solution spreads over the entire substrate by centrifugal force. The continuous rotation spins the solution off the substrate from the edge while the solvent evaporates, leaving a thin polymer layer on the substrate (see Figure 1.1).

Figure 1.1 Illustration of the spin-coating technique for forming polymer thin films. The film becomes thinner as the substrate rotates to bring the polymer solution to the edge, and eventually a uniform thin film forms on the substrate.

Figure 1.1 (cont'd) (Reprinted with permission from *Colloids and Surfaces B: Biointerfaces*, **2005**, 42,115-123) For interpretation of the references to color in this and all other figures, the reader is referred to the electronic version of this dissertation.

The film thickness generated by spin coating depends on the spinning velocity and the coating solution viscosity.[19, 20] Generally, faster rotation and less viscous solutions lead to thinner films. Emslie et al. first modeled the evolution of film thickness as thinning of a Newtonian liquid on a spinning disk.[21] This gives rise to equation (1.1)

$$\frac{dh}{dt} = -\frac{2rw^2h^3}{3\eta_0} \tag{1.1}$$

where h is the liquid film thickness, t is spinning time, r is liquid density, w is spin speed, and η_0 is the initial solution viscosity. When $\frac{dh}{dt}$ reaches a specified evaporation rate, E, the film is essentially immobile as the solvent evaporates to make the solution viscosity too high to maintain flow. Initially, equation (1.2) describes E

$$\mathrm{E} = \mathrm{k}(x_1^0 - x_{1\infty}) \tag{1.2}$$

where k is the mass transfer coefficient (equation (1.3)), x_1^0 is the initial solvent mass fraction in the polymer solution, and $x_{1\infty}$ is the solvent mass fraction that would be in equilibrium with that in the gas phase.[22]

$$\mathrm{k} = \left(\frac{cD_g}{u_g^{\frac{1}{2}} r}\right)\left(\frac{p_1^0 M_1}{RT}\right) w^{1/2} \quad (1.3)$$

In equation (1.3), c is a constant which depends on the gas phase Schmidt number, D_g is the binary diffusivity of the solvent in gas phase, u_g is the kinematic viscosity of the gas phase, p_1^0 is the vapor pressure of the pure solvent at temperature T, M_1 is the solvent molecular weight, and R is gas constant.

Equations (1.1) to (1.3) allow calculation of the wet film thickness h_w shown in equation (1.4).

$$h_w = \left[\left(\frac{3\eta_0}{2\rho\omega^2}\right) k(x_1^0 - x_{1\infty})\right]^{1/3} \quad (1.4)$$

After the coating solution reaches the immobile state, evaporation leads to a final film thickness h_f given by equation (1.5).

$$h_f = (1 - x_1^0) h_w \quad (1.5)$$

Schubert and coworkers suggested that the film thickness also depends on the solute molar mass and molar mass distribution, as the solution viscosity is related to both of these values based on the Mark-Houwink equation, $\eta_0 = KM^a$, where M is the average polymer molar mass and a and K are parameters that depend on the particular polymer-solvent systems.[23]

Spin coating is a simple and fast method that creates uniform thin films with thickness on the order of micrometers and nanometers, and the spin rate

controls the polymer film thickness. However, a typical spin coating process only utilizes 2-5% of the coating solution, because the remaining 95%-98% spins off the substrate.[24] Both loss of expensive polymer solutions and waste disposal contribute to the cost of spin coating. Moreover, the technique is primarily effective on flat substrates.

1.2.2 Dip coating

Dip coating is an especially simple method for manufacturing thin films. Figure 1.2 shows the dip coating process. After vertical immersion in the coating solution for a desired waiting time, pulling the flat substrate out of the solution at a uniform rate leaves a thin polymer solution deposited on both sides. The excess liquid will drain from the substrate, and the volatile solvent evaporates to generate the thin film. A gas flow may accelerate the drying process.

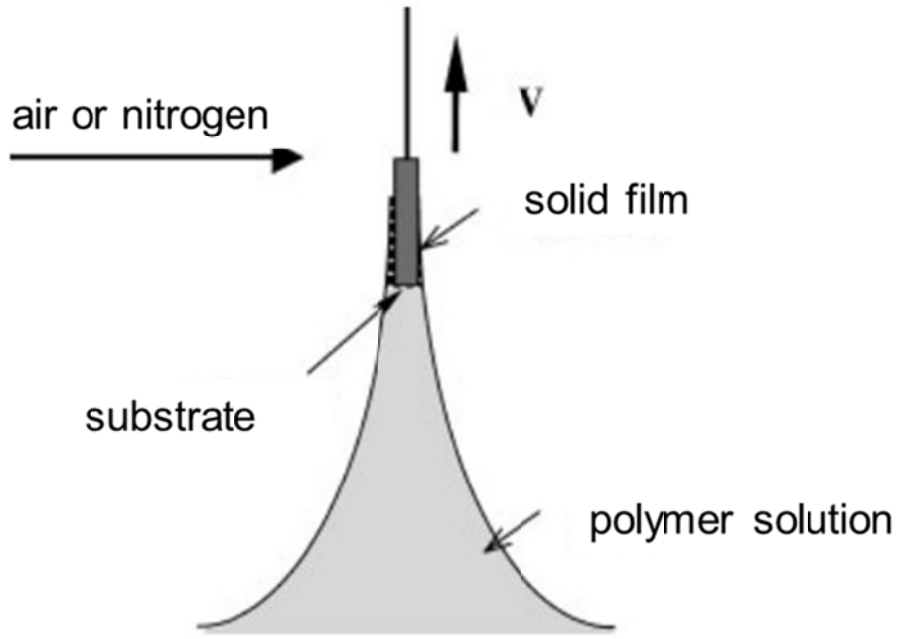

Figure 1.2 Illustration of the dip-coating process. (Reprinted with permission from *Macromol. Mater. Eng.* **2005**, 290,114-121)

The film thickness and morphology are functions of the dip-coating withdrawal speed, temperature and solvent vapor pressure in the gas phase, as well as the polymer concentration in solution and the solvent volatility. Generally, the film deposition falls into one of three regimes based on the dip-coating withdrawal rate. From low to high withdrawal rates, deposition moves from the capillary regime to the intermediate regime to the viscous drag regime, generating a curve of film thickness versus withdraw speed with a lowest point falls in intermediate regime.[25, 26]

Roland and coworkers showed that the in the capillary regime when the dip-coating withdraw rate is smaller than 0.1 mm/s, a combination of convective capillarity and evaporation effects govern the film thickness.[27, 28] Usually in this regime, an ultra-thick film forms as the solvent evaporation rate is faster than the motion of the drying line (vapor, liquid and solid three-phase frontier), leading polymer solution to a continuous upward motion to fill the meniscus by capillary action.

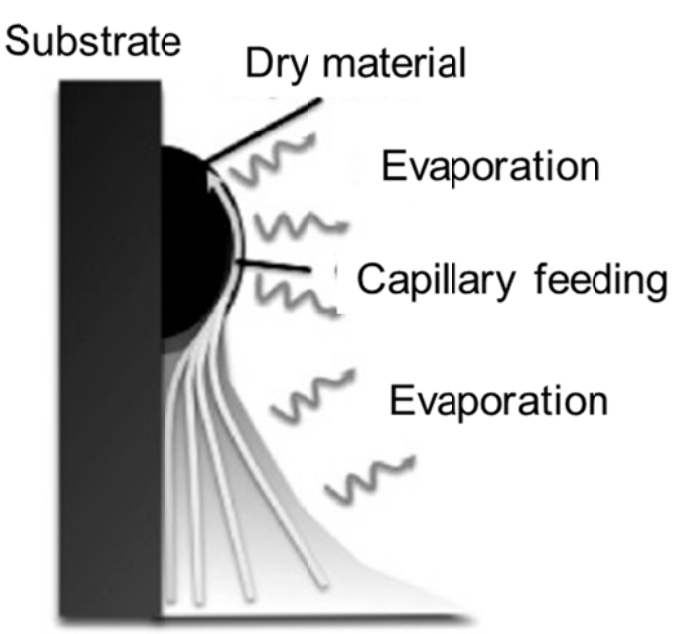

Figure1.3 The capillarity regime associated with low dip-coating rates. (Reprinted with permission from *J. Phys. Chem. C* **2010**, 114, 7637-7645. Copyright (2010) American Chemical Society.)

When the dip-coating speed is between 0.1 to 1 mm/s, a film with minimal thickness forms. At this critical speed range, the thin film thickness could decrease to a few nanometers with dilution of the initial solution. For dip-coating speeds higher than 1 mm/s, a gravity draining force, which removes excess coating on the substrate, prevents ultra-thick film formation. Faustini and coworkers developed a model for the overall film thickness as a function of the dip-coating speed.[26] The model yields equation (1.8)

$$\mathrm{h}_0 = k_i\left(\frac{E}{Lu} + Du^{\frac{2}{3}}\right) \quad (1.8)$$

where h_0 is the film thickness, k_i is a solution composition constant, E is the solvent evaporation rate, L is the substrate width, u is the dip-coating speed and D is a constant representing the solution physical-chemical characteristics, such as fluid viscosity, density and wetting.[26] The dip-coating temperature influences the film thickness by controlling the solvent evaporation rate and drying speed of material above the drying line. Higher temperatures lead to more solution entering the meniscus to generate thicker films. Nevertheless, the temperature does not necessarily affect the viscous drag regime. If the initial solution is highly diluted, which reduces k_i in equation (1.8), the curve representing the film thickness versus the withdrawal speed shifts downward. A few studies examined mesoscopic patterning of

polymer thin films,[29-31] and the composition evolution of supramolecular block copolymer films in dip-coating processes.[27, 28]

The dip-coating technique allows film formation on both sides of an object in a continuous process, and the loss of coating solution is low compared to spin coating or spray coating. However, if not all components in the substrate are submersible, the coating process may require a mask.

1.2.3 Physical/Chemical vapor deposition

Physical vapor deposition (PVD) methods are common techniques for inorganic thin formation in the semiconductor industry. However, PVD of polymers has recently drawn attention because of the development of organic electronic devices. PVD can give a variety of polymer thin films that include fluoropolymers,[32, 33] polyimides,[34-36] vinyl polymers,[37-39] and polypeptides.[40, 41]

In the most primitive PVD of polymers, one simply heats the polymer source material to induce evaporation and subsequent deposition on a substrate (Figure 1.4(a)). This strategy usually requires weak intermolecular interactions in the source material to allow evaporation at low temperatures that avoid thermal degradation of the polymer. This restriction limits the

range of polymers available for direct vapor deposition.

Figure 1.4(b) shows generation of a polymer film through coevaporation of two monomers in vacuum. Because of the vacuum, collisions between two monomers seldom occur in the chamber, and polymerization only happens during annealing of the two monomers absorbed on the substrate. This method is most applicable to polyimide and polyamide deposition.

A third strategy for PVD leading to polymer films employs radical polymerization (Figure 1.4(c)). Initiation occurs through radicals generated in the vacuum chamber, and these species induce polymerization of monomers adsorbed on the substrate. This method yields thin films containing polymers with high molecular weights. In addition to generating free monomer radicals in vacuum, initiators immobilized on the substrate can react with monomer vapor to grow a polymer covalently linked to the surface (Figure 1.4(d)).

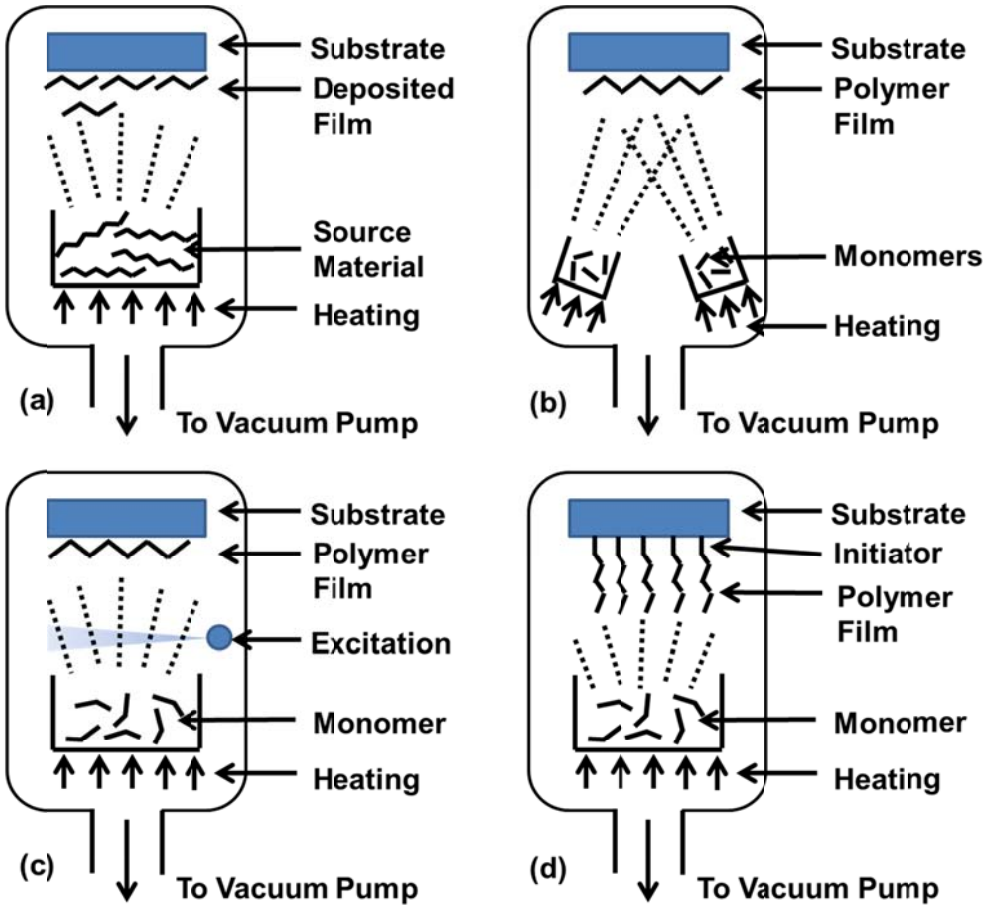

Figure 1.4 Four methods for PVD of polymer thin films. (Redrawn from Preparation of Polymer Thin Films by Physical Vapor Deposition, Wiley-VCH Verlag GmbH & Co. KGaA, 2011)

Chemical vapor deposition (CVD) methods involve chemical reaction of precursor gases brought by a carrier gas to a substrate. The precursor adheres to the substrate and decomposes to generate a thin film and release byproduct, which along with the unreacted precursor flows out of the chamber. Initiated CVD (iCVD) and oxidative CVD (oCVD), in particular, can generate

biocompatible, functional and electrically conducting polymer films.[42] In iCVD, an initiator decomposes into radicals as Scheme 1.1 shows, these radicals react with vinyl monomers, and the product radicals propagate the polymerization. The chain terminates by reaction with any radical species in the reaction chamber. Based on the methods to initiate the chemical reactions, there are different types of CVD, including hot-wire CVD,[43, 44] plasma-enhanced CVD,[45-47] microwave plasma enhanced CVD,[48, 49] and laser CVD[50, 51]. In oCVD, the monomer first reacts with an oxidant to generate cation radicals (Scheme 1.2). Two cation radicals form dimers followed by removal of two protons with the oxidizing agent anion. This process is repeated forming the polymer chain.

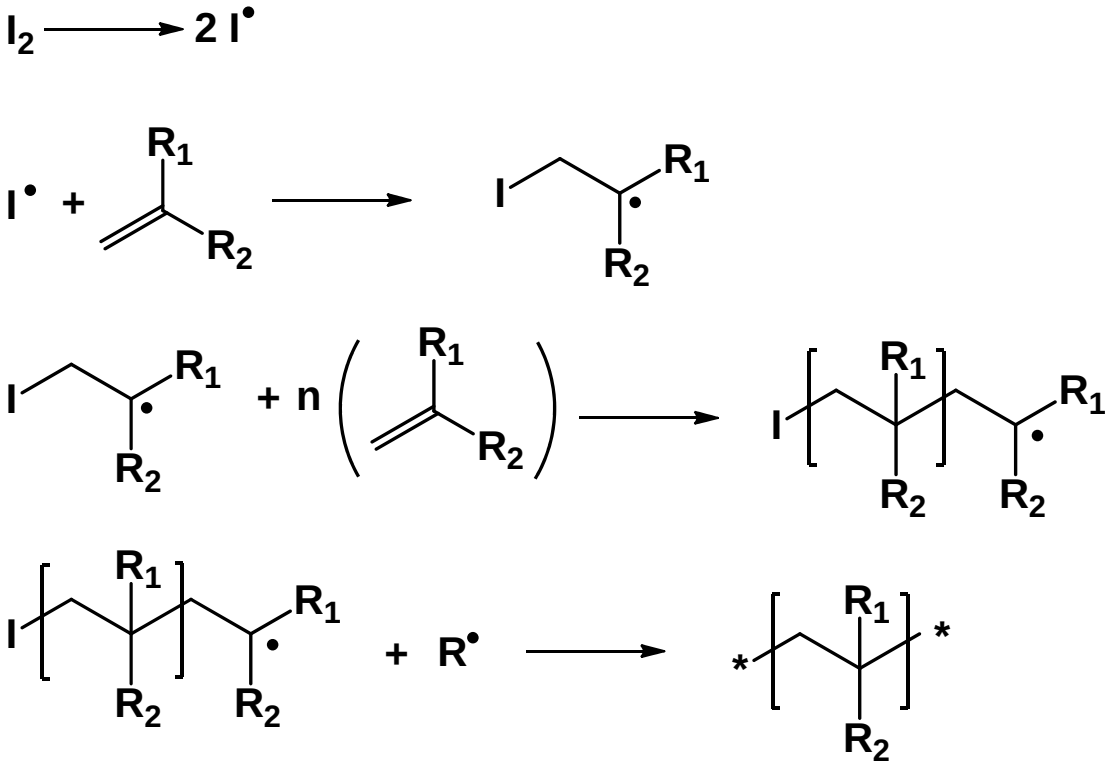

Scheme 1.1 Generic free-radical polymerization mechanism. I_2 represents any initiator and R represents any radical species. See the text for a detailed mechanistic description of the mechanism. (Redrawn from *Phys. Chem. Chem. Phys.* **2009**, 11, 5227-5240)

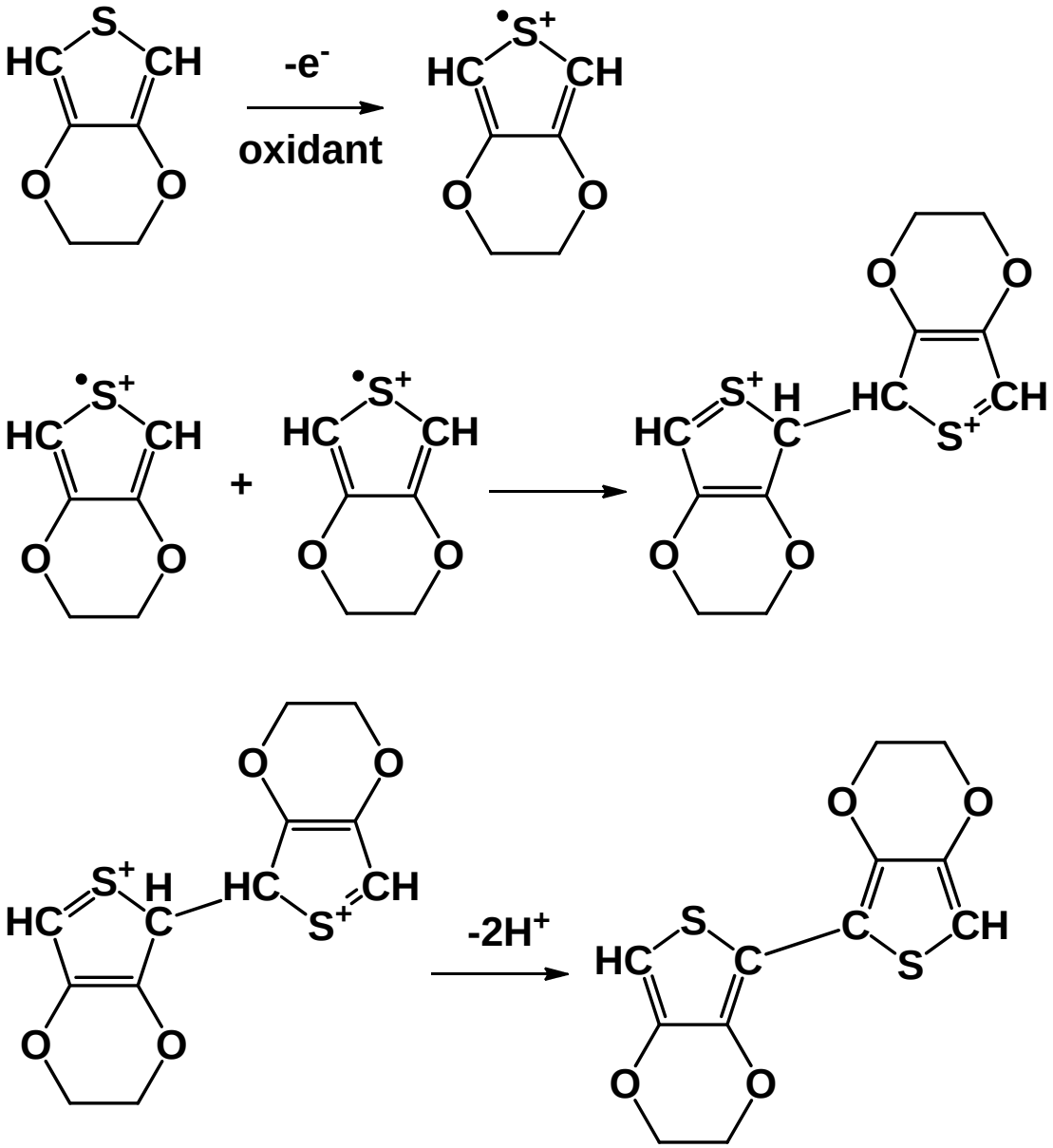

Scheme 1.2 Oxidation polymerization mechanism. See text for a detailed description of the mechanism. (Redrawn from *Phys. Chem. Chem. Phys.* **2009**, 11, 5227-5240)

Unlike PVD, which requires a vacuum below 0.1 mbar to avoid molecular collisions in the chamber,[52] CVD can occur even at atmospheric pressure.

Because CVD is a multidirectional deposition procedure, compared to PVD CVD gives more conformal films.[53] Nevertheless, the poisonous byproducts often produced during the CVD process cause safety and contamination problems. In most cases, films generated by PVD or CVD have weak adhesion to the substrate.

1.2.4 Surface-initiated growth of polymer brushes

Polymer brushes are ultrathin polymer coatings with one chain end or portion of the polymer chain attached to a substrate or interface. For true polymer brushes, the polymers must have a high chain density that forces the polymer chains to extend from the surface.[54] The synthesis of polymer brushes typically occurs through “grafting to” and “grafting from” techniques.[55, 56] The “grafting to” approach involves a chemical reaction or physical interaction between the polymer chain and the substrate (Figure 1.5(a) and 1.5(b)). In the “grafting from” approach polymer chain grows from an initiator immobilized on the substrate (Figure 1.5(c)). The biggest drawback of the copolymer adsorption method (Figure 1.5(a)) is the weak interaction between polymers and the substrate and the resulting film instability.[56] Covalent bonds between polymer chain ends and the substrate provide more robust polymer brushes. Compared to the “grafting from” approach, “grafting to” methods yield

polymer brushes with lower chain densities because steric hindrance prevents incoming polymer chains from approaching covered binding sites to generate dense films.

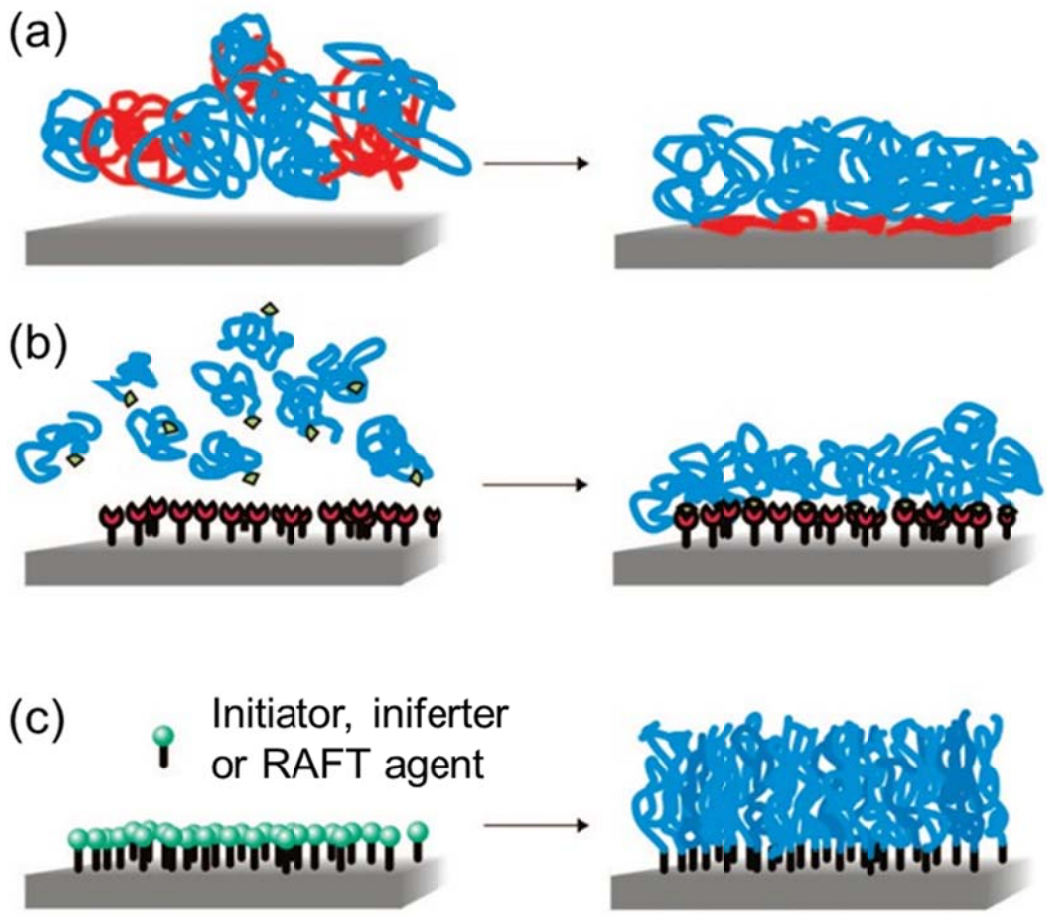

Figure 1.5 Preparation of polymer brushes: (a) Physical adsorption of the red blocks of diblock copolymers to the surface (“grafting to” method); (b) chemical association of the polymer chain end with a complementary functional group on the substrate (“grafting to” method); (c) growth of polymer from surface-tethered initiators (“grafting from” method). (Reprinted with

Figure 1.5 (cont'd) permission from *Chem. Rev.* **2009**, 109, 5437-5527. Copyright (2009) American Chemical Society.)

Cationic,[57-59] anionic,[59-61] ring-opening,[62-64] and ring-opening metathesis polymerization[65-67] are common strategies to grow polymer brushes from a surface. Controlled radical polymerization methods are particularly attractive because they provide control over the polymer brush thickness, composition and architecture with relatively low polydispersity and allow incorporation of a wide range of functional groups into the film. There are many strategies for polymer brush synthesis through controlled radical polymerization, including surface-initiated atom transfer radical polymerization (ATRP),[68-70] surface-initiated reversible-addition fragmentation chain transfer polymerization,[71, 72] surface-initiated nitroxide-mediated polymerization,[73-75] and surface-initiated photoiniferter-mediated polymerization.[76-78]

Surface-initiated ATRP is the most common technique to grow polymer brushes as it utilizes a simple procedure and employs inexpensive catalysts to form versatile polymer brushes. In addition, ATRP affords fine control of the polymer chain length, topology, composition and functionality, as well as robust attachment to the surface.

As Scheme 1.3 shows, the ATRP reaction usually utilizes a transition-metal complex as catalyst (M_t^n-Y/Ligand, where M_t is the metal ion

and Y is another ligand or counterion.). Oxidation of the metal ion in the catalyst accompanied by removal of a halogen atom X from the polymer chain end or initiator (R-X) generates a radical that initiates or propagates the polymerization. The resulting halogen anion compensates the extra charge on the catalyst, and the polymer chain grows with the addition of monomer to the radical at the polymer chain end. A low activation rate constant, k_{act}, compared to the deactivation rate constant, k_{deact}, leads to a low radical density that limits the termination of the polymer chains through radical coupling and disproportionation. A number of parameters control the polymerization rate, including the amount and reactivity of the catalyst, the counterion, solvent, ligand and initiator.

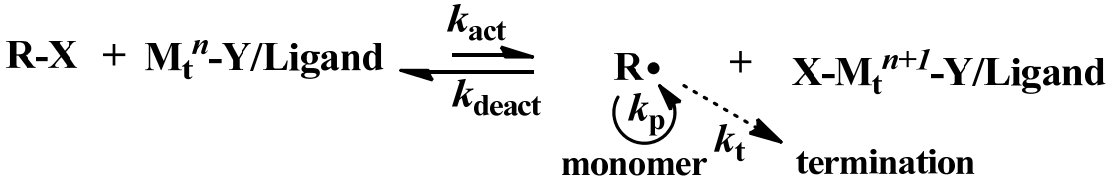

Scheme 1.3 Transition-Metal-Catalyzed ATRP.[79]

1.2.5 Interfacial Polymerization

Interfacial polymerization (IP) is the main technique for fabricating a dense polymer film on a porous support to generate NF or reverse osmosis (RO) membranes. Generally, two monomers react to create a thin polymer film at the interface of immiscible aqueous and organic solutions on a porous support.

Because the film forms a barrier between the immiscible solutions and slows down the reaction, the film can be exquisitely thin (10-100 nm).80 This technique allows the film to have a rough surface to improve the water flux for NF and RO membranes. Several types of polymer films were synthesized by IP, including polyamides,81 polyureas,82 polyesters,83 polyurethanes84 and polysiloxanes.85

Song and coworkers weighed the polyamide layer removed from a substrate to study film growth as a function of trimesoyl chloride (TMC) and p-phenylenediamine (PPD) concentrations and IP time.[86] Figure 1.6 shows a schematic drawing of interfacial polymerization with these monomers. They showed that there is an optimum ratio of TMC and PPD (3.5 g/L TMC and 20 g/L PPD) to achieve the highest crosslinking degree for a dense film, as this film generates the highest NaCl rejection. The film unit area yield reached a plateau within 30 s when the TMC concentration was higher than 1.0 g/L, suggesting a dense barrier formed between two phases to block the PPD diffusion.[87] Filtration experiments show that films fabricated with high TMC concentrations (3.5 g/L or 5.5 g/L) exhibit NaCl rejections >90%, confirming a dense film. At high TMC concentrations (5.5 g/L), the films prepared with different concentration of PPD reach the “self-limiting” stage rapidly,

suggesting a high concentration of TMC is necessary for the "self-limiting" phenomena to occur as PPD diffuses to the interface more easily than TMC.[88]

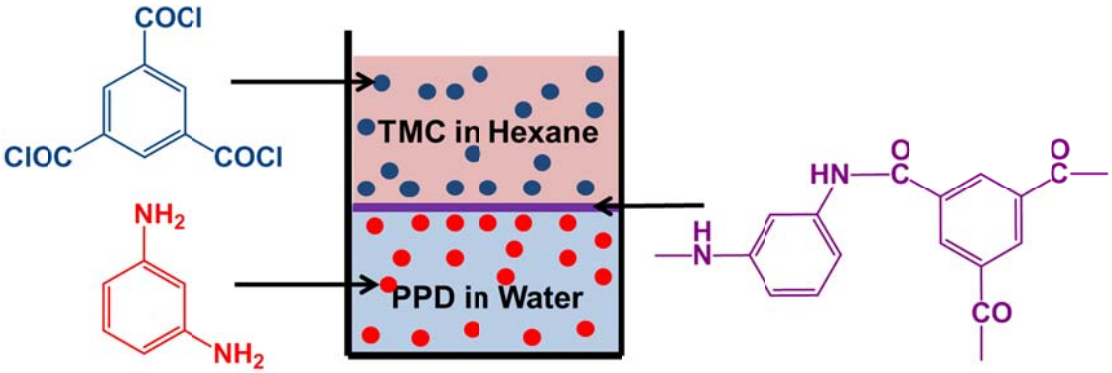

Figure 1.6 Scheme of interfacial polymerization.

Ghosh et al. investigated the impact of the solvent on the thicknesses of polyamide films prepared by IP.[89] Transmission electron microscopy images showed that the film thicknesses were 350±100, 200±100, 150±100, and 100±50 nm for cyclohexane, hexane, isopar, and heptane, respectively, with other polymerization conditions the same. Higher m-phenylenedianmine (MPD) solubility in a given solvent produces thicker films with less crosslinking, as the acetyl chloride groups on TMC react with MPD monomers instead of amine groups within the polymer chains. In addition, the hydrolysis of TMC reduces the number of acetyl chloride groups available within the polymer chains and hence generate a less cross-linked film.

The properties of interfacially polymerized films (e.g. thickness, hydrophobicity, roughness and permeability) are the result of many factors. A partial list of the factors includes monomer concentrations in each phase, monomer ratio, solvent type, reaction time, additives and post treatment (e.g. curing time and curing temperature).[86, 89]

1.2.6 Layer-by-layer assembly

LBL assembly techniques can rapidly provide selective skins for membrane separations,[90] responsive layers in biosensors[91] and capsules for drug delivery.[92] This simple film formation approach relies on adsorption of complementary alternating layers. The affinity between the alternating layers can arise through electrostatic interactions,[93-95] hydrogen bonding,[96-98] covalent bonding,[99-101] hydrophobic forces,[102, 103] and supramolecular interactions.[104, 105] In the most popular LBL method, Decher and coworkers first employed electrostatic interactions between polyanions and polycations to fabricate polymer multilayer films.[93] Typically, this technique employs alternating exposure of charged substrates to oppositely charged species with rinsing between each adsorption step. The deposition can also occur using dip coating,[106] spin coating,[107, 108] spray coating[109] and flow-based techniques.[94] Moreover, polyelectrolytes amenable to LBL methods include

simple polymers, proteins,[94, 110, 111] colloids,[112, 113] DNA,[111, 114] dye molecules,[115, 116] and other charged species.

Figure 1.7 illustrates LBL polyelectrolyte deposition on a flat surface. Initially, immersion of the positively charged substrate in a polyanion solution yields a polyanion layer on the surface because of multiple polyelectrolyte-surface interactions. This is an entropically favored process because the attachment of a single polymer chain releases multiple counter-ions into the deposition solution.[117] Excess polyanion adsorption leads to overcompensation of the positive surface charge and a negatively charged surface. After rinsing, substrate immersion in a polycation solution adds another adsorbed layer and reverses the surface charge. Repetition of this process leads to the desired film thickness or number of layers.[95]

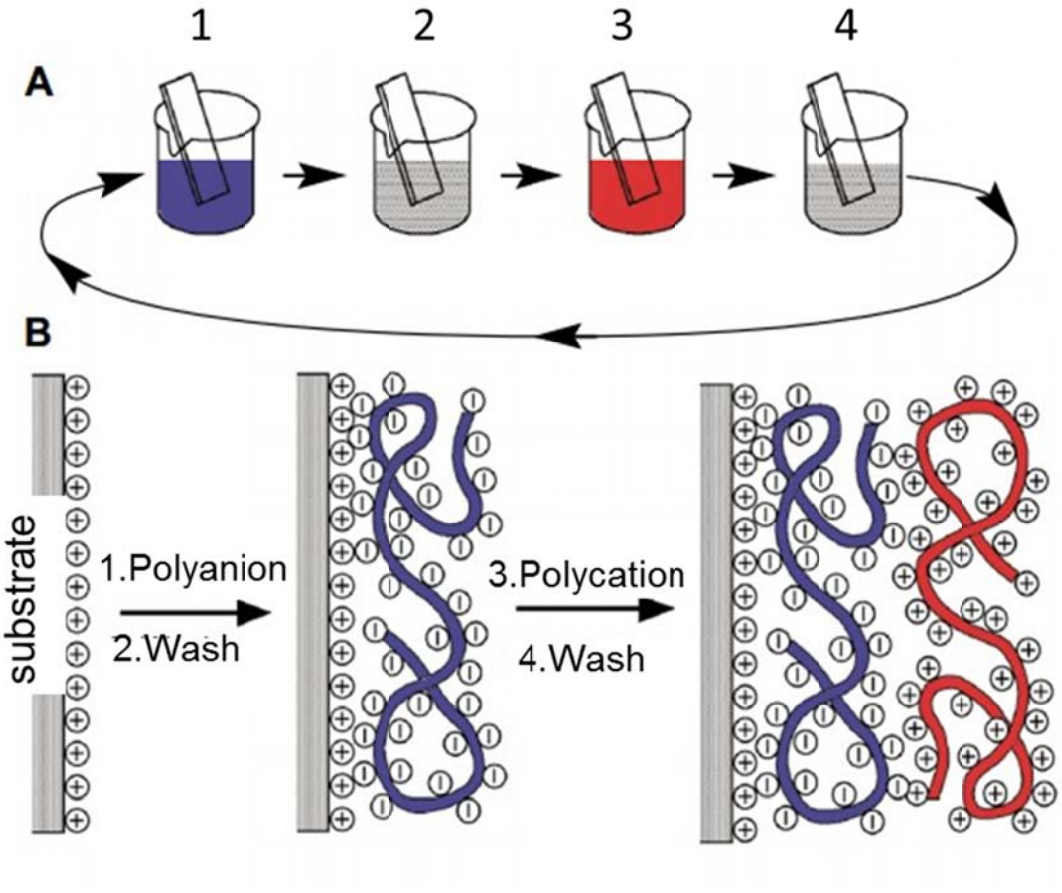

Figure 1.7 LBL assembly of polyelectrolyte bilayers using electrostatic interactions on a flat surface. (Reprinted with permission from *Science* **1997**, 277, 1232-1237)

Below I discuss the factors that influence PEM thicknesses, including polyelectrolyte structure, supporting electrolyte concentration and other deposition conditions (e.g. pH, rinsing protocol, solvent composition, temperature and deposition time).

1.2.6.1 Polyelectrolyte structures

For some polyelectrolyte combinations, e.g. poly(4-sodium styrene sulfonate)/poly(allylamine hydrochloride) (PSS/PAH) and poly(acrylic acid)/poly(allylamine hydrochloride) (PAA/PAH), the PEM thickness increases linearly function with the number of absorbed layers.[118-120] In contrast other polyelectrolyte pairs such as poly(L-glutamic acid sodium salt)/poly(L-lysine hydrochloride) (PGA/PLL) and poly(4-sodium styrene sulfonate)/poly(diallyl dimethyl ammonium chloride) (PSS/PDADMAC) with excess supporting electrolyte show an exponential increase in film thickness as the number of adsorbed bilayers increases.[121-124] (Figure 1.8 shows the structures of these polyelectrolytes.) Such exponential film growth occurs when one of the polyelectrolytes in a pair diffuses into the entire PEM during the deposition. Upon exposure to the next polyelectrolyte, the previously deposited polyelectrolyte “diffuses out” of the PEM film to generate a very thick polyelectrolyte complex. Thus the thickness of each deposition layer increases as the number of layers in the film increases.[125] Usually the polyelectrolyte that diffuses throughout the PEM has a low charge density and high solubility in water.[126]

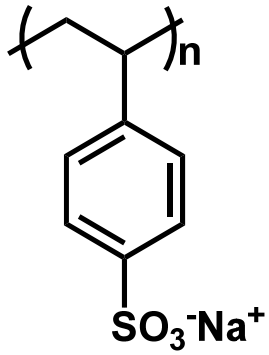

poly(4-sodium styrene sulfonate)

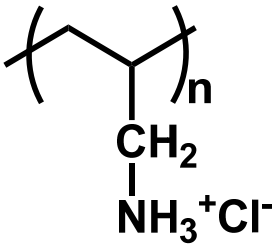

poly(allylamine hydrochloride)

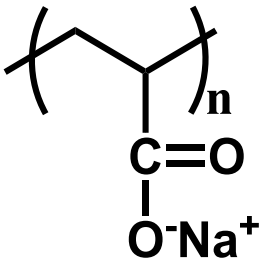

poly(acrylic acid) sodium salt

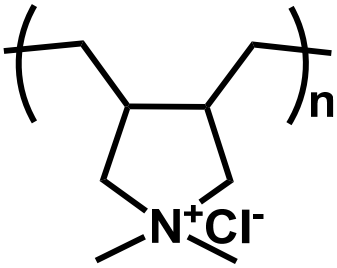

poly(diallyl dimethyl ammonium chloride)

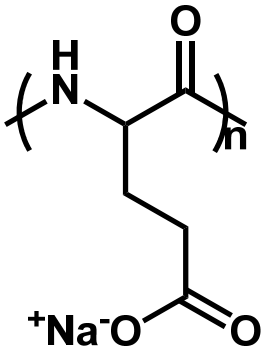

poly(L-glutamic acid sodium salt)

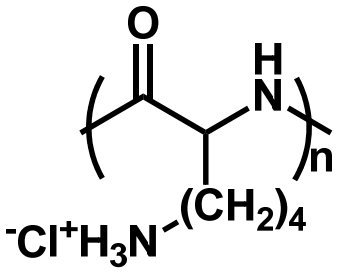

poly(L-lysine hydrochloride)

Figure 1.8 Structure of common polyelectrolytes used in LBL adsorption.

Even when comparing films that all exhibit either linear or exponential growth, the polyelectrolyte architecture affects film thicknesses.[127-130] Ma et

al. showed that a PAH/poly(2-hydroxyethyl methacrylate)-*graft*-poly-(acrylic acid) (PHEMA-*g*-PAA) film with 10 bilayers is about 4 times thicker than a 10-bilayer (PAH/PAA) film deposited at the same pH.[127] Thus the comb shape of the PHEMA-*g*-PAA leads to a much thicker film than adsorption of linear PAH (Figure 1.9 (b)). Choi et al. found that PEMs fabricated with star-shaped PAA and star-shaped poly[2-(dimethylamino) ethyl methacrylate] (PDMAEMA) are two or three times thicker than linear PAA/PDMAEMA films with the same number of deposition cycles (Figure 1.9 (c)).[128]

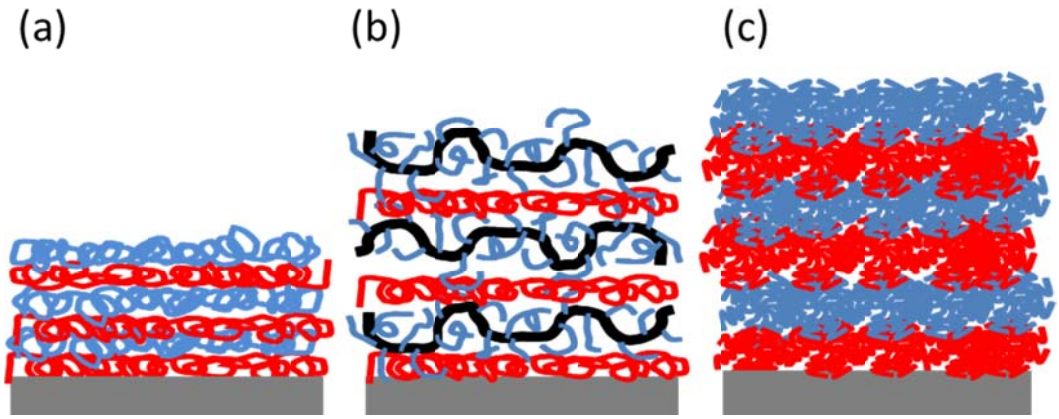

Figure 1.9 Comparison of multilayers containing two linear polymers (a), linear and comb-shaped graft co-polymers (b), and two star-shaped polymers (c).[127, 128]

In addition to the polyelectrolyte composition and architecture, the

polyelectrolyte molecular weight influences the PEM thickness, although initial studies reported mostly weak correlations between molecular weight and thickness. For example, Lösche et al. reported that the thickness of PSS/PAH films is independent of the PSS molecular weight.[131] More recently, Kujawa et al. showed that polyelectrolytes with higher molecular weight (Hyaluronic acid (HA), 360,000 Da; chitosan (CH), 160,000 Da) doubled the thickness of 12-bilayer CH/HA films compared to low molecular weight ones (HA, 30,000 Da; CH, 31,000 Da).[132] In addition, in PSS/PAH adsorption, Milkova and Radeva found that the thickest bilayers result from the use of low molecular weight PSS (70 kDa) rather than 150 kDa or 350 kDa PSS.[133] They suggest this is due to an increase in the surface roughness with the lower molecular weight PSS. Schlenoff et al. demonstrated atypical multilayering characteristics when adsorbing polymers in the 10 kDa range. In this case, the multilayer exhibits loss of materials from the film as the result of the formation of quasisoluble polyelectrolyte complexes.[134]

Several research groups showed that the polyelectrolyte concentration in solution affects the PEM thickness. At low concentrations, film thickness increases as the polyelectrolyte concentration rises,[135-138] but as the concentration continues to increase the film thickness stays nearly constant.[139] Fleer et al. suggest that this correlation stems from the interaction between polyelectrolyte chains and the surface.[140] At low

polyelectrolyte concentrations, a given polymer chain binds to many sites on the surface to give a flat conformation and relatively thin film. On the other hand, high polyelectrolyte concentrations lead to fewer interactions between a given polymer chain and the surface because many polyelectrolytes approach the substrate simultaneously. This should lead to more extended polymers and thicker PEMs.

1.2.5.2 Supporting electrolytes

Addition of salt to deposition solutions is one of the most common methods for increasing the thicknesses of PEMs. When adsorption takes place from solutions without supporting electrolytes, the polymer chains adopt extended conformations to minimize the charge repulsion between the repeating units. Adsorption of these extended chains parallel to the substrate yields thin PEMs. Conversely, supporting electrolyte can screen the charge in the repeating unit, allowing polymers to coil and from loops and tails. As a result, thicker films form from supporting electrolyte solutions, and in solution these films show higher surface charge than films formed in the absence of salt.[139, 141-144] Increased surface charge also leads to more polyelectrolyte adsorption and, hence, thicker films.[139, 143-146] Samanta and coworkers showed that when the salt concentration reaches a critical level, the PEM surface roughness increases dramatically.[147] High roughness leads to

higher surface areas for adsorption and relatively thick films.

In addition to the supporting electrolyte concentration, the salt composition also influences film thickness. According to several studies, the PEM thickness correlates with the Hofmeister ordering of the univalent anions in the supporting electrolyte.[139, 145, 148-151] The interaction between chaotropic anions and polycations is strong and partially neutralizes the polycation charge to generate a thick film (Figure 1.10(a)). On the other hand, the interaction between cosmotropic anions and polycations is weak so the polycation chain stretches to decrease the charge repulsion between repeating units. Thus a flat and thinner multilayer forms in the presence of cosmotropic anions (Figure 1.10(b)). In addition, the least hydrated and highly polarizable cations provide the thickest PEM films due to the higher interaction with charged polyanions.[139, 152] However, compared to anions, the influence of cation composition on the PEM film growth is less significant.

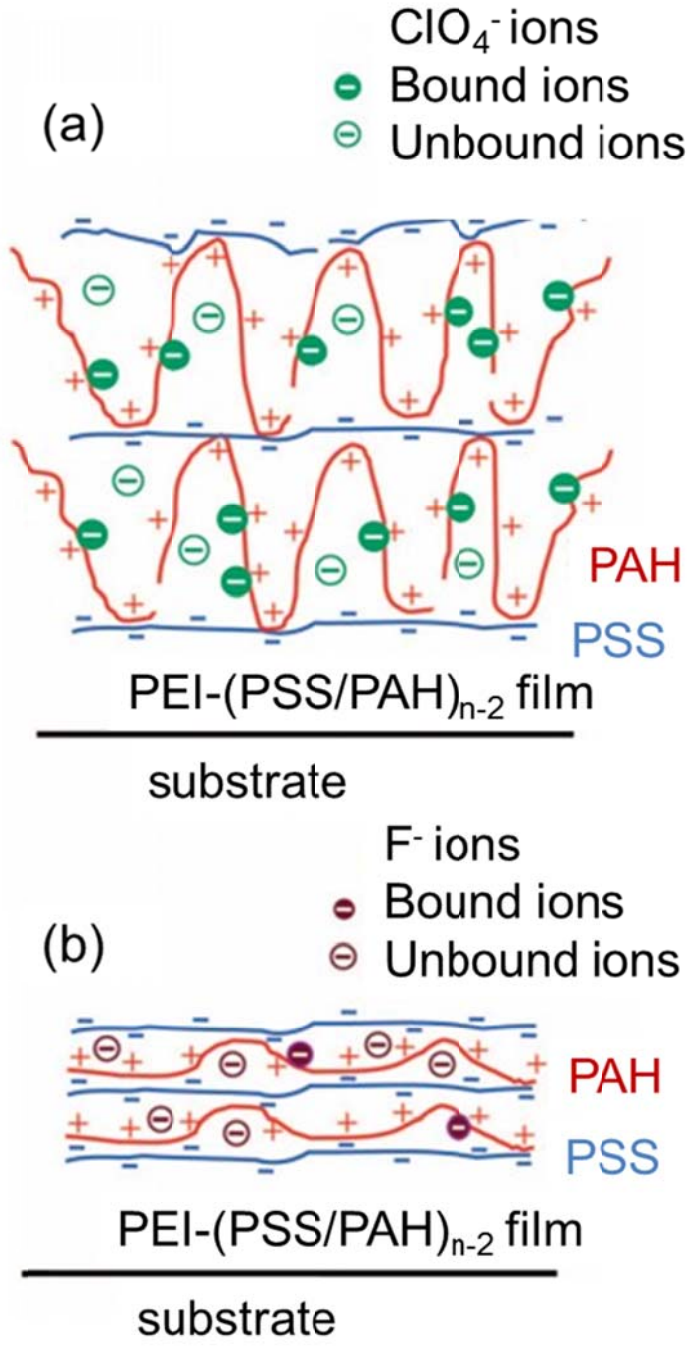

Figure 1.10 PSS/PAH film formation with chaotropic (a) or cosmotropic (b) anions in the supporting electrolytes. (Reprinted with permission from *Langmuir* **2009**, 25, 2282-2289. Copyright (2009) American Chemical Society.)

Dressick and coworkers found that supporting electrolyte salts with divalent anions give rise to higher PEM thickness than salts with monovalent anions.[153] Based on their experimental results, they suggested that PAH aggregated in solution due to intra- and interchain anion bridges through divalent anions such as SO_4^{2-} (Figure 1.11). Because the rigid bridging is relatively stable, PAH does not relax to accommodate additional incoming PAH, leaving thick layers with void defects which were observed by AFM. However, after rinsing with salt solution and water, the removal of divalent anions causes the collapse of the PAH aggregates and eventually the exterior chains exhibit a more open structure and thus voids heal when the PSS is absorbed on the film.

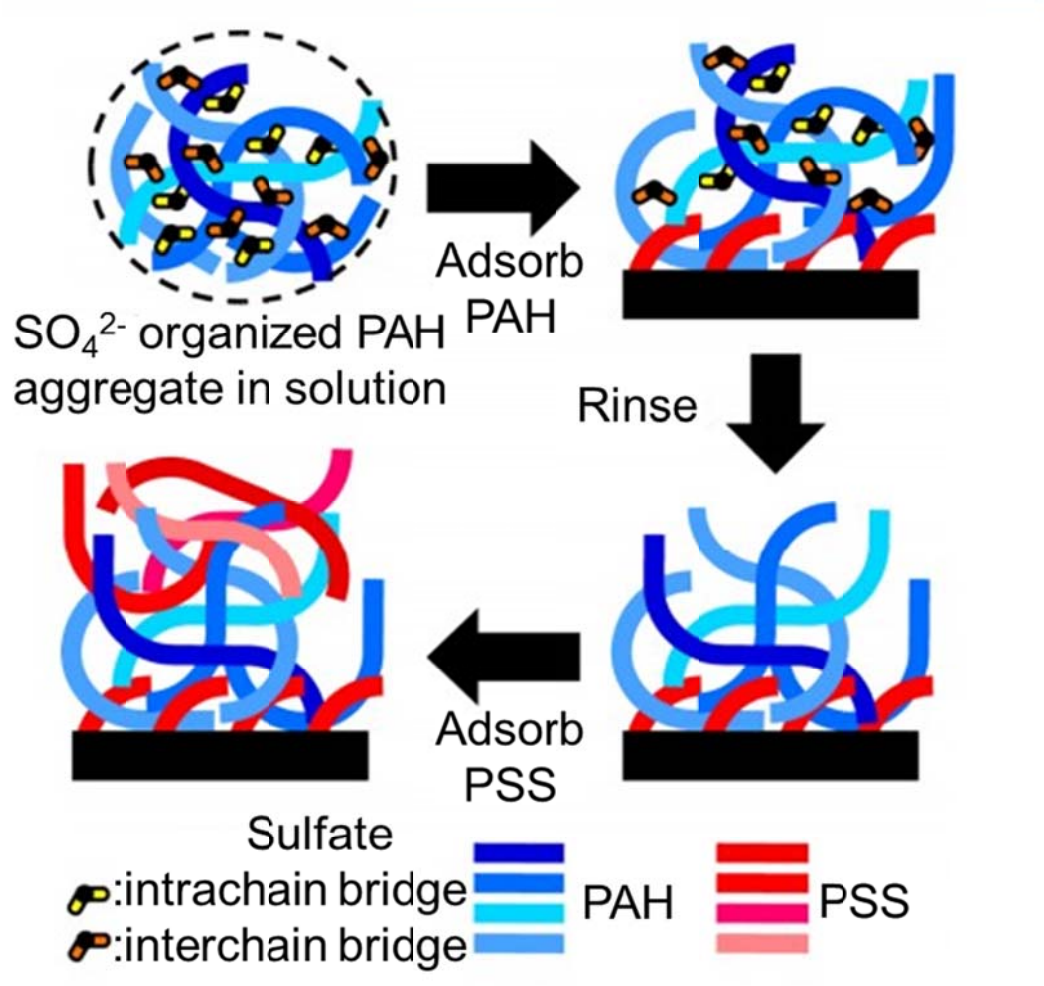

Figure 1.11 Anion-bridging model for PSS/PAH films formed from polyelectrolyte solutions containing sulfate or other divalent bridging anion salts. The different shades of blue or red show the chain entanglement in the multilayer. (Reprinted with permission from *Langmuir* **2012**, 28, 15831-15843. Copyright (2012) American Chemical Society.)

1.2.5.3 Deposition conditions

Other deposition variables such as pH,[154-156] method (simple immersion, spray coating, spin coating or dip coating),[128, 157, 158] rinsing protocol,[151] solvent composition,[139, 159, 160] temperature[161-163] and deposition time[164] all affect PEM deposition.

Choi and coworkers found that spin-assisted LbL deposition generates thinner $(PDMAEMA/PAA)_n$ films than the conventional immersion method (Table 1.1).[128] The spin-assisted method prevents intermixing within the multilayer by limiting diffusion time and provides a smoother PEM surface. However, this result contradicts findings from Kharlampieva et al.,[158] in which a spin-assisted method gave rise to thicker PSS/PAH multilayers than dipping. The difference between these studies might stem from the lower charge density of PDMAEMA compared to PAH. Interdiffusion of polyelectrolytes may be much more important with PDMAEMA than PAH.

Table 1.1 Ellipsometric thicknesses for $(PDMAEMA/PAA)_n$ films formed though dip and spin deposition methods. The polyelectrolyte deposition solution pH was 6 in both cases. (Taken from *J.Am.Chem.Soc.* **2011**, 133, 9592-9606)

	$(PDMAEMA/PAA)_n$ Thickness (nm)		
method	n=9	n=18	n=30
dip	141.3±0.5	514.6±15.0	959.1±39.7
spin	31.6±1.5	70.0±1.0	114.5±0.3

Long et al. studied the influence of solvent on the growth of poly(sodium 2-acrylamido-2-methylpropanesulfonate) (PAMPS)/PDADMAC multilayer films.[159] They employed a quartz crystal microbalance (QCM) with dissipation measurements to investigate the PEM growth as a function of the methanol molar fraction in water (x_M) (Figure 1.12). As equation (1.9) shows, the decrease in the QCM resonant frequency ($\Delta \mathrm{f}$) is proportional to the mass change ($\Delta \mathrm{m}$) after each deposition step as long as the adsorbed layer is rigid and evenly distributed, and much thinner than the crystal.

$$\Delta \mathrm{m} = -\mathrm{C}\frac{\Delta \mathrm{f}}{n} \tag{1.9}$$

In equation (1.9), C is the mass sensitivity constant and n is the overtone number (n = 1, 3, 5, ...). Figure 1.12 shows that the film growth changes from a

linear to an exponential trend as the methanol molar fraction increases. Poptoshev and Caruso observed a similar trend for PSS/PAH multilayer adsorption in mixtures of water and ethanol.[160] The change in PAMPS/PDADMAC growth mode may result from a gradual rise in the surface roughness of the film when polymers become more coiled as the fraction of organic solvent increases. Such increases in roughness lead to more surface area for adsorption of the subsequent layer. As X_M initially increases, the screening of electrostatic repulsion between the charged polyelectrolyte repeating units decreases because the dielectric constant of the solvent drops. This leads to more adsorption of coiled polyelectrolytes. However, both the polyelectrolytes have a minimum ionization degree in 75% methanol, as determined by measuring the conductivity of the polyelectrolyte solution in the solvent mixture. This gives rise to the smallest chain charge density and thereby the most coiled polyelectrolyte conformation.

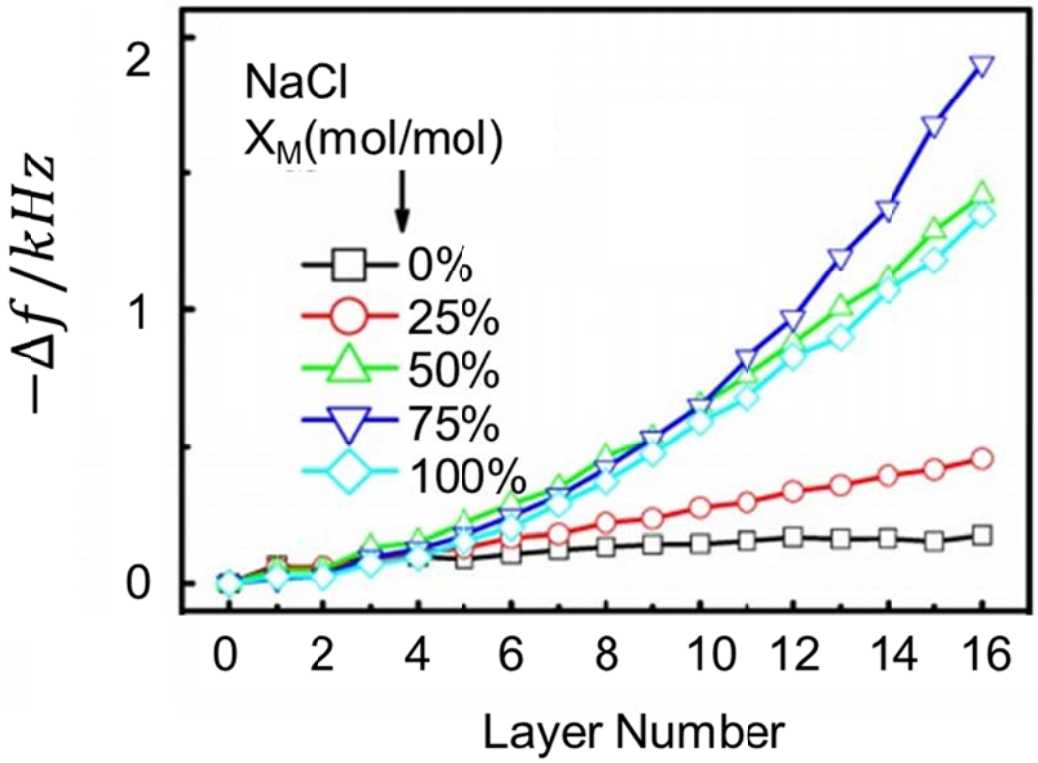

Figure 1.12 The frequency shift as a function of PAMPS/PDADMAC layer number for deposition from solvents with different molar fractions of methanol (X_M). Even and odd layer numbers represent deposition of PDADMAC and PAMPS respectively. Deposition solutions also contained 2.0 mM NaCl. (Reprinted with permission from *Langmuir* **2013**, 29, 3645-3653. Copyright (2013) American Chemical Society.)

1.3 Conducting polymers

With PEMs, the maximum zeta potential is typically around 50 mV.[90, 165] In the future we hope to apply much larger electrical potentials at the surface of

conducting membranes to increase electrostatic exlusion of ions and enhance ion-transport selectivities. Chapter 4 describes our initial studies on depositing conducting polymer films at the surface of filtration membranes, and this section provides an introduction to conducting polymers.

Conducting polymers contain conjugated, delocalized double bonds along their backbones. The polymers are conductive due to the movement of electrons in unoccupied energy states (n-type) or movement of holes in filled energy states (p-type). The conductive electrons or holes result from chemical oxidation or reduction, respectively. Chemical oxidation, for example, removes electrons to generate conductive polymers with positive charge on the repeating unit, and anions compensate this charge to form polymer salts. The oxidation (or reduction) process with compensation of the polymer charge is termed doping and enhances the conductivity of conductive polymers by several orders of magnitude, from the semiconductor to the metal level. Most conductive polymers are p-type, including polyaniline (PAN), poly(3,4-ethylenedioxythiophene) (PEDOT), polypyrrole, and polythiophene. The section below further discusses PAN, which is a major focus of this work.

1.3.1 Polyaniline

Polyaniline (PAN) was first discovered as a conductive polymer in the mid 1980s, although it was first prepared in the 1840s. It has three oxidation states (Figure 1.13), the fully reduced form (leucoemeraldine), the half oxidized form (emeraldine) and the fully oxidized form (pernigraniline). Only the emeraldine salt (doped polyaniline) is highly conductive. The conventional chemical oxidation synthesis method in a protonic acid gives rise to the emeraldine salt form of PAN, or doped PAN. The emeraldine base consists of alternating reduced and oxidized units as shown in figure 1.14. The emeraldine salt could be dedoped (deprotonated) and redoped (protonated) by base and acid.

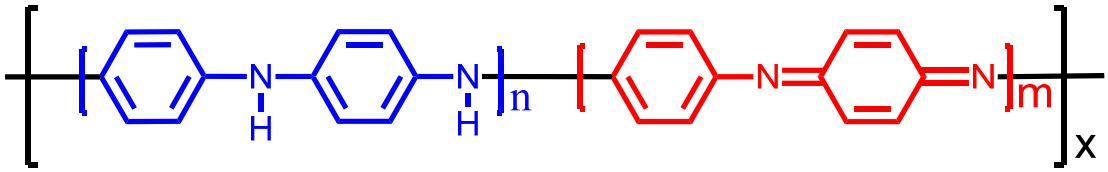

Figure 1.13 Scheme structure of polyaniline with three oxidation states.

n=1 m=0, leucoemeraldine – white or colorless

n=m=0.5, emeraldine- blue

n=0 m=1, pernigraniline – blue or violet

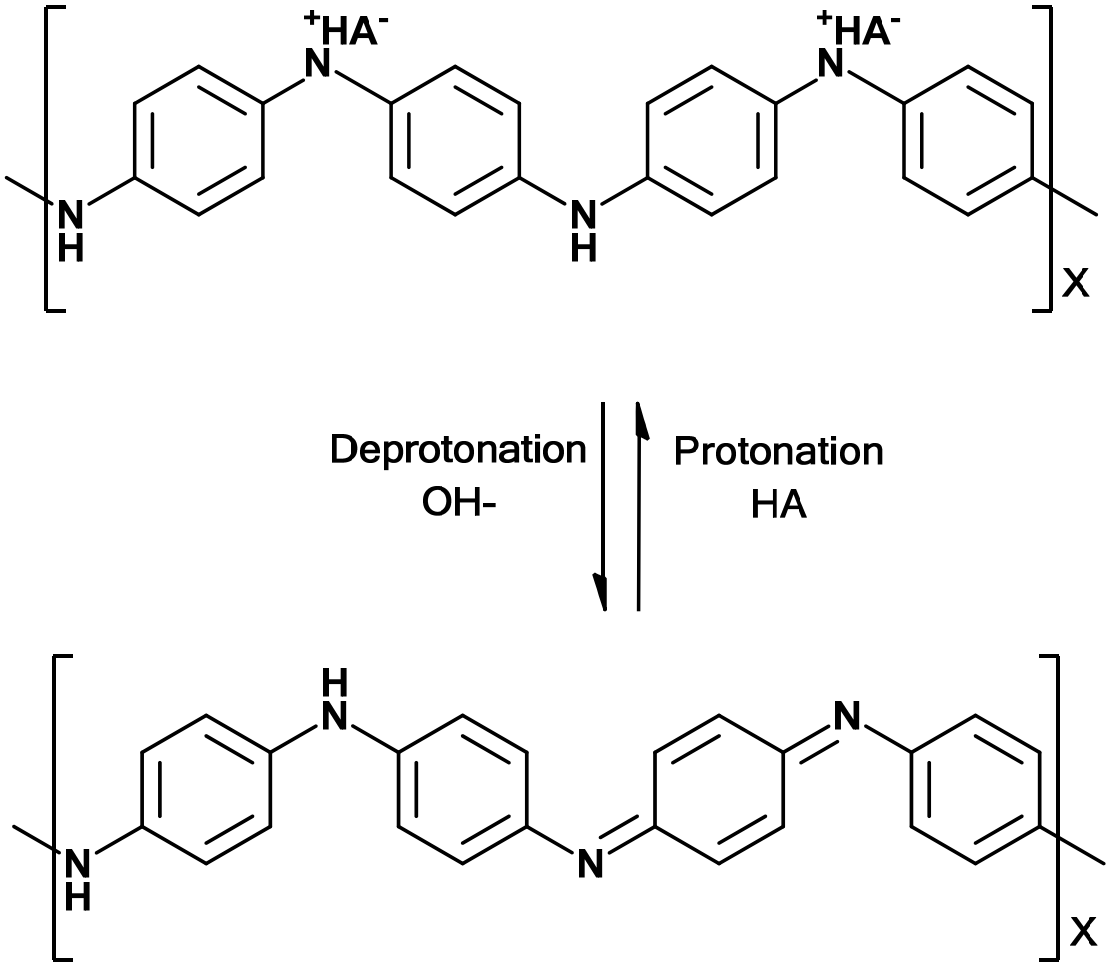

Figure 1.14 Deprotonation (dedoping) and protonation (doping) of polyaniline salt (bottom) and emeraldine base (top).

1.3.2 Synthesis of PAN nanofibers

Polyaniline nanofibers on a membrane surface may enhance the charge density of the selective skin layer upon application of a potential. There are numerous approaches based on chemical oxidative polymerization to

synthesize polyaniline nanofiber coatings including the use of hard templates,[166-169] surfactants,[170-173] electrospinning,[174, 175] interfacial polymerization,[167, 176] and seeding polymerization.[177-179] However, these methods are complex, expensive and include multiple steps. Chiou et al. developed an easy and inexpensive method, dilute polymerization, to synthesize supported, aligned polyaniline nanofibers by exposing the substrates to monomer and oxidant solutions with low concentrations.[180, 181] The mechanism of fiber formation is unclear; however, Chiou et al. suggest a nucleation and growth process, where some nanofibers formed on the substrate serve as the nucleation sites for additional nanofibers. With a higher concentration system, the individual polyaniline nanofibers pack very densely and merge with each other, and the nanofiber structures disappear.

1.4 Ion Separations with Membranes

The focus of this thesis is the development of new membrane coatings for highly selective ion separations. Membrane-based techniques for ion separations or water desalination include NF,[182-184] RO,[182, 185-187] diffusion dialysis,[188-190] electrodialysis,[191, 192] facilitated-transport dialysis,[193-195] forward osmosis,[196, 197] and membrane distillation.[198] Reverses osmosis is now an accepted technique for creating potable water from seawater, whereas

NF is especially useful in water softening and employed in water treatment. Forward osmosis and membrane distillation are emerging techniques for applications such as desalination and food processing, whereas electrodialysis and diffusion dialysis typically aim at synthesis or purification of specific salts. Facilitated transport is a highly selective membrane separation technique that has not yet been widely applied due to technical challenges.[199] This section focuses on the membrane processes examined in this dissertation including NF, diffusion dialysis and electrodialysis.

1.4.1 Nanofiltration

NF is a pressure-driven membrane filtration process similar to RO, but NF requires less transmembrane pressure and provides lower rejection for monovalent ions. Low monovalent ion rejections and high membrane permeabilities make NF membranes more energy efficient than RO systems for water softening and organic pollutant removal.

In some cases, the solution-diffusion model effectively describes the performance of NF membranes. Although more commonly employed with RO, the solution-diffusion model should also apply to “tight” NF membranes, which contain a relatively dense skin on a porous support.[200, 201] In the solution-diffusion model, ions permeate through the membrane due to a

concentration gradient. Equation (1.10) describes the salf flux, J_j, where B is the salt permeability constant and c_{j_0} and c_{j_l} are the salt concentrations on the feed and permeate sides of the membrane, respectively.

$$J_j = \mathrm{B}(c_{j_0} - c_{j_l}) \tag{1.10}$$

The water flux,J_v, depends on the pressure drop across the membrane, $\Delta\mathrm{p}$, the solution osmotic pressure, $\Delta\pi$, and a permeability constant A (equation (1.11)).

$$J_v = \mathrm{A}(\Delta\mathrm{p} - \Delta\pi) \tag{1.11}$$

The membrane performance in terms of salt removal is reported in terms of rejection, R, and selectivity, α, which are defined in equation (1.12) and (1.13),

$$\mathrm{R} = \left(1 - \frac{c_{j_0}}{c_{j_l}}\right) \times 100\% \tag{1.12}$$

$$\alpha = \frac{100 - R_1}{100 - R_2} \tag{1.13}$$

where R_1 and R_2 represent the rejection of solute 1 and solute 2 respectively.

The salt rejections depend on both size-based and Donnan exclusion. In Donnan exclusion, the charged membrane creates a potential that excludes ions with the same charge, particularly multivalent ions. Schaep et al. studied the influence of ion size and charge on salt rejection in NF.[202] For both NF 40 (negatively charged) and UTC 20 (positively charged) membranes whose pore

radii are around 0.4 nm, the rejections of Na_2SO_4, $MgCl_2$ and NaCl were similar, suggesting that charge is not the primary factor in salt rejection by these membranes. However, salt rejection correlated inversely with the salt diffusion coefficients in water. In contrast, for a NTR 7450 membrane, which has larger pores (~0.8nm), Donnan exclusion primarily determined salt rejection.

By optimizing the membrane surface charge, Ouyang et al. achieved a Na^+/Mg^{2+} selectivity of 22 along with a 0.85 $m^3/(m^2$ day) solution flux (4.8 bar transmembrane pressure) using membranes composed of five bilayers of (PSS/PAH) on alumina supports.[90] In addition, Stanton et al. reported Cl^-/SO_4^{2-} selectivities as high as 35 with $(PSS/PAH)_4PSS$ films on alumina supports.[203] By switching the top layer from PSS to PAA, the selectivity increased to about 85 although the water flux dropped about 50%.

NF applications include recovering monovalent ions,[204] softening water,[90, 205] and removing heavy metal ions.[206, 207] Chapter 2 examines the unusual phenomenon of negative ion rejection in NF, where a salt concentration on the permeate side of the membrane is higher than that in the feed. This negative rejection might prove useful for trace ion removal from a multivalent salt solution. That chapter provides a longer discussion of negative rejection.

1.4.2 Diffusion Dialysis

Diffusion dialysis employs a concentration gradient across a selective membrane as the driving force to achieve ion separation or enrichment. Wallace first applied diffusion dialysis as a separation method to enrich radioactive species.[208] He employed 0.01 M $UO_2(NO_3)_2$ as the feed solution for a cation selective membrane, and 2 M nitric acid as the receiving solution (Figure 1.15). Because of the 2 M concentration gradient, protons diffused through the membrane to the feed side, whereas anions could not permeate through the cation exchange membrane. To maintain electrical neutrality, UO_2^+ diffused to the receiving solution with a 28-fold enrichment.

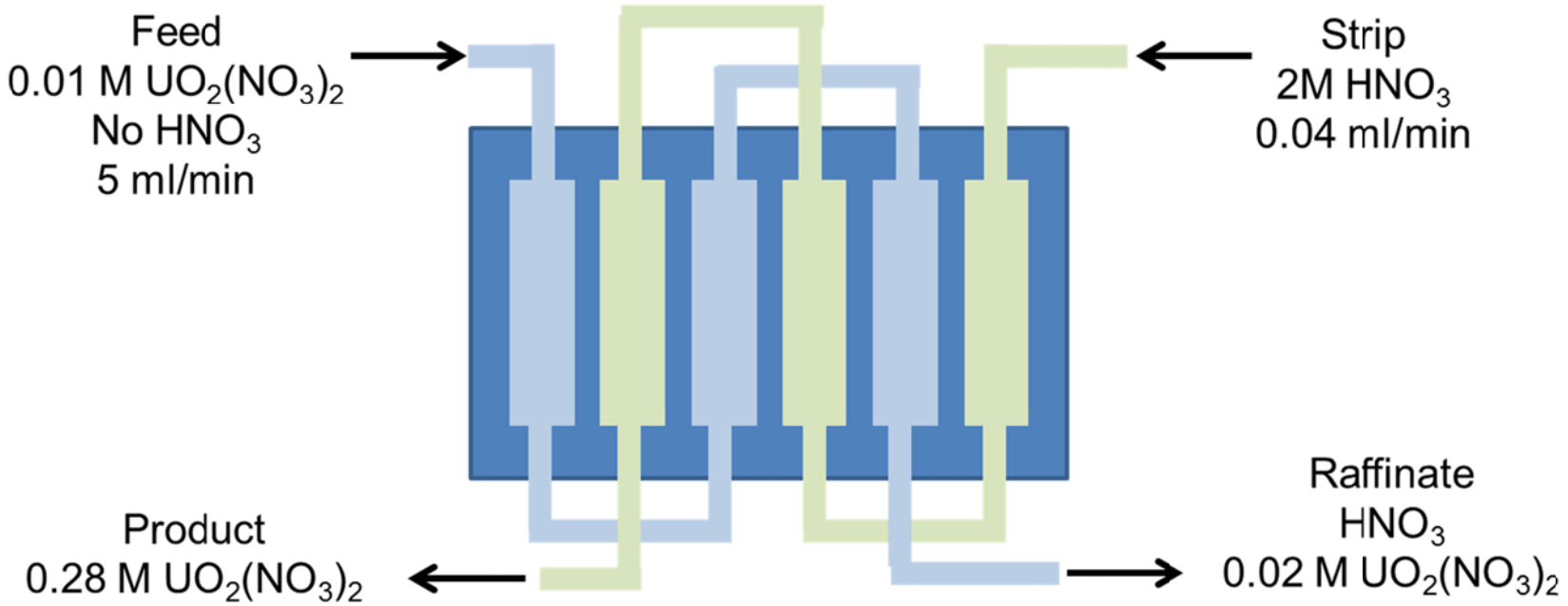

Figure 1.15 Illustration of diffusion dialysis to enrich uranyl nitrate. (Redrawn from *Membrane Technology and Applications.*)[209]

Diffusion dialysis is mostly used for acid recovery from solutions containing heavy metals,[189, 210] or alkali recovery.[211] Oh et al. studied how acid recovery in diffusion dialysis depends on the metal cation.[210] Within the different concentration ranges for each metal ion, the acid recoveries for HNO_3, HCl and H_2SO_4 were 90%, 90% and 70% respectively. The dialysis membrane effectively rejected Fe^{3+}, Cu^{2+}, Ni^{2+}, Cr^{3+} and Zn^{2+}, with the exception of Zn^{2+} in HCl, which showed high leakage. Wang et al. studied the acid adsorption on the anion exchange membranes by obtaining a breakthrough curve of acids as they diffuse through the membrane. The acid adsorption is related to acid concentration and acid species, and both high acid concentration and low valence of the acid species lead to a high permeance.[212]

Chapters 2 and 3 show that membranes containing a $(PSS/PAH)_n$ film on porous alumina exhibit K^+/Mg^{2+} selectivities >350 in diffusion dialysis. The solution ionic strength also influences the membrane permeability. Chapter 2 provides a detailed discussion.

1.4.3 Electrodialysis

Electrodialysis is a separation process that employs electric currents to move ions across membranes. For example, Figure 1.16 shows one method

for desalination using electrodialysis. Salt solutions enter specific cells and the electrical potential drives Na^+ to the left through the cation exchange membrane and Cl^- to the right through the anion-exchange membrane. Because the Na^+ does not permeate through anion exchange membranes and Cl^- does not pass through cation exchange membranes, salt collects in the pickup cells and desalinated water exits from the feed cells. Other applications of electrodialysis include water softening,[213] acid recovery,[214] heavy metal removal,[215] whey desalting,[216] and removal of acids from wine and fruit juice.[217]

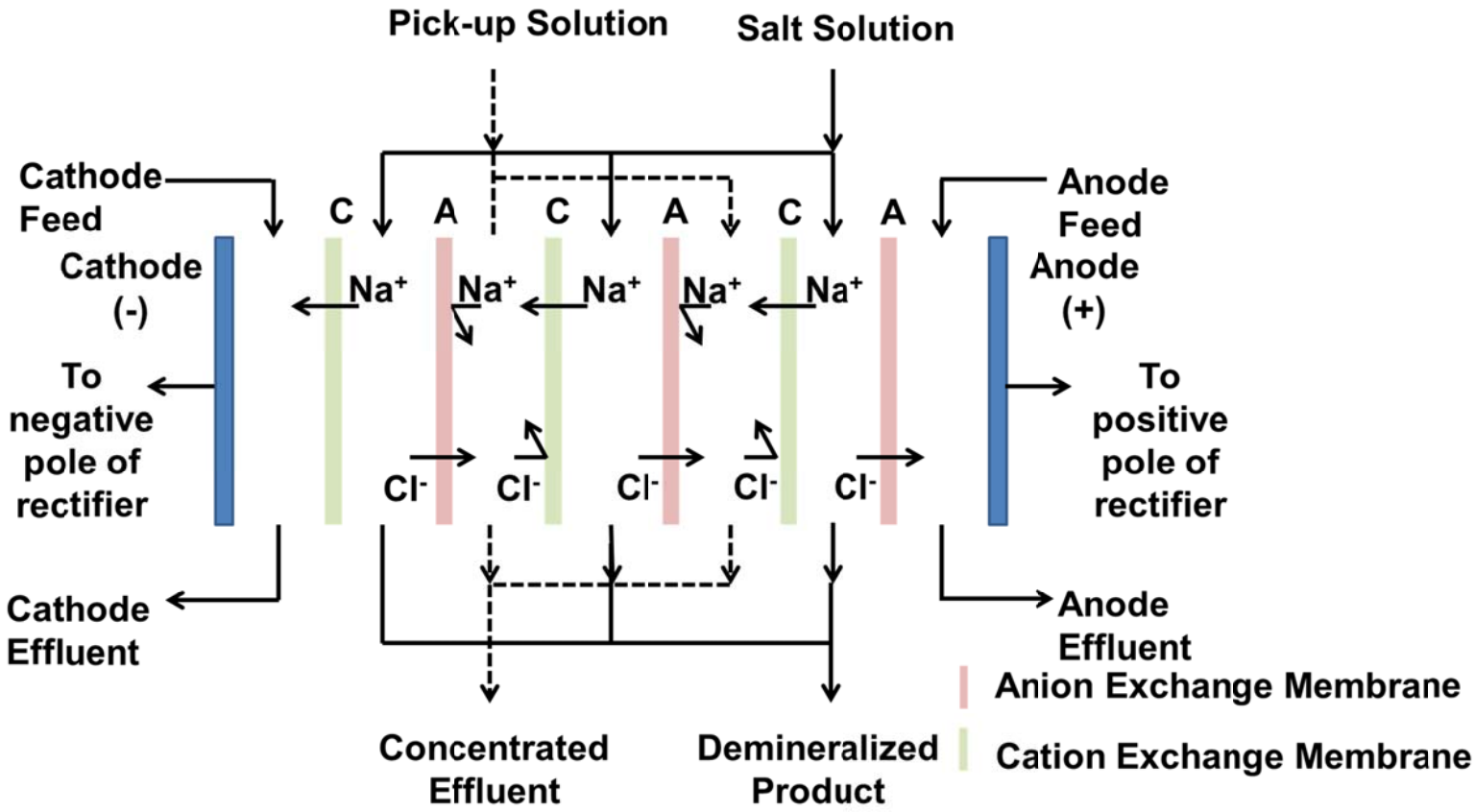

Figure 1.16 Scheme of electrodialysis for desalination. (Redrawn from *Membrane Technology and Applications.*)[209]

Lambert et al. studied the electrodialytic removal of trivalent chromium in wastewaters resulting from leather tanning.[215] After electrodepositing PEI on a Nafion membrane, the selectivity of sodium over chromium increased from 3 to about 16. Mulyati and coworkers employed an anion exchange membrane coated with 15 bilayers of PSS/PAH for electrodialysis.[218] The PSS/PAH coating simultaneously improved the monovalent Cl^-/SO_4^{2-} selectivity and decreased fouling by an anionic surfactant. However, the Cl^-/SO_4^{2-} selectivity was still low.

In Chapter 3, we utilize a PSS/PAH-modified alumina membrane as a monovalent cation selective membrane in electrodialysis and demonstrate a 4-fold increase of monovalent ion flux compared to diffusion dialysis. A PSS/PAH-coated NF membrane shows a 45-fold increase of monovalent flux in electrodialysis compared to diffusion dialysis, and the membrane maintains a monovalent over multivalent ion selectivity higher than 100.

1.5 Dissertation Outline

This dissertation focuses on ion separations that use polymer-modified membranes in diffusion dialysis, electrodialysis, and NF. Chapter 2 investigates the factors behind the high (>350) K^+/Mg^{2+} selectivity of PSS/PAH-modified alumina membranes in diffusion dialysis. Unfortunately,

selectivity is much lower (~16) in NF due to the coupling of water and ion transport through membrane defects. Measurements of transmembrane electrical potentials show that the transference number for Mg^{2+} in $MgCl_2$ solutions, especially at low concentration, approaches zero. However, these high anion/cation selectivities decrease as the solution ionic strength increases. In NF, the high asymmetry of membrane permeabilities to Mg^{2+} and Cl^- creates transmembrane diffusion potentials that lead to negative rejections (the ion concentration in the permeate is larger than in the feed) as low as -200% for trace monovalent cations such as K^+ and Cs^+. Moreover, rejection becomes more negative as the mobility of the trace cation increases. These studies demonstrate that PSS/PAH-modified membranes are attractive for salt purification and water-softening applications.

Chapter 3 compares K^+/Mg^{2+} selectivities and cation fluxes in diffusion dialysis and electrodialysis through membranes coated with PSS/PAH films. In both techniques, K^+/Mg^{2+} selectivities reach values >100, and with $(PSS/PAH)_5$-coated NF membranes the K^+ flux in electrodialysis is 45-times the flux in diffusion dialysis. Thus, the applied electric current can increase flux without decreasing selectivity. However, the K^+ transference number is at most ~0.22 because protons and anions also carry current. Ion fluxes and K^+/Mg^{2+} selectivities depend on the anion of the K^+/Mg^{2+} salts. Sulfate

decreases the surface charge on $(PSS/PAH)_5$-coated membranes and reduces K^+/Mg^{2+} selectivities to ~40 for films on porous alumina in both diffusion dialysis and electrodialysis. Chlorine generated during electrodialysis with chloride salts damages $(PSS/PAH)_5$-coated membranes, and selectivities decline dramatically after 60 min. This work demonstrates that electrodialysis is an applicable method for (PSS/PAH)-modified membranes to achieve high monovalent/multivalent ion separation efficiency.

Chapter 4 demonstrates the successful modification and characterization of different porous supports with conductive polyaniline nanofibers by dilute polymerization. However, the ion separations with these membranes in diffusion dialysis and NF are still under investigation. Preliminary results did not show increases in ion-transport selectivity when applying electrical potentials.

The final chapter briefly summarizes the research and touches on future work, particularly relating to the conductive polymer modified membranes for ion separations.

REFERENCES

REFERENCES

(1) Cheng, C.; Yaroshchuk, A.; Bruening, M. L., *Langmuir* **2013,** 29, 1885-1892.

(2) Garnier, F.; Hajlaoui, R.; Yassar, A.; Srivastava, P., *Science* **1994,** 265, 1684-1686.

(3) Yan, H.; Chen, Z. H.; Zheng, Y.; Newman, C.; Quinn, J. R.; Dotz, F.; Kastler, M.; Facchetti, A., *Nature* **2009,** 457, 679-686.

(4) Ouyang, J. Y.; Chu, C. W.; Szmanda, C. R.; Ma, L. P.; Yang, Y., *Nat. Mater.* **2004,** 3, 918-922.

(5) Ling, Q. D.; Liaw, D. J.; Zhu, C. X.; Chan, D. S. H.; Kang, E. T.; Neoh, K. G., *Prog. Polym. Sci.* **2008,** 33, 917-978.

(6) Cho, J. H.; Lee, J.; Xia, Y.; Kim, B.; He, Y. Y.; Renn, M. J.; Lodge, T. P.; Frisbie, C. D., *Nat. Mater.* **2008,** 7, 900-906.

(7) Noh, Y. Y.; Zhao, N.; Caironi, M.; Sirringhaus, H., *Nat. Nanotechnol.* **2007,** 2, 784-789.

(8) Kim, J. Y.; Kim, S. H.; Lee, H. H.; Lee, K.; Ma, W. L.; Gong, X.; Heeger, A. J., *Adv. Mater.* **2006,** 18, 572-576.

(9) Erb, T.; Zhokhavets, U.; Gobsch, G.; Raleva, S.; Stuhn, B.; Schilinsky, P.; Waldauf, C.; Brabec, C. J., *Adv. Funct. Mater.* **2005,** 15, 1193-1196.

(10) Koidis, C.; Logothetidis, S.; Kapnopoulos, C.; Karagiannidis, P. G.; Laskarakis, A.; Hastas, N. A., *Mater. Sci. Eng. B-Adv. Funct. Solid-State Mater.* **2011,** 176, 1556-1561.

(11) Guha, S.; Adil, D.; Ukah, N. B.; Gupta, R. K.; Ghosh, K., *Appl. Phys. A-Mater. Sci. Process.* **2011,** 105, 547-554.

(12) Tsai, Y.-C.; Li, S.-C.; Chen, J.-M., *Langmuir* **2005,** 21, 3653-3658.

(13) Muguruma, H.; Hiratsuka, A.; Karube, I., *Anal. Chem.* **2000,** 72, 2671-2675.

(14) Myler, S.; Eaton, S.; Higson, S. P. J., *Anal. Chim. Acta* **1997,** 357, 55-61.

(15) Koehler, J. A.; Ulbricht, M.; Belfort, G., *Langmuir* **1997,** 13, 4162-4171.

(16) Andreeva, D. V.; Skorb, E. V.; Shchukin, D. G., *ACS Appl. Mater. Interfaces* **2010,** 2, 1954-1962.

(17) Frau, A. F.; Pernites, R. B.; Advincula, R. C., *Ind. Eng. Chem. Res.* **2010,** 49, 9789-9797.

(18) Li, P. H.; Wu, G. S.; Xu, R. Z.; Wang, W. H.; Wu, S. L.; Yeung, K. W. K.; Chu, P. K., *Mater. Lett.* **2012,** 89, 51-54.

(19) Hall, D. B.; Underhill, P.; Torkelson, J. M., *Polym. Eng. Sci.* **1998,** 38, 2039-2045.

(20) Lawrence, C. J., *Phys. Fluids* **1988,** 31, 2786-2795.

(21) Emslie, A. G.; Bonner, F. T.; Peck, L. G., *J. Appl. Phys.* **1958,** 29, 858-862.

(22) Bornside, D. E.; Macosko, C. W.; Scriven, L. E., *J. Electrochem. Soc.* **1991,** 138, 317-320.

(23) Schubert, D. W.; Dunkel, T., *Mater. Res. Innov.* **2003,** 7, 314-321.

(24) Sahu, N.; Parija, B.; Panigrahi, S., *Indian J. Phys.* **2009,** 83, 493-502.

(25) Grosso, D., *J. Mater. Chem.* **2011,** 21, 17033-17038.

(26) Faustini, M.; Louis, B.; Albouy, P. A.; Kuemmel, M.; Grosso, D., *J. Phys. Chem. C* **2010,** 114, 7637-7645.

(27) Roland, S.; Pellerin, C.; Bazuin, C. G.; Prud'homme, R. E., *Macromolecules* **2012,** 45, 7964-7972.

(28) Roland, S.; Prud'homme, R. E.; Bazuin, C. G., *ACS Macro Letters* **2012,** 1, 973-976.

(29) Bormashenko, E.; Pogreb, R.; Stanevsky, O.; Bormashenko, Y.; Stein, T.; Gaisin, V. Z.; Cohen, R.; Gendelman, O. V., *Macromol. Mater. Eng.* **2005,** 290, 114-121.

(30) Bormashenko, E.; Schechter, A.; Stanevsky, O.; Stein, T.; Balter, S.; Musin, A.; Bormashenko, Y.; Pogreb, R.; Barkay, Z.; Aurbach, D., *Macromol. Mater. Eng.* **2008,** 293, 872-877.

(31) Sohn, J. Y.; Im, J. S.; Shin, J.; Nho, Y. C., *J. Solid State Electrochem.* **2012,** 16, 551-556.

(32) Usui, H.; Koshikawa, H.; Tanaka, K., *J. Vac. Sci. Technol. A-Vac. Surf. Films* **1995,** 13, 2318-2324.

(33) Huber, N.; Heitz, J.; Bauerle, D., *Eur. Phys. J.-Appl. Phys* **2005,** 29, 231-238.

(34) Salem, J. R.; Sequeda, F. O.; Duran, J.; Lee, W. Y.; Yang, R. M., *J. Vac. Sci. Technol. A-Vac. Surf. Films* **1986,** 4, 369-374.

(35) Takahashi, Y.; Iijima, M.; Inagawa, K.; Itoh, A., *J. Vac. Sci. Technol. A-Vac. Surf. Films* **1987,** 5, 2253-2256.

(36) Usui, H.; Watanabe, M.; Arai, C.; Hibi, K.; Tanaka, K., *Jpn. J. Appl. Phys. Part 1 - Regul. Pap. Brief Commun. Rev. Pap.* **2005,** 44, 2810-2814.

(37) Masao, T.; Hideki, O.; Norimasa, O., *Thin Solid Films* **1994,** 251, 36-39.

(38) Yun, W. M.; Jang, J.; Nam, S.; Jeong, Y. J.; Kim, L. H.; Park, S.; Seo, S. J.; Park, C. E., *J. Mater. Chem.* **2012,** 22, 25395-25401.

(39) Kawakami, A.; Otsuki, E.; Fujieda, M.; Kita, H.; Taka, H.; Sato, H.; Usui, H., *Jpn. J. Appl. Phys.* **2008,** 47, 1279-1283.

(40) Duran, H.; Ogura, K.; Nakao, K.; Vianna, S. D. B.; Usui, H.; Advincula, R. C.; Knoll, W., *Langmuir* **2009,** 25, 10711-10718.

(41) Hyun, J.; Chilkoti, A., *Macromolecules* **2001,** 34, 5644-5652.

(42) Baxamusa, S. H.; Im, S. G.; Gleason, K. K., *Phys. Chem. Chem. Phys.* **2009,** 11, 5227-5240.

(43) Lau, K. K. S.; Lewis, H. G. P.; Limb, S. J.; Kwan, M. C.; Gleason, K. K., *Thin Solid Films* **2001,** 395, 288-291.

(44) Martin, T. P.; Chan, K.; Gleason, K. K., *Thin Solid Films* **2008,** 516, 681-683.

(45) Thyen, R.; Weber, A.; Klages, C. P., *Surf. Coat. Technol.* **1997,** 97, 426-434.

(46) Chan, K.; Kostun, L. E.; Tenhaeff, W. E.; Gleason, K. K., *Polymer* **2006,** 47, 6941-6947.

(47) Trujillo, N. J.; Baxamusa, S. H.; Gleason, K. K., *Chem. Mat.* **2009,** 21, 742-750.

(48) Yang, J.; Gao, J. C., *Mater. Sci. Technol.* **2008,** 24, 261-265.

(49) Barranco, A.; Cotrino, J.; Yubero, F.; Girardeau, T.; Camelio, S.; Gonzalez-Elipe, A. R., *Surf. Coat. Technol.* **2004,** 180, 244-249.

(50) Caricato, A. P.; Luches, A., *Appl. Phys. A-Mater. Sci. Process.* **2011,** 105, 565-582.

(51) Kowalewska, A.; Kupcik, J.; Pola, J.; Stanczyk, W. A., *Polymer* **2008,** 49, 857-866.

(52) Reichelt, K.; Jiang, X., *Thin Solid Films* **1990,** 191, 91-126.

(53) Alf, M. E.; Asatekin, A.; Barr, M. C.; Baxamusa, S. H.; Chelawat, H.; Ozaydin-Ince, G.; Petruczok, C. D.; Sreenivasan, R.; Tenhaeff, W. E.; Trujillo, N. J.; Vaddiraju, S.; Xu, J. J.; Gleason, K. K., *Adv. Mater.* **2010,** 22, 1993-2027.

(54) Milner, S. T., *Science* **1991,** 251, 905-914.

(55) Barbey, R.; Lavanant, L.; Paripovic, D.; Schuwer, N.; Sugnaux, C.; Tugulu, S.; Klok, H. A., *Chem. Rev.* **2009,** 109, 5437-5527.

(56) Jain, P.; Baker, G. L.; Bruening, M. L., Applications of Polymer Brushes in Protein Analysis and Purification. In *Annual Review of Analytical Chemistry*, Annual Reviews: Palo Alto, 2009; Vol. 2, pp 387-408.

(57) Jordan, R.; Ulman, A., *J. Am. Chem. Soc.* **1998,** 120, 243-247.

(58) Jordan, R.; West, N.; Ulman, A.; Chou, Y. M.; Nuyken, O., *Macromolecules* **2001,** 34, 1606-1611.

(59) Advincula, R., Polymer brushes by anionic and cationic Surface-Initiated Polymerization (SIP). In *Surface-Initiated Polymerization I*, Jordan, R., Ed. Springer-Verlag Berlin: Berlin, 2006; Vol. 197, pp 107-136.

(60) Fan, X. W.; Zhou, Q. Y.; Xia, C. J.; Cristofoli, W.; Mays, J.; Advincula, R., *Langmuir* **2002,** 18, 4511-4518.

(61) Advincula, R.; Zhou, Q. G.; Park, M.; Wang, S. G.; Mays, J.; Sakellariou, G.; Pispas, S.; Hadjichristidis, N., *Langmuir* **2002,** 18, 8672-8684.

(62) Jaworek, T.; Neher, D.; Wegner, G.; Wieringa, R. H.; Schouten, A. J., *Science* **1998,** 279, 57-60.

(63) Zeng, H. L.; Gao, C.; Yan, D. Y., *Adv. Funct. Mater.* **2006,** 16, 812-818.

(64) Yoon, K. R.; Lee, Y. W.; Lee, J. K.; Choi, I. S., *Macromol. Rapid Commun.* **2004,** 25, 1510-1513.

(65) Jeon, N. L.; Choi, I. S.; Whitesides, G. M.; Kim, N. Y.; Laibinis, P. E.; Harada, Y.; Finnie, K. R.; Girolami, G. S.; Nuzzo, R. G., *Appl. Phys. Lett.* **1999,** 75, 4201-4203.

(66) Schwab, P.; Grubbs, R. H.; Ziller, J. W., *J. Am. Chem. Soc.* **1996,** 118, 100-110.

(67) Kong, B.; Lee, J. K.; Choi, I. S., *Langmuir* **2007,** 23, 6761-6765.

(68) Jain, P.; Dai, J. H.; Baker, G. L.; Bruening, M. L., *Macromolecules* **2008,** 41, 8413-8417.

(69) Grajales, S. T.; Dong, X. J.; Zheng, Y.; Baker, G. L.; Bruening, M. L., *Chem. Mat.* **2010,** 22, 4026-4033.

(70) Teuchert, C.; Michel, C.; Hansen, F.; Park, D. Y.; Beckham, H. W.; Wenz, G., *Macromolecules* **2013,** 46, 2-7.

(71) Stenzel, M. H.; Zhang, L.; Huck, W. T. S., *Macromol. Rapid Commun.* **2006,** 27, 1121-1126.

(72) Zhai, G. Q.; Yu, W. H.; Kang, E. T.; Neoh, K. G.; Huang, C. C.; Liaw, D. J., *Ind. Eng. Chem. Res.* **2004,** 43, 1673-1680.

(73) Husseman, M.; Malmstrom, E. E.; McNamara, M.; Mate, M.; Mecerreyes, D.; Benoit, D. G.; Hedrick, J. L.; Mansky, P.; Huang, E.; Russell, T. P.; Hawker, C. J., *Macromolecules* **1999,** 32, 1424-1431.

(74) Cimen, D.; Caykara, T., *J. Appl. Polym. Sci.* **2013,** 129, 383-390.

(75) Parvole, J.; Montfort, J. P.; Reiter, G.; Borisov, O.; Billon, L., *Polymer* **2006,** 47, 972-981.

(76) Krause, J. E.; Brault, N. D.; Li, Y. T.; Xue, H.; Zhou, Y. B.; Jiang, S. Y., *Macromolecules* **2011,** 44, 9213-9220.

(77) Nakayama, Y.; Matsuda, T., *Macromolecules* **1996,** 29, 8622-8630.

(78) Nakayama, Y.; Sudo, M.; Uchida, K.; Matsuda, T., *Langmuir* **2002,** 18, 2601-2606.

(79) Edmondson, S.; Osborne, V. L.; Huck, W. T. S., *Chem. Soc. Rev.* **2004,** 33, 14-22.

(80) Zhao, J.; Zhang, Y.; Su, Y.; Liu, J.; Zhao, X.; Peng, J.; Jiang, Z., *J. Membr. Sci.* **2013,** 445, 1-7.

(81) Kim, I.-C.; Jeong, B.-R.; Kim, S.-J.; Lee, K.-H., *Desalination* **2013,** 308, 111-114.

(82) Siddhan, P.; Jassal, M.; Agrawal, A. K., *J. Appl. Polym. Sci.* **2007,** 106, 786-792.

(83) Tang, B.; Zou, C.; Wu, P., *J. Membr. Sci.* **2010,** 365, 276-285.

(84) Lu, S.; Xing, J.; Zhang, Z.; Jia, G., *J. Appl. Polym. Sci.* **2011,** 121, 3377-3383.

(85) Provatas, A.; Matisons, J.; Clarke, S.; Graiver, D.; Lomas, W., *Macromolecules* **2000,** 33, 9156-9159.

(86) Song, Y. J.; Sun, P.; Henry, L. L.; Sun, B. H., *J. Membr. Sci.* **2005,** 251, 67-79.

(87) Chai, G. Y.; Krantz, W. B., *J. Membr. Sci.* **1994,** 93, 175-192.

(88) Porter, M. C., In *Handbook of Industrial Membrane Technology*, Noyes Publisher: New Jersey, USA, 1990; pp 314-333.

(89) Ghosh, A. K.; Jeong, B.-H.; Huang, X.; Hoek, E. M. V., *J. Membr. Sci.* **2008,** 311, 34-45.

(90) Ouyang, L.; Malaisamy, R.; Bruening, M. L., *J. Membr. Sci.* **2008,** 310, 76-84.

(91) Ram, M. K.; Bertoncello, P.; Ding, H.; Paddeu, S.; Nicolini, C., *Biosens. Bioelectron.* **2001,** 16, 849-856.

(92) Caruso, F.; Trau, D.; Mohwald, H.; Renneberg, R., *Langmuir* **2000,** 16, 1485-1488.

(93) Decher, G.; Hong, J. D., *Ber. Bunsen-Ges. Phys. Chem. Chem. Phys.* **1991,** 95, 1430-1434.

(94) Xu, F.; Wang, W. H.; Tan, Y. J.; Bruening, M. L., *Anal. Chem.* **2010,** 82, 10045-10051.

(95) Decher, G., *Science* **1997,** 277, 1232-1237.

(96) Sukhishvili, S. A.; Granick, S., *Macromolecules* **2002,** 35, 301-310.

(97) Stockton, W. B.; Rubner, M. F., *Macromolecules* **1997,** 30, 2717-2725.

(98) Sukhishvili, S. A.; Granick, S., *J. Am. Chem. Soc.* **2000,** 122, 9550-9551.

(99) Such, G. K.; Quinn, J. F.; Quinn, A.; Tjipto, E.; Caruso, F., *J. Am. Chem. Soc.* **2006,** 128, 9318-9319.

(100) Zhang, Y.; He, H.; Gao, C.; Wu, J. Y., *Langmuir* **2009,** 25, 5814-5824.

(101) Kohli, P.; Blanchard, G. J., *Langmuir* **2000,** 16, 4655-4661.

(102) Kotov, N. A., *Nanostruct. Mater.* **1999,** 12, 789-796.

(103) Khopade, A. J.; Mohwald, H., *Adv. Funct. Mater.* **2005,** 15, 1088-1094.

(104) Crespo-Biel, O.; Dordi, B.; Reinhoudt, D. N.; Huskens, J., *J. Am. Chem. Soc.* **2005,** 127, 7594-7600.

(105) Naseer, M. M.; Hameed, S., *Crystengcomm* **2012,** 14, 4247-4250.

(106) Habibi, M. H.; Zendehdel, M., *Curr. Nanosci.* **2010,** 6, 642-647.

(107) Schlicke, H.; Schroder, J. H.; Trebbin, M.; Petrov, A.; Ijeh, M.; Weller, H.; Vossmeyer, T., *Nanotechnology* **2011,** 22.

(108) Chiarelli, P. A.; Johal, M. S.; Holmes, D. J.; Casson, J. L.; Robinson, J. M.; Wang, H. L., *Langmuir* **2002,** 18, 168-173.

(109) Bruening, M.; Dotzauer, D., *Nat. Mater.* **2009,** 8, 449-450.

(110) Lvov, Y.; Ariga, K.; Ichinose, I.; Kunitake, T., *J. Am. Chem. Soc.* **1995,** 117, 6117-6123.

(111) Decher, G.; Lehr, B.; Lowack, K.; Lvov, Y.; Schmitt, J., *Biosens. Bioelectron.* **1994,** 9, 677-684.

(112) Ariga, K.; Hill, J. P.; Ji, Q. M., *Phys. Chem. Chem. Phys.* **2007,** 9, 2319-2340.

(113) Malikova, N.; Pastoriza-Santos, I.; Schierhorn, M.; Kotov, N. A.; Liz-Marzan, L. M., *Langmuir* **2002,** 18, 3694-3697.

(114) Johnston, A. P. R.; Mitomo, H.; Read, E. S.; Caruso, F., *Langmuir* **2006,** 22, 3251-3258.

(115) Tokuhisa, H.; Hammond, P. T., *Adv. Funct. Mater.* **2003,** 13, 831-839.

(116) Fukumoto, H.; Yonezawa, Y., *Thin Solid Films* **1998,** 327, 748-751.

(117) Bucur, C. B.; Sui, Z.; Schlenoff, J. B., *J. Am. Chem. Soc.* **2006,** 128, 13690-13691.

(118) Ruths, J.; Essler, F.; Decher, G.; Riegler, H., *Langmuir* **2000,** 16, 8871-8878.

(119) Ramsden, J. J.; Lvov, Y. M.; Decher, G., *Thin Solid Films* **1995,** 254, 246-251.

(120) Buchner, K.; Ehrhardt, N.; Cahill, B. P.; Hoffmann, C., *Thin Solid Films* **2011,** 519, 6480-6485.

(121) Hübsch, E.; Fleith, G.; Fatisson, J.; Labbé, P.; Voegel, J. C.; Schaaf, P.; Ball, V., *Langmuir* **2005,** 21, 3664-3669.

(122) Lavalle, P.; Gergely, C.; Cuisinier, F. J. G.; Decher, G.; Schaaf, P.; Voegel, J. C.; Picart, C., *Macromolecules* **2002,** 35, 4458-4465.

(123) Porcel, C.; Lavalle, P.; Decher, G.; Senger, B.; Voegel, J. C.; Schaaf, P., *Langmuir* **2007,** 23, 1898-1904.

(124) Adusumilli, M.; Bruening, M. L., *Langmuir* **2009,** 25, 7478-7485.

(125) Lavalle, P.; Picart, C.; Mutterer, J.; Gergely, C.; Reiss, H.; Voegel, J.-C.; Senger, B.; Schaaf, P., *J. Phys. Chem. B* **2003,** 108, 635-648.

(126) Hoda, N.; Larson, R. G., *J. Phys. Chem. B* **2009,** 113, 4232-4241.

(127) Ma, Y.; Dong, J.; Bhattacharjee, S.; Wijeratne, S.; Bruening, M. L.; Baker, G. L., *Langmuir* **2013,** 29, 2946-2954.

(128) Choi, I.; Suntivich, R.; Plamper, F. A.; Synatschke, C. V.; Müller, A. H. E.; Tsukruk, V. V., *J. Am. Chem. Soc.* **2011,** 133, 9592-9606.

(129) Khopade, A. J.; Caruso, F., *Nano Lett.* **2002,** 2, 415-418.

(130) Li, C.; Mitamura, K.; Imae, T., *Macromolecules* **2003,** 36, 9957-9965.

(131) Lösche, M.; Schmitt, J.; Decher, G.; Bouwman, W. G.; Kjaer, K., *Macromolecules* **1998,** 31, 8893-8906.

(132) Kujawa, P.; Moraille, P.; Sanchez, J.; Badia, A.; Winnik, F. M., *J. Am. Chem. Soc.* **2005,** 127, 9224-9234.

(133) Milkova, V.; Radeva, T., *Colloid Surf. A-Physicochem. Eng. Asp.* **2013,** 424, 52-58.

(134) Sui, Z.; Salloum, D.; Schlenoff, J. B., *Langmuir* **2003,** 19, 2491-2495.

(135) Wang, L. Y.; Fu, Y.; Wang, Z. Q.; Fan, Y. G.; Zhang, X., *Langmuir* **1999,** 15, 1360-1363.

(136) Bertrand, P.; Jonas, A.; Laschewsky, A.; Legras, R., *Macromol. Rapid Commun.* **2000,** 21, 319-348.

(137) Voigt, U.; Jaeger, W.; Findenegg, G. H.; Klitzing, R. V., *J. Phys. Chem. B* **2003,** 107, 5273-5280.

(138) Garg, A.; Heflin, J. R.; Gibson, H. W.; Davis, R. M., *Langmuir* **2008,** 24, 10887-10894.

(139) Dubas, S. T.; Schlenoff, J. B., *Macromolecules* **1999,** 32, 8153-8160.

(140) Fller, G. J. C. S., M. A.; Scheutjens, J.M.H.M; Cosgrove, T.; Vincent, B., *Polymers at interfaces*. Chapman & Hall: Cambridge, U.K.: 1993.

(141) Schwarz, B.; Schönhoff, M., *Colloids Surf., A* **2002,** 198–200, 293-304.

(142) Guzman, E.; Ritacco, H.; Rubio, J. E. F.; Rubio, R. G.; Ortega, F., *Soft Matter* **2009,** 5, 2130-2142.

(143) Blomberg, E.; Poptoshev, E.; Caruso, F., *Langmuir* **2006,** 22, 4153-4157.

(144) Boddohi, S.; Killingsworth, C. E.; Kipper, M. J., *Biomacromolecules* **2008,** 9, 2021-2028.

(145) Dodoo, S.; Steitz, R.; Laschewsky, A.; von Klitzing, R., *Phys. Chem. Chem. Phys.* **2011,** 13, 10318-10325.

(146) Lefaux, C. J.; Zimberlin, J. A.; Dobrynin, A. V.; Mather, P. T., *J. Polym. Sci., Part B: Polym. Phys.* **2004,** 42, 3654-3666.

(147) Samanta, T.; Mukherjee, M., *Polymer* **2012,** 53, 5393-5403.

(148) El Haitami, A. E.; Martel, D.; Ball, V.; Nguyen, H. C.; Gonthier, E.; Labbe, P.; Voegel, J. C.; Schaaf, P.; Senger, B.; Boulmedais, F., *Langmuir* **2009,** 25, 2282-2289.

(149) Salomaki, M.; Laiho, T.; Kankare, J., *Macromolecules* **2004,** 37, 9585-9590.

(150) Salomaki, M.; Tervasmaki, P.; Areva, S.; Kankare, J., *Langmuir* **2004,** 20, 3679-3683.

(151) Feldoto, Z.; Varga, I.; Blomberg, E., *Langmuir* **2010,** 26, 17048-17057.

(152) Wong, J. E.; Zastrow, H.; Jaeger, W.; von Klitzing, R., *Langmuir* **2009,** 25, 14061-14070.

(153) Dressick, W. J.; Wahl, K. J.; Bassim, N. D.; Stroud, R. M.; Petrovykh, D. Y., *Langmuir* **2012,** 28, 15831-15843.

(154) Aulin, C.; Varga, I.; Claessont, P. M.; Wagberg, L.; Lindstrom, T., *Langmuir* **2008,** 24, 2509-2518.

(155) Lulevich, V. V.; Vinogradova, O. I., *Langmuir* **2004,** 20, 2874-2878.

(156) Schoeler, B.; Poptoshev, E.; Caruso, F., *Macromolecules* **2003,** 36, 5258-5264.

(157) Patel, P. A.; Dobrynin, A. V.; Mather, P. T., *Langmuir* **2007,** 23, 12589-12597.

(158) Kharlampieva, E.; Kozlovskaya, V.; Chan, J.; Ankner, J. F.; Tsukruk, V. V., *Langmuir* **2009,** 25, 14017-14024.

(159) Long, Y. C.; Wang, T.; Liu, L. D.; Liu, G. M.; Zhang, G. Z., *Langmuir* **2013,** 29, 3645-3653.

(160) Poptoshev, E.; Schoeler, B.; Caruso, F., *Langmuir* **2004,** 20, 829-834.

(161) Salomaki, M.; Vinokurov, I. A.; Kankare, J., *Langmuir* **2005,** 21, 11232-11240.

(162) Tan, H. L.; McMurdo, M. J.; Pan, G. Q.; Van Patten, P. G., *Langmuir* **2003,** 19, 9311-9314.

(163) Buscher, K.; Graf, K.; Ahrens, H.; Helm, C. A., *Langmuir* **2002,** 18, 3585-3591.

(164) Lvov, Y.; Yamada, S.; Kunitake, T., *Thin Solid Films* **1997,** 300, 107-112.

(165) Egueh, A.-N. D.; Lakard, B.; Fievet, P.; Lakard, S.; Buron, C., *Journal of Colloid and Interface Science* **2010,** 344, 221-227.

(166) Jackowska, K.; Biegunski, A. T.; Tagowska, M., *J. Solid State Electrochem.* **2008,** 12, 437-443.

(167) Zhang, X.; Chan-Yu-King, R.; Jose, A.; Manohar, S. K., *Synth. Met.* **2004,** 145, 23-29.

(168) Parthasarathy, R. V.; Martin, C. R., *Chem. Mat.* **1994,** 6, 1627-1632.

(169) Mazur, M.; Tagowska, M.; Palys, B.; Jackowska, K., *Electrochem. Commun.* **2003,** 5, 403-407.

(170) Han, J.; Dai, J.; Zhou, C. Q.; Guo, R., *Polym. Chem.* **2013,** 4, 313-321.

(171) Chen, C. F.; Lei, I. A.; Chiu, W. Y., *J. Appl. Polym. Sci.* **2012,** 126, E195-E205.

(172) Li, G. C.; Zhang, Z. K., *Macromolecules* **2004,** 37, 2683-2685.

(173) Carswell, A. D. W.; O'Rear, E. A.; Grady, B. P., *J. Am. Chem. Soc.* **2003,** 125, 14793-14800.

(174) Attout, A.; Yunus, S.; Bertrand, P., *Polym. Eng. Sci.* **2008,** 48, 1661-1666.

(175) Hong, K. H.; Kang, T. J., *J. Appl. Polym. Sci.* **2006,** 99, 1277-1286.

(176) Li, R. Q.; Chen, Z.; Li, J. Q.; Zhang, C. H.; Guo, Q., *Synth. Met.* **2013,** 171, 39-44.

(177) Wang, D. H.; Ma, F. H.; Qi, S. H.; Song, B. Y., *Synth. Met.* **2010,** 160, 2077-2084.

(178) Zhang, X. Y.; Goux, W. J.; Manohar, S. K., *J. Am. Chem. Soc.* **2004,** 126, 4502-4503.

(179) Xing, S. X.; Zhao, C.; Jing, S. Y.; Wang, Z. C., *Polymer* **2006,** 47, 2305-2313.

(180) Chiou, N.-R.; Lui, C.; Guan, J.; Lee, L. J.; Epstein, A. J., *Nat. Nanotechnol.* **2007,** 2, 354-357.

(181) Chiou, N. R.; Epstein, A. J., *Adv. Mater.* **2005,** 17, 1679-1683.

(182) Jin, W. Q.; Toutianoush, A.; Tieke, B., *Langmuir* **2003,** 19, 2550-2553.

(183) Schaep, J.; Van der Bruggen, B.; Uytterhoeven, S.; Croux, R.; Vandecasteele, C.; Wilms, D.; Van Houtte, E.; Vanlergberghe, F., *Desalination* **1998,** 119, 295-301.

(184) Mika, A. M.; Childs, R. F.; Dickson, J. M., *Desalination* **1999,** 121, 149-158.

(185) Greenlee, L. F.; Lawler, D. F.; Freeman, B. D.; Marrot, B.; Moulin, P., *Water Res.* **2009,** 43, 2317-2348.

(186) Li, D.; Wang, H. T., *J. Mater. Chem.* **2010,** 20, 4551-4566.

(187) Li, L. X.; Dong, J. H.; Nenoff, T. M.; Lee, R., *J. Membr. Sci.* **2004,** 243, 401-404.

(188) Luo, J. Y.; Wu, C. M.; Xu, T. W.; Wu, Y. H., *J. Membr. Sci.* **2011,** 366, 1-16.

(189) Xu, T. W.; Yang, W. H., *J. Membr. Sci.* **2001,** 183, 193-200.

(190) Simons, R., *Desalination* **1993,** 89, 325-341.

(191) Vallejo, E.; Pourcelly, G.; Gavach, C.; Mercier, R.; Pineri, M., *J. Membr. Sci.* **1999,** 160, 127-137.

(192) Sata, T.; Yang, W. K., *J. Membr. Sci.* **2002,** 206, 31-60.

(193) Cussler, E. L.; Aris, R.; Bhown, A., *J. Membr. Sci.* **1989,** 43, 149-164.

(194) Noble, R. D., *J. Membr. Sci.* **1991,** 56, 229-234.

(195) Nghiem, L. D.; Mornane, P.; Potter, I. D.; Perera, J. M.; Cattrall, R. W.; Kolev, S. D., *J. Membr. Sci.* **2006,** 281, 7-41.

(196) Cath, T. Y.; Childress, A. E.; Elimelech, M., *J. Membr. Sci.* **2006,** 281, 70-87.

(197) Yip, N. Y.; Tiraferri, A.; Phillip, W. A.; Schiffman, J. D.; Elimelech, M., *Environ. Sci. Technol.* **2010,** 44, 3812-3818.

(198) Lawson, K. W.; Lloyd, D. R., *J. Membr. Sci.* **1997,** 124, 1-25.

(199) Fallanza, M.; Ortiz, A.; Gorri, D.; Ortiz, I., *J. Membr. Sci.* **2013,** 444, 164-172.

(200) Yaroshchuk, A.; Martínez-Lladó, X.; Llenas, L.; Rovira, M.; de Pablo, J., *J. Membr. Sci.* **2011,** 368, 192-201.

(201) Cséfalvay, E.; Pauer, V.; Mizsey, P., *Desalination* **2009,** 240, 132-142.

(202) Schaep, J.; Van der Bruggen, B.; Vandecasteele, C.; Wilms, D., *Sep. Purif. Technol.* **1998,** 14, 155-162.

(203) Stanton, B. W.; Harris, J. J.; Miller, M. D.; Bruening, M. L., *Langmuir* **2003,** 19, 7038-7042.

(204) Wen, X.; Ma, P.; Chaoliang, Z.; He, Q.; Deng, X., *Sep. Purif. Technol.* **2006,** 49, 230-236.

(205) Homayoonfal, M.; Akbari, A.; Mehrnia, M. R., *Desalination* **2010,** 263, 217-225.

(206) Murthy, Z. V. P.; Choudhary, A., *J. Rare Earths* **2011,** 29, 974-978.

(207) Murthy, Z. V. P.; Choudhary, A., *Desalination* **2011,** 279, 428-432.

(208) Wallace, R. M., *Ind. Eng. Chem. Process Des. Dev.* **1967,** 6, 423-431.

(209) Baker, R. W., *Membrane technology and applications*. John Wiley & Sons, Ltd: West Sussex, England, 2004.

(210) Oh, S. J.; Moon, S. H.; Davis, T., *J. Membr. Sci.* **2000,** 169, 95-105.

(211) Hao, J. W.; Wu, Y. H.; Xu, T. W., *J. Membr. Sci.* **2013,** 425, 156-162.

(212) Wang, K.; Xing, W.; Zhong, Z.; Fan, Y., *Sep. Purif. Technol.* **2013,** 110, 144-149.

(213) Lee, H.-J.; Song, J.-H.; Moon, S.-H., *Desalination* **2013,** 314, 43-49.

(214) Vallois, C.; Sistat, P.; Roualdès, S.; Pourcelly, G., *J. Membr. Sci.* **2003,** 216, 13-25.

(215) Lambert, J.; Avila-Rodriguez, M.; Durand, G.; Rakib, M., *J. Membr. Sci.* **2006,** 280, 219-225.

(216) Diblikova, L.; Curda, L.; Homolova, K., *Desalin. Water Treat.* **2010,** 14, 208-213.

(217) Postel, W.; Prasch, E., *Weinwirtschaft* **1978,** 114, 28-32.

(218) Mulyati, S.; Takagi, R.; Fujii, A.; Ohmukai, Y.; Matsuyama, H., *J. Membr. Sci.* **2013,** 431, 113-120.

Chapter 2 Fundamentals of Selective Ion Transport through Multilayer Polyelectrolyte Membranes

2.1 Introduction

Layer-by-layer adsorption of polycations and polyanions on porous supports is a convenient method for controlled formation of ultrathin membrane skins.[1, 2] Although this multistep procedure may be cumbersome for large-scale membrane applications, polyelectrolyte multilayers (PEMs) on porous supports provide a unique platform for examining mechanisms of ion transport.[3, 4] Commercial membranes, such as those formed by interfacial polymerization, are very effective in water treatment but determining the properties of the membrane skin is challenging.[5-9] Deposition of PEMs on well-defined supports such as nanoporous alumina gives membrane skins whose thickness and surface charge controllably vary with the number of adsorbed layers. Transport properties also depend on the specific polyelectrolytes and the deposition conditions, i.e. pH and ionic strength.[10-14] Under optimized conditions, ultrathin PEMs can serve as the selective skins in pervaporation,[15-18] gas-separation,[19, 20] nanofiltration (NF),[21-24] and forward osmosis membranes.[25-28]

Similar to reverse osmosis (RO), NF involves pressure-driven passage of

water or another solvent through a membrane. However, RO membranes are denser than NF membranes, so NF requires lower pressures for a given flux, and monovalent ion rejections are typically lower in NF than RO. The solution-diffusion model,[29] which assumes that transport through the membrane occurs solely by diffusion, adequately describes RO, but NF membranes may contain pores large enough to allow for some convective salt transport.[30, 31] Supported PEMs behave as NF membranes, selectively rejecting divalent ions.[21, 23] Moreover, the well-defined structure of PEMs gives a convenient system to examine the applicability of the solution-diffusion model through a combination of NF experiments and diffusion dialysis.

Tieke and coworkers first reported Na^+/Mg^{2+} diffusion dialysis selectivities as high as 113 with 60-bilayer protonated poly(allylamine) (PAH)/poly(4-styrenesulfonate) (PSS) films on a porous polymer support. Films with 5 and 10 bilayers showed selectivities between 30 and 40.[14] In later dead-end, single-salt NF experiments, the Na^+/Mg^{2+} selectivity was only 10 for 0.01 M chloride salt solutions, even with a 60-bilayer polyvinylamine/polyvinyl sulfate film. Nevertheless, selectivities appeared to be higher at lower salt concentrations (0.001 M) where Mg^{2+} rejections approached 100%.[32] Ouyang and coworkers achieved 95% Mg^{2+} rejection along with a Na^+/Mg^{2+} selectivity of 22 using feed solutions containing both NaCl and $MgCl_2$ and porous alumina membranes coated with $(PSS/PAH)_5$

films.[21] However, they presented no diffusion dialysis studies, so testing of the solution-diffusion model was not possible.

In addition to simple diffusion, electric fields that arise spontaneously due to different membrane permeabilities to cations and anions also influence ion transport across NF and RO membranes. This is especially evident in NF of mixed salt solutions, where the concentration of a given ion may be higher in the permeate than in the feed (negative rejection).[21, 33, 34] In particular with solutions containing both NaCl and $MgCl_2$, NF through $(PSS/PAH)_4$ membranes results in small negative Na^+ rejections (about -30%)[21] because the PEMs are more permeable to Cl^- and Na^+ than Mg^{2+}.[14] Initial passage of excess Cl^- creates a negative potential that pulls extra Na^+ through the membrane (see Figure 2.1).

This study examines the mechanisms of cation transport through PEMs deposited on nanoporous alumina. Specifically, we first combine diffusion dialysis and NF experiments to determine whether the solution-diffusion model applies to NF through PEMs. Second, we measure transmembrane potentials to investigate the selectivity of the PEMs for anions over cations at various salt concentrations. These studies also include an examination of diffusion dialysis and NF as a function of salt concentrations. Finally, we study negative rejections of trace ions, which depend on both the electric potential developed across the membrane (due to anion/cation selectivity) and the membrane

permeability to the trace ions.

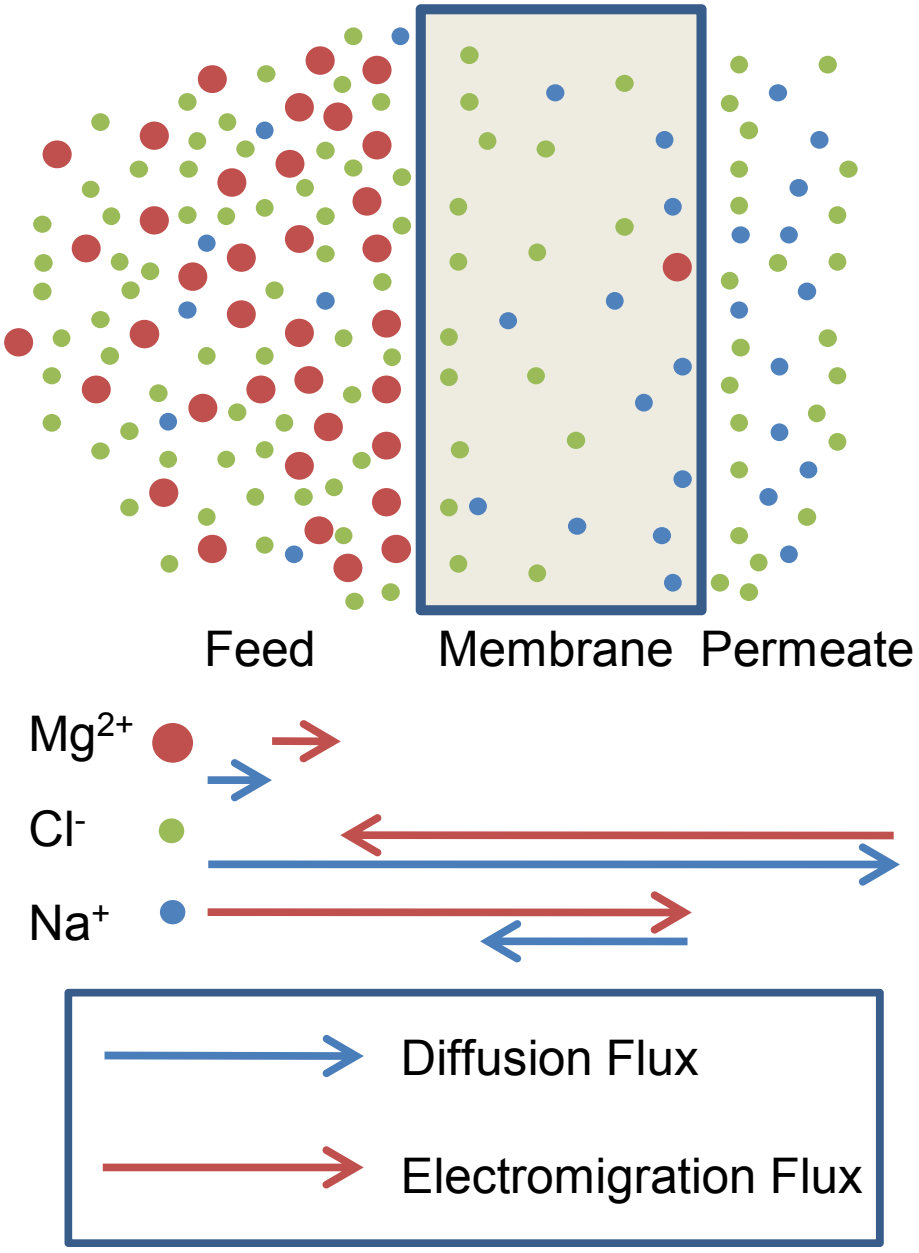

Figure 2.1 Schematic, qualitative drawing of ion distributions and transport during NF of a solution containing $MgCl_2$ and trace amounts of NaCl. The high permeability of Cl^- relative to Mg^{2+} leads to a negative electric potential drop across the membrane. This potential enhances the transport of trace Na^+ ions

Figure 2.1 (cont'd) and can lead to higher concentrations of Na^+ in the permeate than in the feed. The arrows qualitatively show the relative fluxes due to diffusion (blue) and electromigration (red) for each ion. In the absence of convection, the total flux is the sum of the arrows.

2.2 Experimental Section

2.2.1 Materials

Poly(sodium 4-styrenesulfonate) (M_W=70,000 Da) and poly(allylamine hydrochloride) (M_W=15,000 Da) were obtained from Aldrich. Salts were purchased from Columbus Chemical with the exception of CsCl (Aldrich) and LiCl (Jade Scientific). LiCl and CsCl are hygroscopic, so we prepared stock solutions from freshly opened bottles. All chemicals were used as received without further purification. Deionized water (Milli-Q system, 18.2 MΩcm) was employed in all experiments. The pH of the polyelectrolyte solutions was adjusted with dilute aqueous HCl or NaOH.

2.2.2 Film Deposition

Porous alumina membranes (0.02 μm Whatman Anodisk filters, all membranes were used from the same box unless specified otherwise) were treated with UV/O_3 (Boekel UV-Clean Model 135500) for 15 min and placed in

a home-built O-ring holder that exposes only the feed side of the membrane to polyelectrolyte solutions. The deposition solutions (pH 2.3) contained 0.02 M (with respect to the repeating unit) polyelectrolytes along with 1 M NaCl for PAH and 0.5 M NaCl for PSS. The low deposition pH is common for PSS/PAH films,[35] and addition of 1 M NaCl to PAH adsorption solutions leads to a high surface charge for monovalent/multivalent ion separations.[21] Polyelectrolyte multilayers were adsorbed by alternatively exposing the top surface of the membrane to polyanion and polycation solutions for 5 min with 1 min rinsing with deionized water between each deposition step. PEMs usually contained four PSS/PAH bilayers to allow high water flux while still providing full coverage of the support.[11, 21]

2.2.3 Nanofiltration

NF experiments were performed with a home built system described previously.[22] Briefly, the crossflow apparatus was pressurized with N_2, and a centrifugal pump circulated the feed solution across the membranes at 26 mL/min to minimize concentration polarization. A stainless steel prefilter (Mott Corp.) removes rust or insoluble particles prior to passing solution over the membrane. The exposed membrane external area was 1.7 cm^2. After 18 h of filtration to reach steady state, permeate aliquots (<10 mL) were collected for periods ranging from 30 min to 2 h, and the feed solution was sampled at the

end of the experiment. The feed volume was initially 2 L. The concentrations of most cations were determined using inductively couple plasma-optical emission spectroscopy (Varian 710-ES). Cs^+ was analyzed by atomic emission spectroscopy (Varian AA240), and nitrobenzene was analyzed by UV-Vis absorbance measurements (Perkin Elmer Lambda 40). The rejection, *Re*, was calculated with equation (2.1), where C_f and C_p are the feed and permeate concentrations, respectively. Selectivity, for ion 1 over ion 2, $\alpha_{1/2}$, was calculated using equation (2.2).

$$Re = \frac{C_f - C_p}{C_f} \quad (2.1)$$

$$\alpha_{1/2} = \frac{C_{1,p}/C_{1,f}}{C_{2,p}/C_{2,f}} = \frac{100 - Re_1}{100 - Re_2} \quad (2.2)$$

Multiple permeate samples from each of at least two membranes were collected for determination of ion rejections and solution fluxes. The ± values represent standard deviations of at least 4 values.

2.2.4 Diffusion Dialysis

Diffusion dialysis was performed as described previously.[36] A membrane was sandwiched between the source and receiving cells, and the solutions in each cell (initially 90 mL each) were stirred vigorously. The cells exposed a membrane area of 2.1 cm^2. One-mL aliquots were withdrawn periodically from the receiving cell to monitor the analyte concentration as a function of

time, and similar aliquots were taken from the source phase to maintain equal volumes. Because the diffusion flux is relatively small, the concentration gradient across the membrane is essentially constant. Moreover, the transporting salt concentration in the source phase was limited to 0.01 M to minimize osmosis. In most experiments, the receiving phase was initially deionized water. For diffusion dialysis experiments as a function of solution composition, we added a background salt in equal concentrations to both the source and receiving reservoirs to keep osmosis and diffusion of the added salt negligible. At least three membranes were used to obtain the diffusion fluxes, and ± values represent standard deviations where n is typically 3.

2.2.5 Membrane Potential

Membrane potential measurements were carried out using the diffusion dialysis apparatus (no convective flow) with solutions containing different salt concentrations on each side of the membrane. Before measuring the transmembrane potential, the two Ag/AgCl reference electrodes (saturated KCl, CH Instruments) were placed in the receiving phase solution to determine the electric potential difference between these electrodes. This potential drop was subtracted from the membrane potential reading, which was obtained when the reference electrodes were placed on the different sides of the membrane. The difference between the junction potentials of the electrodes in

the source and receiving solutions was also subtracted (see Appendix A). To minimize the diffusion boundary layers at the membrane surface, both solutions were stirred vigorously. Solution activity coefficients for KCl,[37, 38] $MgSO_4$,[39] and $MgCl_2$[40] were usually obtained by interpolation of literature data. For $MgCl_2$ at concentrations ≤0.00464 M, activity coefficients were estimated from the Debye-Hückel equation. Three membranes were used to obtain values of the membrane potential, and ± values represent standard deviations.

2.3 Results and Discussion

Ion transport through PEMs may include diffusion, convection, and electromigration components, and the film permeability often varies with the solution composition.[41] Thus, ion flux is a complicated function of salt concentrations and transmembrane volume flow. To evaluate the effects of different variables on transport, this section first examines salt permeabilities in diffusion dialysis where transmembrane volume flow is negligible. Subsequent NF studies show that transmembrane volume flow significantly enhances ion transport, and measurements of membrane potentials assess relative permeabilities of cations and anions. Finally, NF measurements with mixed salts at varying concentrations show remarkable negative rejections due to spontaneously-arising transmembrane electric potentials that result from

higher membrane permeabilities to anions than cations.

2.3.1Diffusion Dialysis

In dialysis experiments, ions diffuse across a membrane from a concentrated source phase to a dilute receiving phase. Figure 2.2 shows the evolution of the receiving phase K^+ and Mg^{2+} concentrations during aqueous dialysis of 0.01 M $MgCl_2$ or 0.01 M KCl through a porous alumina membrane coated with a $(PSS/PAH)_4$ film. (The receiving phase initially contains deionized water.) Based on the slopes in Figure 2.2 and in similar replicate experiments, the flux of KCl is $2.4\pm0.5 \times 10^{-9}$ mol cm^{-2} s^{-1}, whereas the flux of $MgCl_2$ is $<7 \times 10^{-12}$ mol cm^{-2} s^{-1}. As Table 2.1 shows, these fluxes lead to a remarkable K^+/Mg^{2+} selectivity >350, and in dialysis with a source phase solution containing both $MgCl_2$ and KCl, the fluxes of each cation are essentially similar to those in single-salt experiments. Tieke and coworkers performed dialysis using $(PSS/PAH)_{60}$ films on porous poly(acrylonitrile)/poly(ethylene terephthalate) supports and achieved a Na^+/Mg^{2+} selectivity of 113 with source phase concentrations of 0.1 M.[14] The support and number of layers in the film as well as the source phase concentration likely affect selectivities.

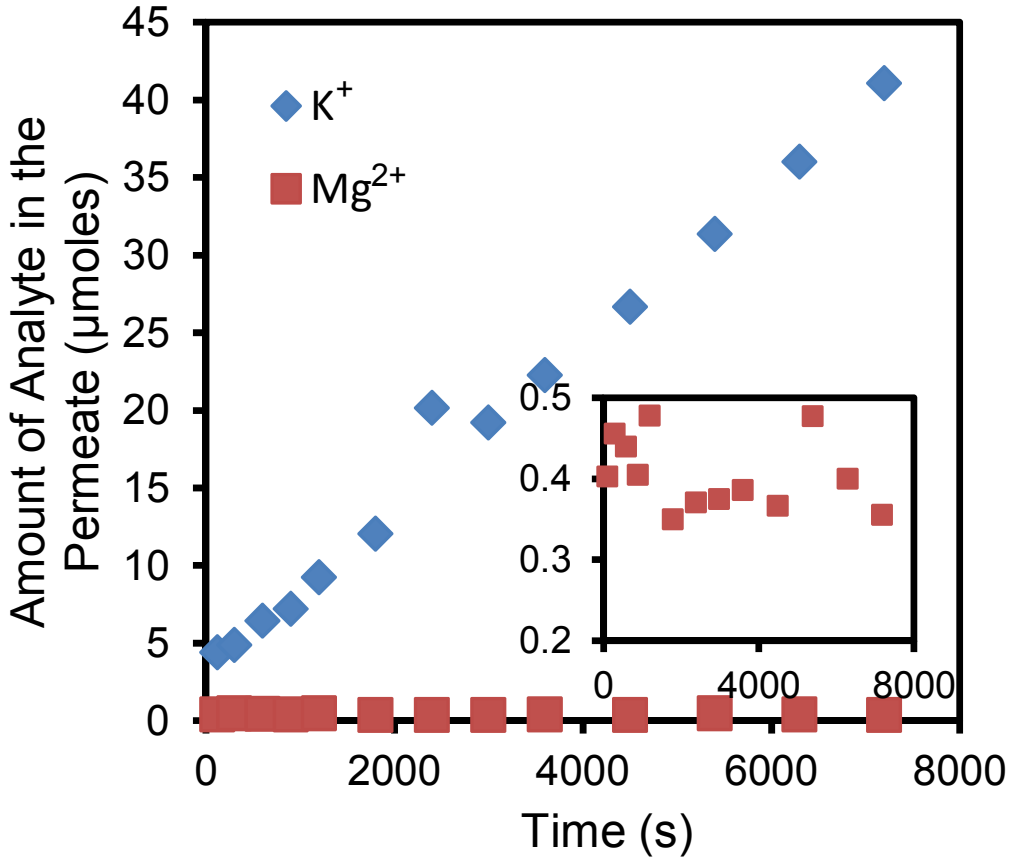

Figure 2.2 Amount of KCl (blue diamonds) or $MgCl_2$ (red squares) in the receiving phase as a function of time in diffusion dialysis of 0.01 M KCl or 0.01 M $MgCl_2$ through a porous alumina membrane coated with a $(PSS/PAH)_4$ film. The inset shows an enlarged region for the $MgCl_2$.

Dialysis using porous alumina coated with a $(PSS/PAH)_4PSS$ film gives salt fluxes (Table 2.1) similar to those with $(PSS/PAH)_4$-coated membranes. Hence, the surface charge is not a dominant factor in controlling transport, and the K^+/Mg^{2+} selectivity likely results primarily from the difference in hydrated ion sizes (or solvation energies) rather than charge exclusion. Previous SEM

images of these membranes show that the interiors of the pores are open, and selectivity only increases dramatically after full coverage of the support.[11, 21] Thus the primary effect of the polyelectrolyte adsorption results from the film on the surface and not adsorption within pores.[42] The relatively dense PEM structure is essentially impermeable to Mg^{2+} (hydrated diameter of 8 Å) but much more permeable to K^{+} (hydrated diameter of 3 Å).[43] Studies with the transport of neutral molecules suggest that the effective pore diameter in $(PSS/PAH)_7$ films is around 0.8-1.0 nm, which is consistent with the exclusion of Mg^{2+}.[36]

Table 2.1 Ion fluxes and selectivities in diffusion dialysis of KCl and $MgCl_2$ through bare porous alumina membranes and similar membranes coated with $(PSS/PAH)_4$ and $(PSS/PAH)_4PSS$ films.

Membrane	Ion	Single Salt Ion Flux (nmol cm^{-2} s^{-1})	Selectivity (K^+/Mg^{2+})
Bare Alumina	K^+	6.43±0.65	1.47±0.15
	Mg^{2+}	4.36±0.04	
$(PSS/PAH)_4$-coated Alumina	K^+	2.39±0.50	>350
	Mg^{2+}	<0.007	
$(PSS/PAH)_4PSS$-coated Alumina	K^+	3.09±0.18	276±93
	Mg^{2+}	0.011±0.004	

Ion fluxes through these composite membranes are affected by both the PEM and the alumina support. In each of these membrane regions, equation (2.3) describes the salt flux, J, where ΔC is the concentration gradient across the region and P is the local permeance.

$$J = P\Delta C \tag{2.3}$$

According to the series resistance model,[44] equation (4) describes the permeance of the PEM, P_{film}, where $P_{composite}$ is the permeance of the PEM-coated membrane and

$$P_{film} = \frac{P_{composite}P_{support}}{P_{support}-P_{composite}} \quad (2.4)$$

$P_{support}$ is the permeance of the bare alumina. We calculated the values of $P_{composite}$ and $P_{support}$ for KCl using equation (2.3) with 0.01 M for ΔC and diffusion fluxes of 6.4 and 2.4 nmol cm^{-2} s^{-1} through the bare and modified membranes, respectively. Equation (2.4) then reveals that the permeance of the PEM, P_{film}, is 3.8 μm/s. In contrast, the PEM permeance to $MgCl_2$ is <0.007 μm/s.

2.3.2 Nanofiltration

In NF with PEM-coated porous alumina, a pressure drop forces water across the membrane while the feed solution flows parallel (crossflow) to the membrane surface. If water and ion transport occur solely by independent diffusion, the solution-diffusion model should describe the ion rejection. In this model, equation (3) still describes the salt flux across the membrane, with $P = P_{film}$. Assuming negligible concentration polarization in the feed solution, or $\Delta C_{film} = C_f - C_p$, equation (2.5) describes the salt rejection based on the solution-diffusion model,

$$Re = 1 - \frac{P_{film}}{J_v+P_{film}} \quad (2.5)$$

where J_v is the volumetric flux through the membrane (see Appendix A for more details on the solution-diffusion model).

Table 2.2 shows experimental and predicted salt rejections in NF with alumina membranes coated with $(PSS/PAH)_4$ films. We predicted the rejections using the P_{film} values from diffusion dialysis, the experimental values of J_v, and equation (2.5). Notably, the solution-diffusion model greatly over predicts the NF rejections. Although the K^+/Mg^{2+} selectivity in NF is 16, which is similar to the Na^+/Mg^{2+} selectivity in our previous work,[21] this selectivity is much lower than the value of >350 observed in diffusion dialysis.

Table 2.2 Experimental and predicted ion rejections and K^+/Mg^{2+} selectivities in NF[a] of 0.01 M KCl or 0.01 M $MgCl_2$ through porous alumina membranes coated with $(PSS/PAH)_4$ films. The table also presents values of the solution flux through the membrane.

Predicted Values[b]			Experimental Values				
Rejection (%)		Selectivity (K^+/Mg^{2+})	Rejection (%)		Solution Flux (m^3/m^2/day)		Selectivity (K^+/Mg^{2+})
K^+	Mg^{2+}		K^+	Mg^{2+}	K^+	Mg^{2+}	
85.3±4.3	>99.96	>350	47.3±4.4	96.7±0.7	1.91±0.07	1.61±0.07	16.0±1.3

[a]NF occurred with a transmembrane pressure of 5 bar and a crossflow rate of 26 mL/min.

[b]The predicted values were calculated from the diffusion dialysis results and the solution-diffusion model.

The lower than expected rejections in NF likely stem from convective transport of ions. However, given the assumption of a ~20 nm[21] thick polyelectrolyte layer, the permeability coefficients estimated from the diffusion dialysis data are 4 and 7 orders of magnitude lower than the bulk diffusivities for KCl and $MgCl_2$, respectively. Such strongly reduced diffusivities are hardly compatible with the picture of a nanoporous medium, which is required to have noticeable convective coupling in a defect-free matrix. Thus, the increased passage of $MgCl_2$ in NF most likely stems from convection through film imperfections that arise due to inhomogeneities in the alumina support. Some SEM images reveal defects in the alumina skin layer on the porous alumina supports (see Appendix A Figure A5), and such imperfections will likely lead to defects in the PEM. NF rejections and diffusion dialysis fluxes seem to vary when we use membranes taken from different boxes, and SEM images suggest that the defect density varies from box to box (see Appendix A). Therefore, the data above were all obtained using one box of alumina supports.

Concentration polarization may also decrease K^+/Mg^{2+} selectivity in NF compared to diffusion dialysis. However, the Mg^{2+} rejection is not a strong function of either crossflow rate or permeate flux, so concentration polarization is not the primary factor leading to low rejection. Moreover the concentration polarization factors needed to make the NF results consistent with dialysis data seem unreasonably high (see Appendix A for a longer discussion of concentration polarization).

2.3.3 Membrane Potential

The rate of salt diffusion through a membrane depends on the solubility and diffusivity of both the cation and the anion, but transport experiments typically assess only a composite salt permeance. In contrast, electrical potential drops across membranes exposed to salt concentration gradients inherently reveal the relative permeabilities of cations and anions. Ideally, the electrical potential drop across the membrane, E, is a function of the transference numbers of the cation and anion, t_+ and t_-, respectively, according to equation (2.6).[45]

$$E = \left(\frac{t_+}{z_+} + \frac{t_-}{z_-}\right)\frac{RT}{F} ln \frac{a_1}{a_2} \quad (2.6)$$

In this equation, R is the gas constant, z_+ and z_- represent the charges of the cation and anion, respectively, T is the temperature, F is the Faraday constant and a_1 and a_2 are the salt activities in the source and receiving phase solutions, respectively. The transference numbers depend on the charge, concentration, and diffusivity of each ion, as equation (2.7) shows for the cation.

$$t_+ = \frac{|z_+|C_+D_+}{|z_+|C_+D_+ + |z_-|C_-D_-} \quad (2.7)$$

In this equation, C_+ and C_- are the concentrations and D_+ and D_- are the diffusion coefficients of the cation and anion, respectively. Because for $MgCl_2$ most of the mass transport resistance of the coated membrane stems

from the PEM, the transference number is essentially that in the film, and the support can be neglected. For KCl, the transference number reflects the selectivity of both the support and the PEM.

Figure 2.3 shows the potential drop across $(PSS/PAH)_4$- and $(PSS/PAH)_4PSS$-coated alumina membranes as a function of $\log(a_1/a_2)$ for $MgCl_2$ solutions. (In these experiments, the receiving phase concentration is always 0.001 M). For low source phase concentrations, the slopes of the linear fits to data for both types of membranes are around -57 mV, indicating that the transference number for Mg^{2+} is essentially zero. For completely selective membranes with no permeability to Mg^{2+}, the slope would be -59 mV. The low Mg^{2+} transference number is consistent with the negligible $MgCl_2$ flux in diffusion dialysis. Regardless of whether the film terminates with PAH or PSS, the membrane is much less permeable to Mg^{2+} than Cl^-, suggesting that size exclusion or a difference in ion solvation energies is the dominant mechanism behind the low Mg^{2+} transference number. The high electric field across the PEM (as high as 35,000 V/cm) is common in interfaces and double layers.[45]

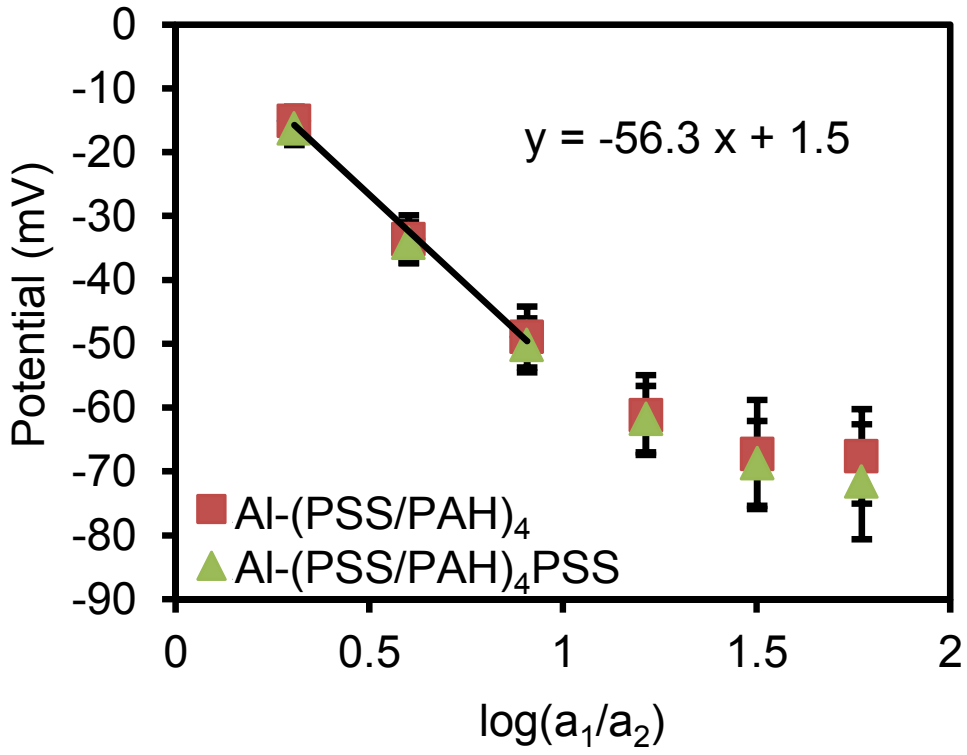

Figure 2.3 Transmembrane potential as a function of $\log(a_1/a_2)$, where a_1 and a_2 are the activities of $MgCl_2$ in the source and receiving phases, respectively. The source phase $MgCl_2$ concentrations ranged from 0.001 to 0.0215 M, whereas the receiving phase always contained 0.001 M $MgCl_2$. Squares and triangles represent alumina membranes coated with $(PSS/PAH)_4$ and $(PSS/PAH)_4PSS$ films, respectively.

At the higher source phase concentrations in Figure 2.3, the decrease in slope implies that the Mg^{2+} transference number increases with the $MgCl_2$ concentration. Fixing the source to receiving phase concentration ratio at 2,

while varying the concentrations in both solutions more clearly reveals the influence of ionic strength on transference number. As Figure 2.4(a) shows, the Mg^{2+} transference number increases from around zero with a 0.0043 M $MgCl_2$ source phase to 0.42 in a 0.20 M $MgCl_2$ source phase. This trend occurs with both $(PSS/PAH)_4$ and $(PSS/PAH)_4PSS$ films, suggesting that the increasing transference number at high ionic strength is not simply due to screening of surface charge and that the membrane becomes more permeable to Mg^{2+} as the $MgCl_2$ concentrations increases. Farhat and Schlenoff provided evidence that at high ionic strength polycations and polyanions dissociate to create more ion-exchange sites and enhance transport.[41] Control experiments with uncoated porous alumina also show more permeability to Cl^- than Mg^{2+}, presumably because the alumina is positively charged. However, the effect is much smaller than in coated membranes (Figure 2.4(a)). At the lowest concentrations, the potential drops across bare membranes are only -8.3 mV compared to -16.7 mV across membranes coated with $(PSS/PAH)_4$ films.

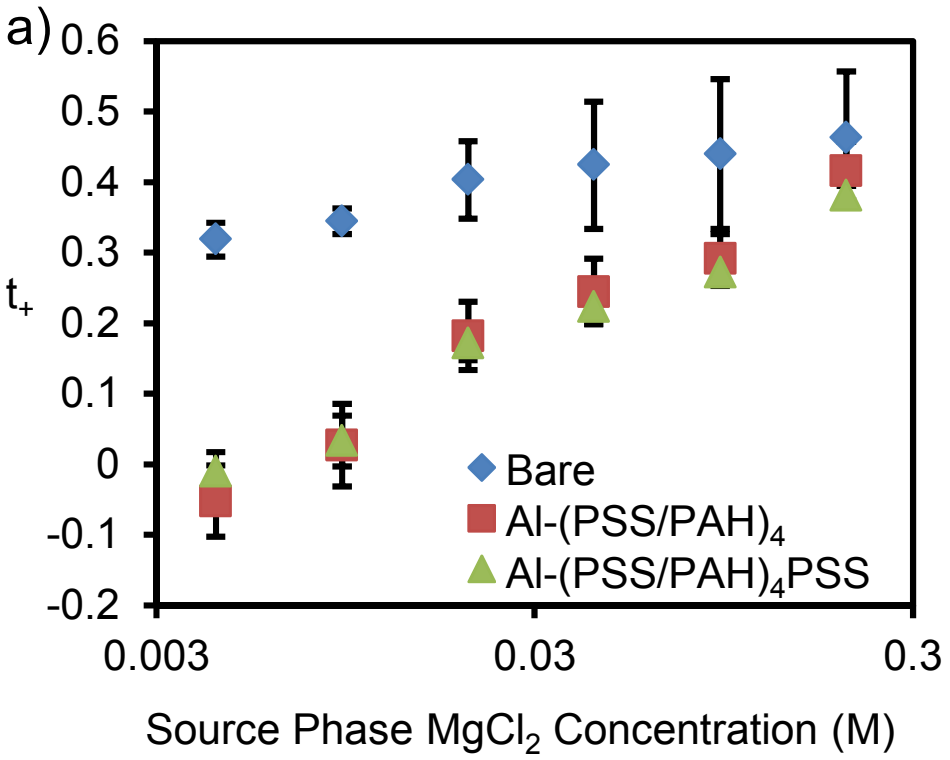
a)
0.6
0.5
0.4
0.3
0.2
0.1
0
-0.1
-0.2
t+
Bare
Al-(PSS/PAH)4
Al-(PSS/PAH)4PSS
0.003
0.03
0.3
Source Phase MgCl2 Concentration (M)

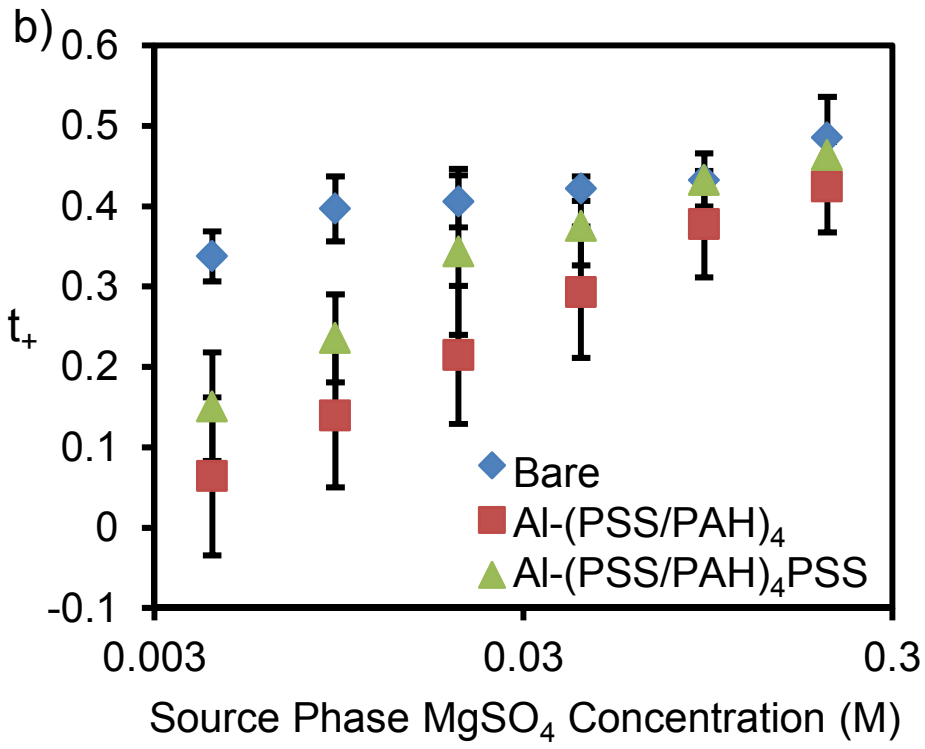
b)
0.6
0.5
0.4
0.3
0.2
0.1
0
-0.1
t+
Bare
Al-(PSS/PAH)4
Al-(PSS/PAH)4PSS
0.003
0.03
0.3
Source Phase MgSO4 Concentration (M)

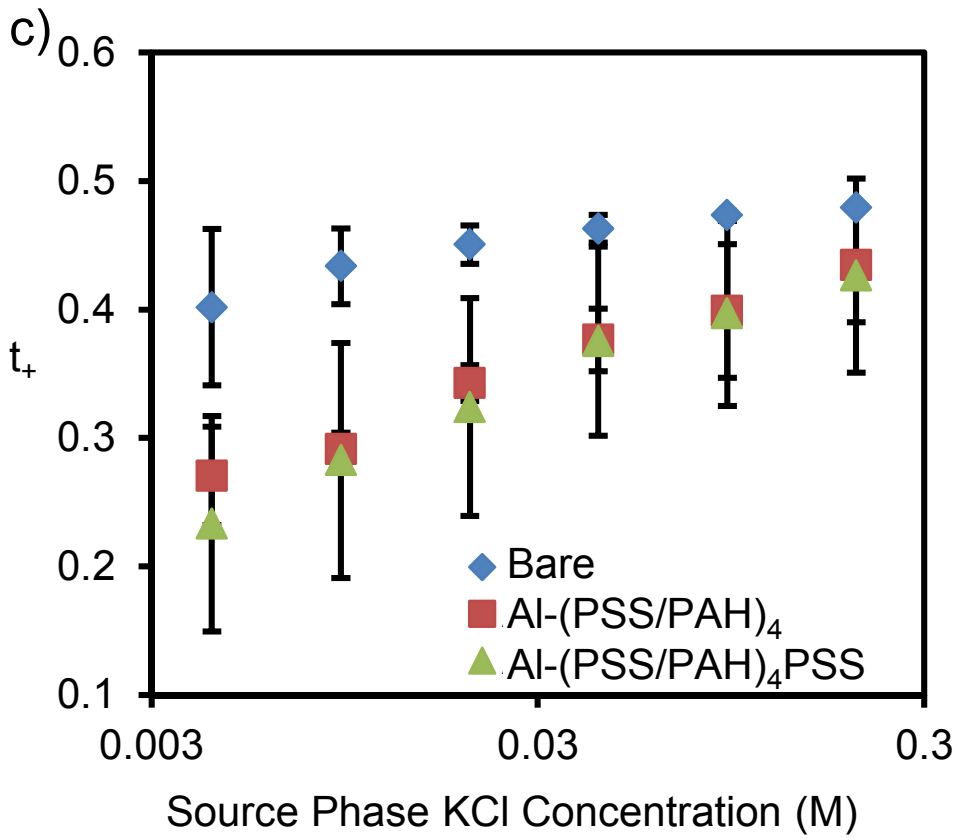

Figure 2.4 Transference numbers of cations as a logarithmic function of the a) $MgCl_2$ b) $MgSO_4$ and c) KCl source phase concentrations (from 0.0043 M to 0.20 M) employed in transmembrane potential measurements with bare alumina membranes (diamonds), $(PSS/PAH)_4$-coated membranes (squares) and $(PSS/PAH)_4PSS$ membranes (triangles). The ratios of the source and receiving phase concentrations are 2 in all cases.

Despite the large size of SO_4^{2-} relative to Cl^-, the Mg^{2+} transference numbers for $MgSO_4$ diffusion through $(PSS/PAH)_4$-coated membranes are only slightly smaller than those with $MgCl_2$ (compare Figures 2.4(a) and

2.4(b)). The Mg^{2+} transference number is <0.1 with 0.0043 M $MgSO_4$ in the source phase (Figure 2.4(b)). The PSS-terminated membrane likely electrostatically excludes SO_4^{2-},[23] and this might explain why in the case of $MgSO_4$, the Mg^{2+} transference numbers are a little higher for $(PSS/PAH)_4PSS$ films than $(PSS/PAH)_4$ films.

Interestingly, at source phase concentrations of 0.0043 M, even KCl shows a cation transference number of only ~0.25 (Figure 2.4(c)). This is in contrast to aqueous solutions where the potassium and chloride transference numbers are nearly equal.[45] The low cation transference number stems in part from the positively charged alumina substrate, which excludes cations, but the K^+ transference number is significantly lower for membranes coated with $(PSS/PAH)_4$ and $(PSS/PAH)_4PSS$ than for bare alumina. The low K^+ transference number suggests a slight positive charge on these films.[46]

2.3.4 Diffusion Dialysis and Nanofiltration as a Function of Solution Composition

The transmembrane potential measurements suggest that the membrane permeability to Mg^{2+} increases with the ionic strength of the surrounding solution. To further assess the effect of ionic strength on ion transport, we performed diffusion dialysis of 0.01 M KCl while adding equal amounts of $MgCl_2$ to the source and receiving reservoirs. Figure 2.5 shows that on going

from 0 to 0.0464 M $MgCl_2$ in both the source and receiving phases, the K^+ flux increases by a factor of ~1.6. Corresponding addition of $MgCl_2$ to both source and receiving phases in diffusion dialysis with bare alumina does not increase flux. Thus the primary effect of $MgCl_2$ addition is an increase in the permeability of the polyelectrolyte film to KCl. Similarly, the Mg^{2+} permeability (0.01 M $MgCl_2$ in the source phase) increases ~1.5 times upon the addition of 0.119 M KCl to both source and receiving phases. (The addition of 0.119 M KCl gives the same solution ionic strength as the addition of 0.0464 M $MgCl_2$ to 0.01M KCl.)

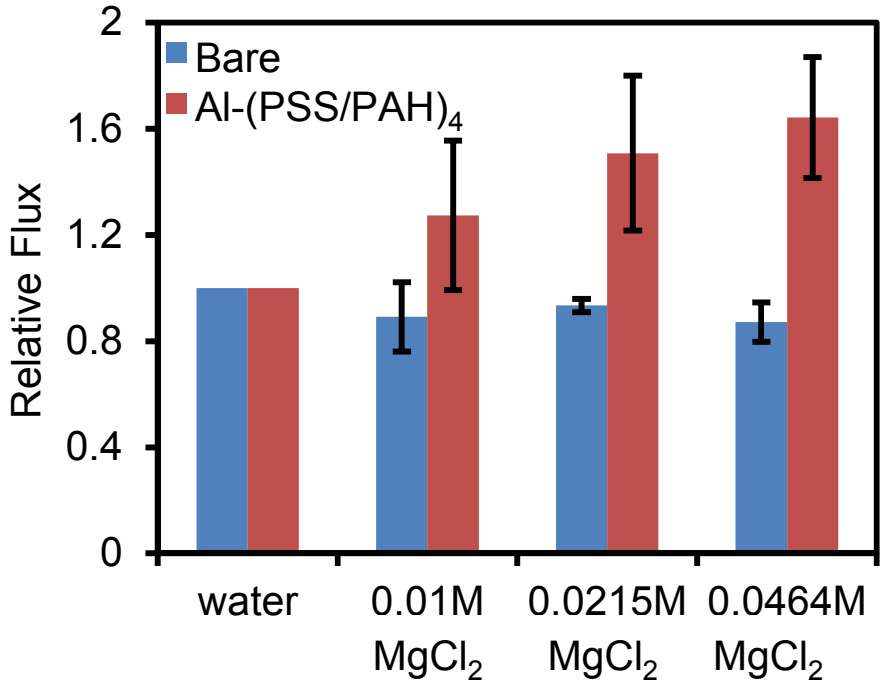

Figure 2.5 Normalized K^+ fluxes in diffusion dialysis of 0.01 M KCl through bare and $(PSS/PAH)_4$-coated alumina membranes. All experiments occurred with 0.01 M KCl as the source phase, and the $MgCl_2$ concentrations in the source and receiving phases varied simultaneously from 0 to 0.0464 M. Fluxes are normalized to those with no $MgCl_2$, which were 6.4 nmol cm^{-2} s^{-1} and 2.4 nmol cm^{-2} s^{-1}, for bare and coated membranes, respectively. (All experiments with diffusion dialysis as a function of salt composition were performed using alumina supports from a new box.)

Compared to diffusion dialysis, NF may show different trends in ion flux as a function of ionic strength because ion transport occurs in part through convective coupling with water flux. As Figure 2.6(a) shows, within

experimental uncertainty, the $MgCl_2$ rejection in NF is constant with feed concentrations ranging from 0.001 M to 0.0232 M $MgCl_2$ (rejection ranged from 98.6 to 98.8%). At an even higher feed concentration (0.0464 M), the rejection decreases slightly to 96.9%. The results in Figure 2.6(a) are mostly consistent with a primary Mg^{2+} transport mechanism of convective coupling, probably through defects. In transport through defects the Mg^{2+} flux should be proportional to the $MgCl_2$ feed concentration, and rejection should be independent of concentration.

2.3.5 Negative Rejections in Nanofiltration.

Diffusion potentials created by $MgCl_2$ transport through imperfection-free regions of the membrane may affect the transport of other charged species. This should be particularly true for K^+ because diffusion through the defect-free region may dominate its transport. To examine the effects of $MgCl_2$ on the transport of other species in NF, we added trace amounts of nitrobenzene (0.10 mM) and KCl (0.5% of the concentration of $MgCl_2$) to the NF solutions. The nitrobenzene rejection is ~20%, regardless of $MgCl_2$ concentration, suggesting that the presence of $MgCl_2$ has a marginal effect on the overall membrane permeability. Consistent with minimal variation in film permeability to nitrobenzene, the water flux is also relatively constant at

essentially equal driving pressures. We varied the applied pressure to keep the driving force, applied pressure minus osmotic pressure, for solution flux approximately constant, and the solution flux ranged from 0.63 m^3/m^2/day to 0.86 m^3/m^2/day over the range of $MgCl_2$ feed concentrations in Figure 2.6.

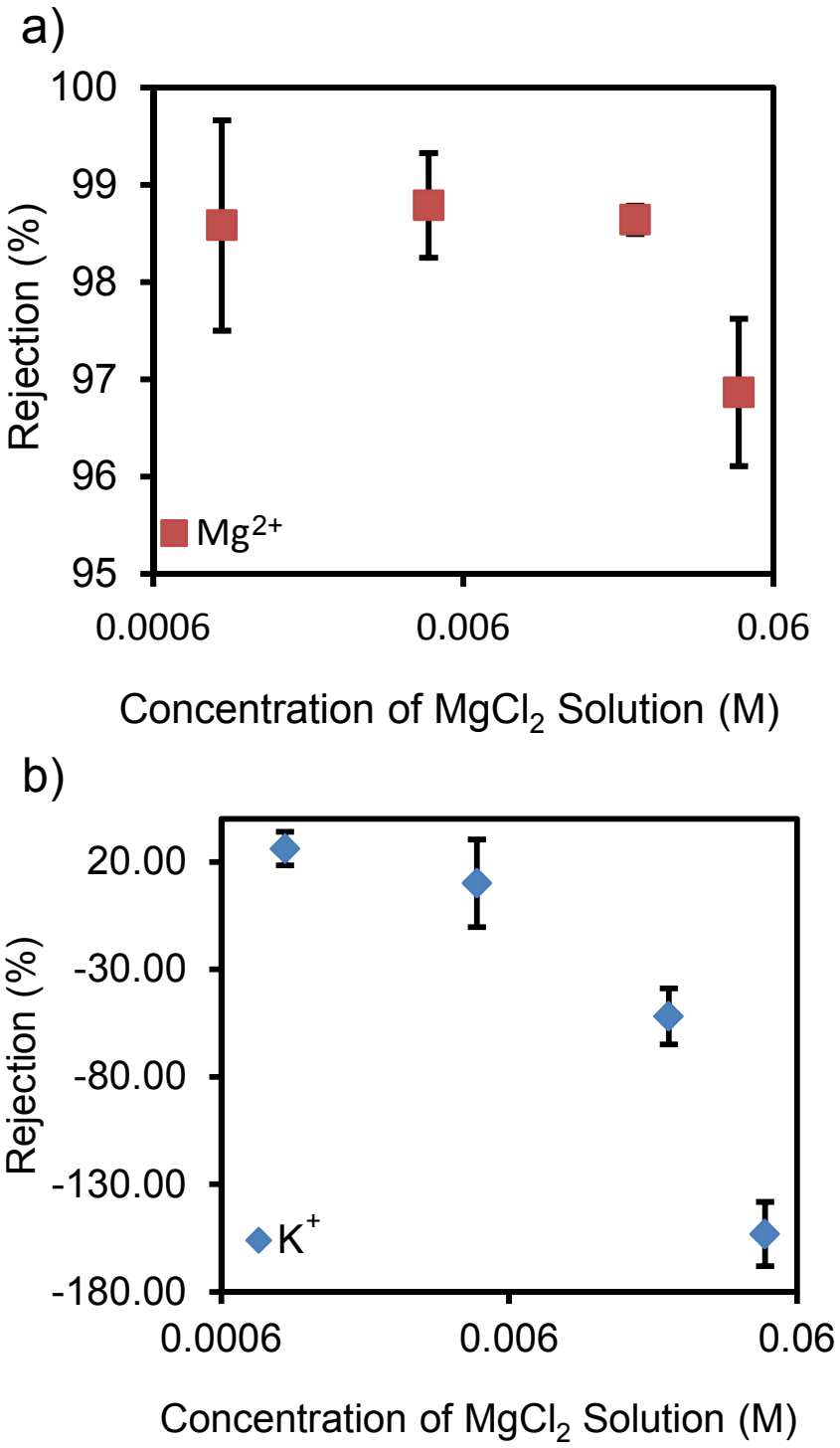

Figure 2.6 Rejections of a) $MgCl_2$ and b) trace KCl in NF through porous alumina membranes coated with $(PSS/PAH)_4$ films. The $MgCl_2$ feed concentrations ranged from 0.0010 M to 0.0464 M while the KCl concentration

Figure 2.6 (cont'd) was 0.5% of that for $MgCl_2$. Both graphs are from the same experiments repeated with more than 3 membranes. The applied pressure was adjusted from 2.8 to 6 bar to keep the difference between the applied pressure and osmotic pressure approximately the same and maintain a nearly constant volume flux. The crossflow rate was 26 mL/min.

In contrast to $MgCl_2$, Figure 2.6(b) shows that NF rejection of K^+ decreases significantly with increasing $MgCl_2$ concentrations and becomes highly negative. At the highest Mg^{2+} feed concentration, the amount of K^+ in the permeate is 2.5 times that in the feed. The negative rejection reflects a negative electrical potential drop (from feed to permeate) across the membrane that enhances K^+ and Mg^{2+} transport while decreasing transport of Cl^- to maintain zero current (see Figure 2.1). However, the reason for the decreasing K^+ rejection with increasing $MgCl_2$ concentration is not readily evident because the transference numbers obtained from membrane potentials decrease with increasing $MgCl_2$ concentration (see Figure 2.4(a)). Increased permeability to K^+ with increasing $MgCl_2$ concentrations (Figure 2.5) can compensate a fraction of the decreased membrane potentials at higher $MgCl_2$ concentrations, but this may not account for the 3-fold increase in K^+ passage on going from 0.0010 M to 0.0464 M $MgCl_2$ as the dominant salt.

The high negative rejections might stem from selective convective

transport of Cl^- over Mg^{2+} in the defect-free region of the matrix. Such a mechanism should increase transmembrane potentials and give more negative rejections with increases in permeate flux. However, Figure 2.7 clearly shows less negative K^+ rejection as flux increases. In fact, the concentration of K^+ in the permeate is almost proportional to the solution flux. This shows that K^+ flux, which predominantly occurs through diffusion and electrical migration, is essentially independent of solution flux, and higher permeate flow rates simply dilute the K^+. Thus, selective convective transport of Cl^- over Mg^{2+} does not contribute to negative rejection. Currently, we do not have a satisfactory explanation for why the K^+ NF rejection becomes more negative with increasing concentrations of $MgCl_2$, although increases in film permeability may contribute to this phenomenon. The Mg^{2+} rejection is relatively independent of solution flux (see Figure 2.7 and Figure A4 in Appendix A), so for this highly rejected ion, convective coupling (presumably mostly through defects) is important because diffusion through the membrane is very slow.

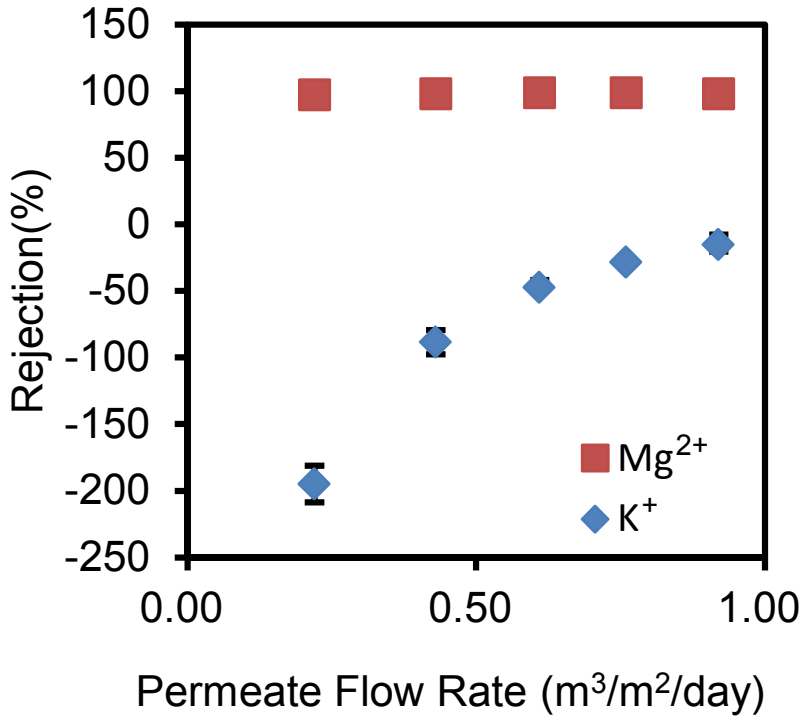

Figure 2.7 $MgCl_2$ and KCl rejections as a function of permeate flow rate in NF of 0.0215 M $MgCl_2$, 0.11 mM KCl through porous alumina coated with a $(PSS/PAH)_4$ film. The Mg^{2+} rejections range from 97.1% to 98.7%. The applied pressure varied from 2 to 5 bar, and the crossflow rate was 26 mL/min. (Figure A4 shows an enlarged plot of the Mg^{2+} rejection.)

Consistent with negative rejection stemming from electrical migration, the trace cation rejection varies with the mobility of the cation. Figure 2.8(a) shows rejections of trace Li^+, K^+, and Cs^+. The mobility of Li^+ is about half that of K^+ and Cs^+, and the amount of Li^+ passing through the membrane is indeed about half that for the other alkali ions, as reflected by the -40% rejection of Li^+

and the -200% rejection of K^+ and Cs^+.

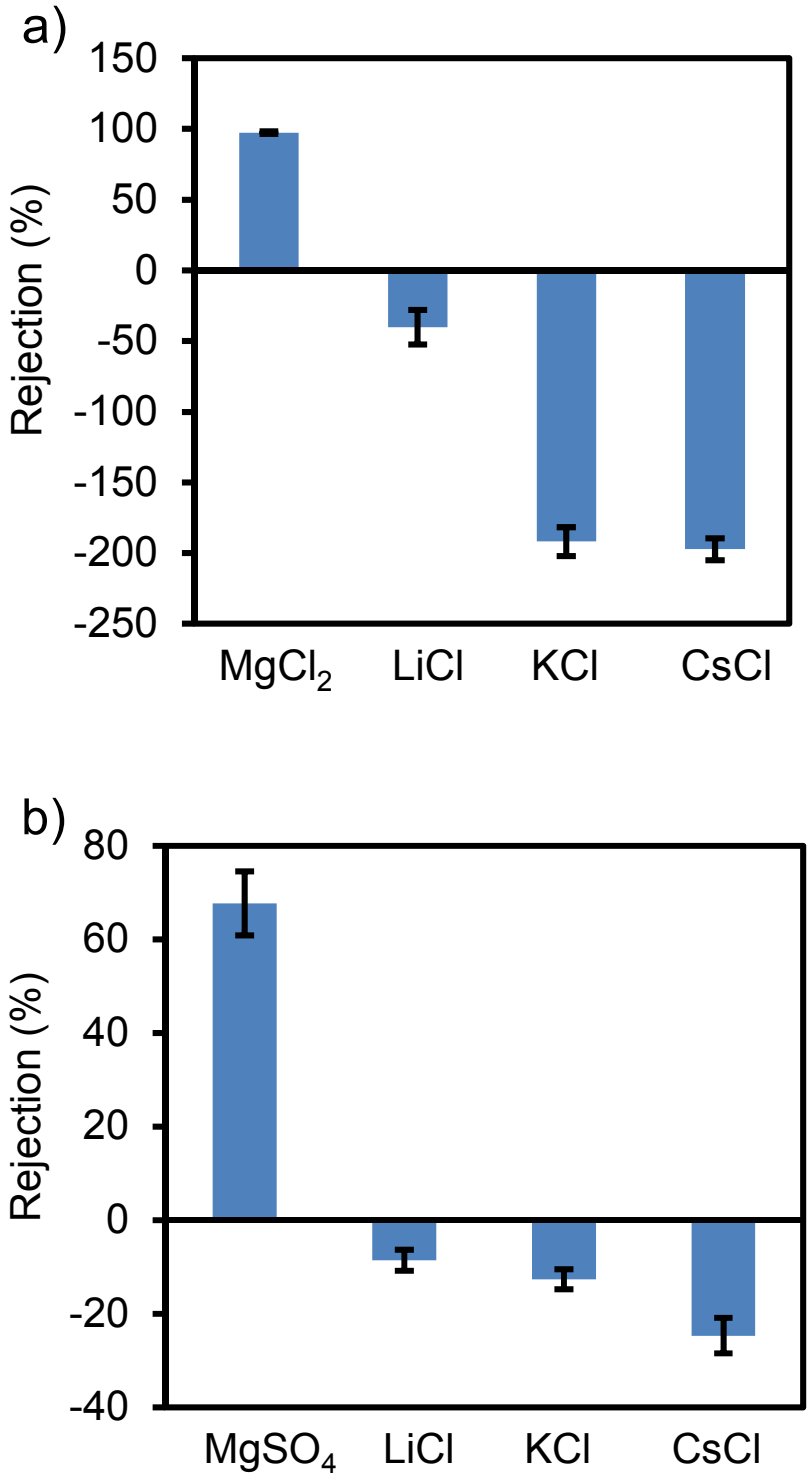

Figure 2.8 Ion rejections during NF of solutions containing a) 0.0464 M $MgCl_2$

Figure 2.8 (cont'd) or b) 0.0464 M $MgSO_4$. Both feed solutions also contained 0.232 mM LiCl, 0.232 mM KCl and 0.232 mM CsCl. NF occurred at 6 bar through porous alumina membranes coated with a $(PSS/PAH)_4$ film. The crossflow rate was 26 mL/min.

When $MgSO_4$ is the dominant salt instead of $MgCl_2$, the rejection of Mg^{2+} decreases to 67%. This is consistent with the higher transference numbers of Mg^{2+} in $MgSO_4$ than in $MgCl_2$. The lower diffusion potential across the membrane with $MgSO_4$ relative to that with $MgCl_2$ also leads to less negative rejections of monovalent cations (compare Figures 2.8(a) and 2.8(b)). Nevertheless, the monovalent-ion negative rejections still follow the ion mobility trend, where LiCl has the smallest magnitude of negative rejection while CsCl has the most negative rejection.

2.4 Conclusion

PSS/PAH films show remarkable K^+/Mg^{2+} selectivities >350 in diffusion dialysis. However, the corresponding selectivity in nanofiltration is only 16, suggesting that convective transport of Mg^{2+} occurs (probably through membrane imperfections). Nevertheless, the extremely high dialysis selectivities might prove useful in electrodialysis, and we are investigating this possibility. Transmembrane electric potentials under concentration gradients

show that PSS/PAH films are selectively permeable to anions, but this selectivity decreases with increasing salt concentrations. In nanofiltration, the differences in Mg^{2+} and Cl^{-} permeabilities give rise to electrical potentials across the membrane that lead to negative K^{+} rejections as low as -200%. The magnitude of negative rejection increases with the trace ion mobility and might prove useful in selective removal of alkali cations from electrolyte mixtures containing multiply charged cations.

APPENDIX

A1. Determination of Transmembrane Potentials

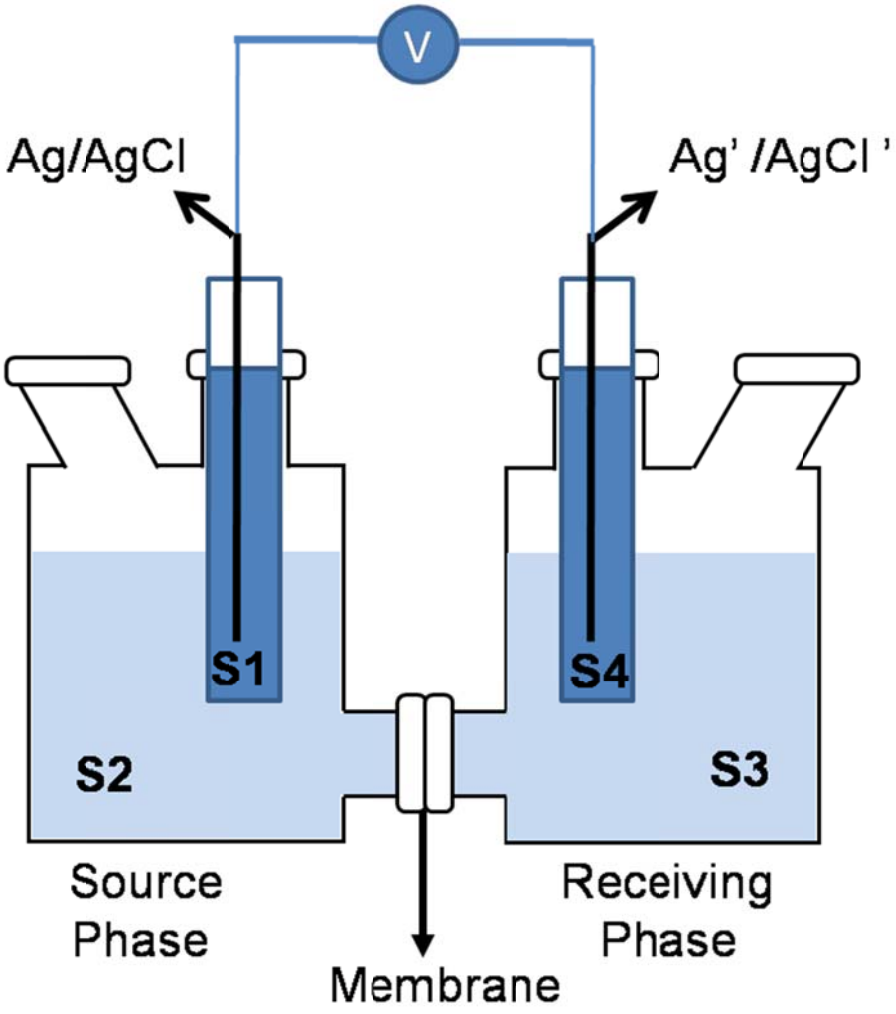

Figure A1. Apparatus for measuring transmembrane potentials. The symbols S1 to S4 denote various solutions separated by either frits or membranes. S1 and S4 are saturated KCl solutions, and S2 and S3 indicate the solutions in the source and receiving phases, respectively. The diagram does not show the stirrers on each side of the membrane.

Figure A1 illustrates the experimental setup for transmembrane potential measurements. As equation (A1) illustrates, the electrical potential drop between the

$$\phi^{Ag'} - \phi^{Ag} = \left(\phi^{Ag'} - \phi^{S4}\right) + (\phi^{S4} - \phi^{S3}) + (\phi^{S3} - \phi^{S2}) + (\phi^{S2} - \phi^{S1}) + (\phi^{S1} - \phi^{Ag}) \quad \text{(A1)}$$

two electrodes (Ag' and Ag) includes a series of potential drops. In this equation, ϕ represents the electric potential in each of the phases as indicated in the diagram. Of course, we are only interested in the transmembrane potential, $(\phi^{S3} - \phi^{S2})$. Thus, we need to determine or estimate the other potential drops. To determine $\left(\phi^{Ag'} - \phi^{S4}\right) + (\phi^{S1} - \phi^{Ag})$, we put both reference electrodes in the receiving phase and measure the potential difference between the two electrodes. In this case, because both reference electrodes contain the same filling solution and they are immersed in the same solution, the junction potentials at the two reference electrode-solution interfaces should cancel. In the actual measurement of transmembrane potential, however, the reference electrodes are immersed in two different solutions and the junction potentials will not cancel exactly. To approximate these junction potentials, $(\phi^{S4} - \phi^{S3})$ and $(\phi^{S2} - \phi^{S1})$, we employ equation (A2), which is also known as the Henderson equation.[47] In this equation,

$$\mathrm{E_j} = \phi^{\beta} - \phi^{\alpha} = \frac{\sum_i \frac{|z_i|\mu_i}{z_i}[C_i(\beta) - C_i(\alpha)]}{\sum_i |z_i|\mu_i[C_i(\beta) - C_i(\alpha)]} \frac{RT}{F} \ln \frac{\sum_i |z_i|\mu_i C_i(\alpha)}{\sum_i |z_i|\mu_i C_i(\beta)} \quad \text{(A2)}$$

$\mathrm{E_j}$ is the junction potential, z_i is the ion charge, μ_i is the ion mobility, C_i is the ion concentration, and α and β denote different solution phases.

Using the measured potential, $\left(\phi^{Ag'} - \phi^{Ag}\right)$ along with the estimated values for the junction potentials, $(\phi^{S2} - \phi^{S1})$ and $(\phi^{S4} - \phi^{S3})$, and the measured value for $\left(\phi^{Ag'} - \phi^{S4}\right) + (\phi^{S1} - \phi^{Ag})$ with the reference electrodes in the same solution, we can determine $(\phi^{S3} - \phi^{S2})$.

Tables A1 to A3 list typical values of the measured potentials, calculated junction potentials and activity coefficients.

Table A1. Example Data from $MgCl_2$ membrane potential measurements with a $(PSS/PAH)_4$-modified membrane. The table also gives activity coefficients, junction potentials, and reference electrode potential differences employed to calculate the Mg^{2+} transference number. The subscripts s and r denote the source and receiving phase.

Experiment	**1**	**2**	**3**	**4**	**5**	**6**
C_s (M)[a]	0.0043	0.00928	0.02	0.043	0.0928	0.2
${\gamma_\pm}^{s}$[b]	0.77	0.68	0.68	0.61	0.53	0.50
C_r (M)[c]	0.00215	0.00464	0.01	0.0215	0.0464	0.1
${\gamma_\pm}^{r}$[d]	0.83	0.76	0.71	0.67	0.60	0.52
$\left(\phi^{Ag'} - \phi^{S4}\right) + \left(\phi^{S1} - \phi^{Ag}\right)$ (mV)	0.7	0.0	-0.2	-0.4	-0.7	-1.6
$\phi^{Ag'} - \phi^{Ag}$(mV)	-14.3	-12.6	-10.5	-8.6	-7.4	-5.9
$\phi^{S2} - \phi^{S1}$(mV)	-3.01	-2.54	-2.02	-1.36	-0.50	0.69
$\phi^{S4} - \phi^{S3}$(mV)	3.37	2.96	2.50	1.96	1.29	0.40
$\phi^{S3} - \phi^{S2}$ (mV)	-15.36	-13.02	-10.78	-8.80	-7.49	-5.39
t_+	0.01	0.08	0.23	0.29	0.32	0.46

[a] C_s denotes the salt concentration in the source phase.

[b] ${\gamma_\pm}^{s}$ denotes the average activity coefficient of the salt solution in the source phase.

[c] C_f denotes the salt concentration in the source phase.

[d] ${\gamma_\pm}^{r}$ denotes the average activity coefficient of the salt solution in the receiving phase.

Table A2. Example Data from $MgSO_4$ membrane potential measurements with a $(PSS/PAH)_4$-modified membrane. The table also gives activity coefficients, junction potentials, and reference electrode potential differences employed to calculate the Mg^{2+} transference number. The subscripts s and r denote the source and receiving phase.

Experiment	**1**	**2**	**3**	**4**	**5**	**6**
C_s (M)[a]	0.0043	0.00928	0.02	0.043	0.0928	0.2
$\gamma_{\pm}{}^{s}$[b]	0.55	0.43	0.33	0.25	0.18	0.13
C_r (M)[c]	0.00215	0.00464	0.01	0.0215	0.0464	0.1
$\gamma_{\pm}{}^{rd}$	0.66	0.53	0.42	0.32	0.24	0.18
$\left(\phi^{Ag'} - \phi^{S4}\right) + \left(\phi^{S1} - \phi^{Ag}\right)$ (mV)	0.4	-0.1	0.0	-0.1	0.0	0.0
$\phi^{Ag'} - \phi^{Ag}$(mV)	-5.2	-4.1	-2.9	-1.8	-0.7	0.0
$\phi^{S2} - \phi^{S1}$ (mV)	-3.07	-2.67	-2.27	-1.84	-1.35	-0.80
$\phi^{S4} - \phi^{S3}$(mV)	3.40	3.02	2.63	2.23	1.79	1.30
$\phi^{S3} - \phi^{S2}$(mV)	-5.93	-4.35	-3.26	-2.09	-1.14	-0.50
t_+	0.03	0.15	0.22	0.32	0.40	0.45

[a] C_s denotes the salt concentration in the source phase.

[b] $\gamma_{\pm}{}^{s}$ denotes the average activity coefficient of the salt solution in the source phase.

[c] C_f denotes the salt concentration in the source phase.

[d] $\gamma_{\pm}{}^{r}$ denotes the average activity coefficient of the salt solution in the receiving phase.

Table A3. Example Data from KCl membrane potential measurements with a $(PSS/PAH)_4$-modified membrane. The table also gives activity coefficients, junction potentials, and reference electrode potential differences employed to calculate the K^+ transference number. The subscripts s and r denote the source and receiving phase.

Experiment	**1**	**2**	**3**	**4**	**5**	**6**
C_s (M)[a]	0.0043	0.00928	0.02	0.043	0.0928	0.2
$\gamma_{\pm}{}^{s}$[b]	0.93	0.90	0.87	0.82	0.75	0.72
C_r (M)[c]	0.00215	0.00464	0.01	0.0215	0.0464	0.1
$\gamma_{\pm}{}^{rd}$	0.95	0.93	0.90	0.86	0.82	0.77
$\left(\phi^{Ag'} - \phi^{S4}\right) + \left(\phi^{S1} - \phi^{Ag}\right)$ (mV)	0.3	1.5	1.1	0.3	0.3	0.2
$\phi^{Ag'} - \phi^{Ag}$ (mV)	-7.1	-5.0	-3.7	-3.0	-1.8	-0.9
$\phi^{S2} - \phi^{S1}$(mV)	-3.36	-2.99	-2.62	-2.25	-1.88	-1.51
$\phi^{S4} - \phi^{S3}$(mV)	3.69	3.32	2.95	2.58	2.22	1.85
$\phi^{S3} - \phi^{S2}$(mV)	-7.73	-6.83	-5.13	-3.63	-2.44	-1.44
t_+	0.27	0.30	0.35	0.39	0.42	0.46

[a] C_s denotes the salt concentration in the source phase.

[b] $\gamma_{\pm}{}^{s}$ denotes the average activity coefficient of the salt solution in the source phase.

[c] C_f denotes the salt concentration in the source phase.

[d] $\gamma_{\pm}{}^{r}$ denotes the average activity coefficient of the salt solution in the receiving phase.

A2. Salt Rejection Based on the Solution Diffusion Model

The solution diffusion model assumes that equation (A3) describes the flux, J_i, of a given species i across a membrane, where C_f and C_p are the concentrations of species i at the feed and permeate sides of the membrane, respectively.

$$J_i = P_i \Delta C_i = P_i (C_f - C_p) \quad \text{(A3)}$$

(P_i is the product of the partition and diffusion coefficients.) Equation (A4) defines rejection, *Re*.

$$Re = \frac{C_f - C_p}{C_f} \quad \text{(A4)}$$

We also note that

$$J_i = J_v C_p \quad \text{(A5)}$$

where J_V is the volumetric flux across the membrane. Equating equation (A3) and (A5) yields

$$C_p = \frac{P_{film}(C_f - C_p)}{J_v} \quad \text{(A6)}$$

Substituting this expression for C_p in equation (A4) gives

$$Re = \frac{C_f - \frac{P_{film}(C_f - C_p)}{J_v}}{C_f} \quad \text{(A7)}$$

Simplification of this expression noting the definition of rejection in equation (A4) leads to

$$\mathrm{Re} = 1 - \frac{P_{film}\mathrm{Re}}{J_v} \tag{A8}$$

and reorganization yields equation (A9).

$$Re = 1 - \frac{P_{film}}{J_v + P_{film}} \tag{A9}$$

A3. Salt Rejection with Concentration Polarization

Because the PEMs exclude ions such as Mg^{2+}, their concentration will rise at the membrane surface, even with a high cross flow rate. Figure A2 qualitatively shows the concentration profile of an ion that is rejected by the membrane in NF.

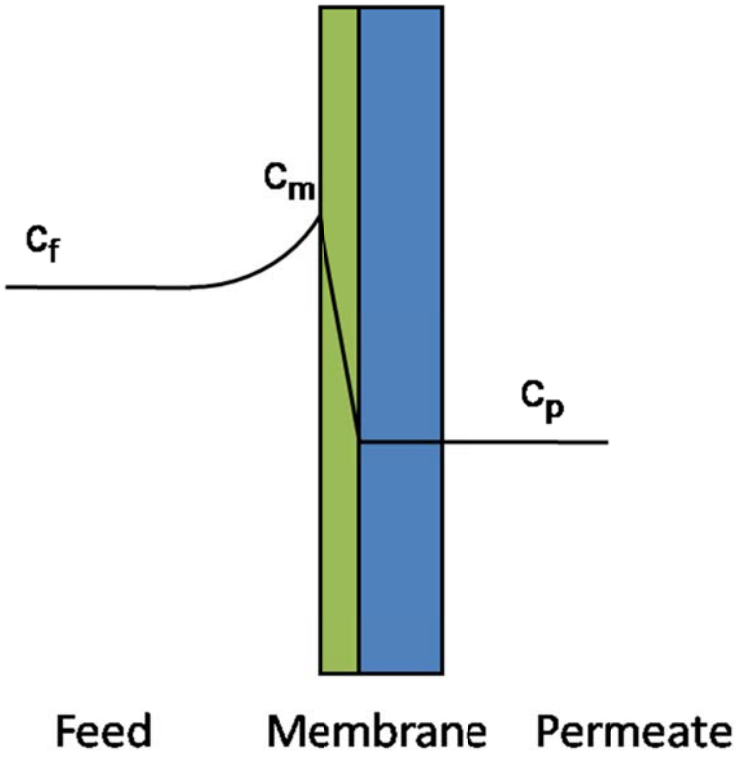

Figure A2. Salt concentration profile in the nanofiltration cell.

To account for concentration polarization, in Equation (A6) C_f should be replaced with C_m, the salt concentration at the membrane surface. Noting that

$$C_m = \beta C_f \quad \text{(A10)}$$

Equation (A6) becomes

$$C_p = \frac{P_{film}(\beta C_f - C_p)}{J_v} \quad \text{(A11)}$$

Substituting this expression for C_p in Equation (A4) and considerable simplification gives Equation (A12).

$$Re = 1 - \frac{P_{film}\beta}{J_v + P_{film}} \quad \text{(A12)}$$

A4. Is Concentration Polarization Responsible for Unexpectedly Low Mg^{2+} Rejections in Nanofiltration

In concentration polarization, convective flux to the membrane surface and salt rejection lead to an enhanced salt concentration, C_m, at the membrane surface, which increases the salt flux. Equation (A13) shows how the concentration polarization factor, C_m/C_f or β, varies with the transmembrane flow rate in the case of a simple homogenous system with a single mass transfer coefficient k.[30] The approximation assumes that the ion concentration is much smaller in the permeate than in the feed.

$$\frac{C_m - Cp}{C_f - c_p} = exp\frac{J_v}{k} \cong \frac{C_m}{C_f} = \beta \quad \text{(A13)}$$

Flow along the membrane surface reduces concentration polarization by decreasing the thickness of the stagnant boundary layer and increasing k. Although the membranes in this study are circular so the concentration polarization is not homogeneous over the membrane surface, enhanced crossflow will nevertheless decrease the local concentration polarization. Figure A3 shows how $MgCl_2$ rejection varies with the volumetric crossflow rate. (We cannot accurately determine the linear crossflow velocity because the height of the feed channel depends on the compression of the o-ring that seals the membrane cell. However, assuming no o-ring compression, the linear velocity is around 23 cm/s for a crossflow rate of 26 mL/min). Increasing the crossflow rate from 3.5 to 98 mL/min increases rejection from 97% to 99%, but the rejection plateaus at crossflow rates >50 mL/min. This suggests that concentration polarization is not a large factor in decreasing the rejections relative to those deduced from diffusion dialysis. Moreover, based on equation (A12), the concentration polarization polarization factor, β, would have to be 88 to account for the increase in salt flux in NF relative to diffusion dialysis. For a simple model of the mass transfer coefficient as D/δ, where D is the diffusion coefficient and δ is the boundary layer thickness, a concentration polarization factor of 88 would require a boundary layer thickness of 0.3 mm (Mg^{2+} diffusion coefficient[48] of 1.2 x 10^{-5} cm^2/s). Given the crossflow rate and cell height (0.4 mm without o-ring compression), such a boundary layer thickness is not realistic. Even with a 10-fold concentration polarization factor,

the calculated $MgCl_2$ NF rejection would be 99.6% using the upper limit of the P_{film} value from diffusion dialysis.

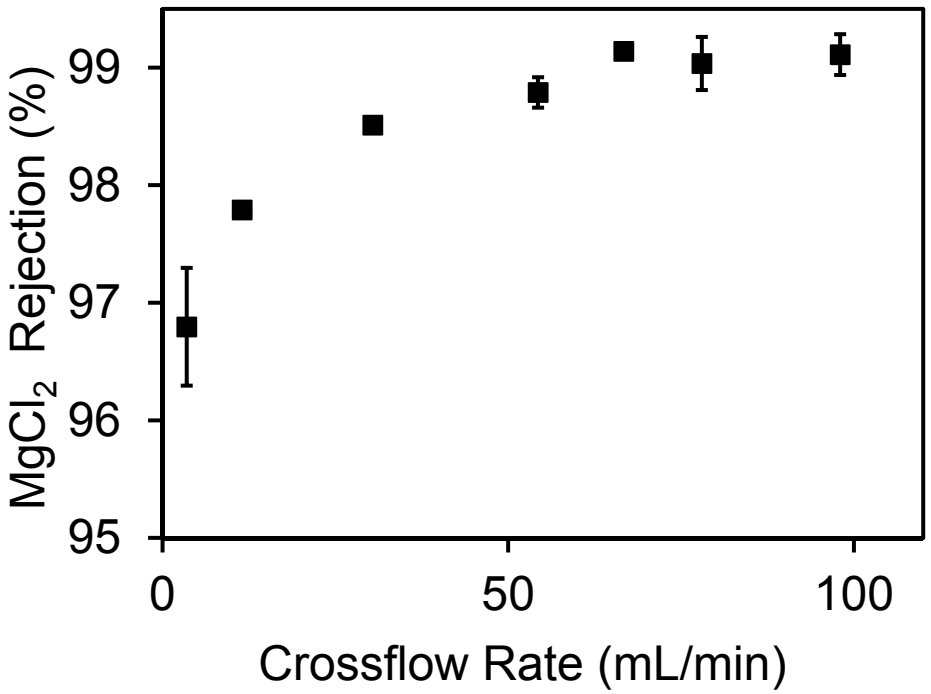

Figure A3 $MgCl_2$ rejection as a function of crossflow rate during NF of 0.0215 M $MgCl_2$ through a porous alumina membrane coated with a $(PSS/PAH)_4$ film. The transmembrane pressure was 5 bar.

As equations (A12) and (A13) illustrate, both concentration polarization and rejection vary with the volume flux across the membrane, which is a function of the transmembrane pressure. In the absence of concentration polarization, higher fluxes should lead to an increase in rejection due to dilution of the permeate, assuming that water and ion transport are not completely

coupled. If concentration polarization is severe, however, increases in volume flux can lead to decreases in rejections due to the exponential increases in β (assuming negligible permeate concentrations). Figure A4 suggests that rejection initially increases slowly with J_v, but then levels off when increasing concentration polarization offsets increases in rejection due to greater water flux. However, the changes in rejection are relatively small for a four-fold increase in J_v. Even at the low volumetric fluxes (0.22 m^3/m^2/day) where concentration polarization is small, rejections calculated from diffusion permeabilities using $Re = 1 - \frac{P_{film}}{J_v + P_{film}}$ (equation (2.5) in the discussion) are 99.7%, whereas the measured rejection is only 97%. This represents a ten-fold difference between predicted and measured salt passage.

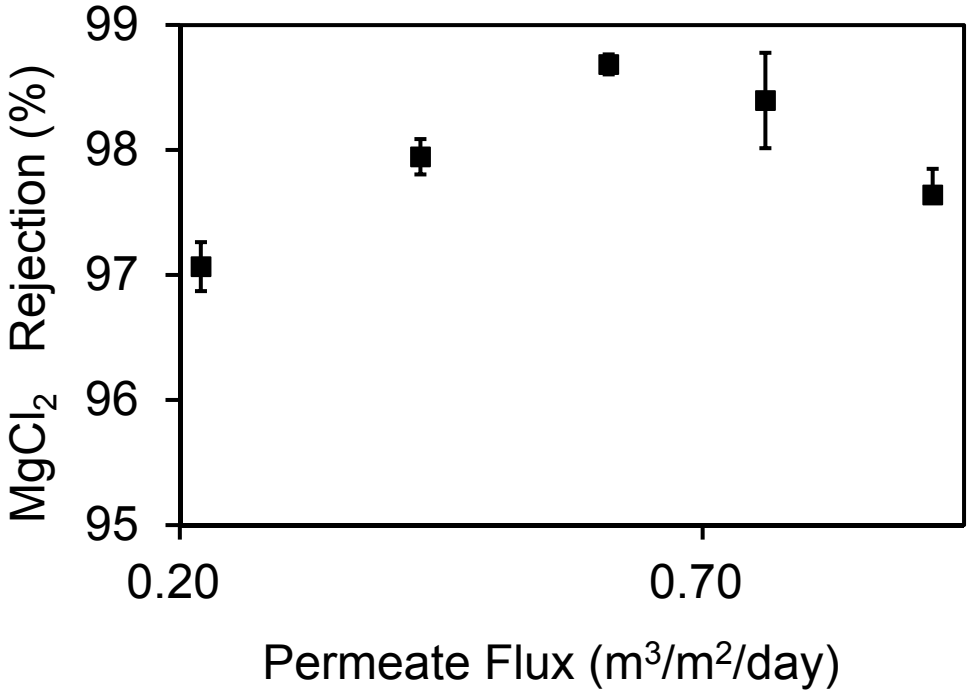

Figure A4. $MgCl_2$ rejection as a function of permeate flux in NF of 0.0215 M $MgCl_2$ and trace 0.11 mM KCl through a porous alumina membrane coated with a $(PSS/PAH)_4$ film. The osmotic pressure of the 0.0215 M $MgCl_2$ is ~1.4 bar, which allows us to vary the flow rate using transmembrane pressures ranging from 2 to 5 bar. The crossflow rate was 26 mL/min.

In summary, concentration polarization does not account for the large increases in ion flux in NF as compared to diffusion dialysis. Convective transport through defects in the porous support (see the paper and below) is likely the dominant effect.

A5. Imperfections in Porous Alumina Supports

The porous alumina supports in this study all came from the same box except those used for the diffusion dialysis studies as a function of background salt composition. Compared to the old box of nanoporous alumina, coated membranes prepared with the new box of membranes give ~5 times higher Mg^{2+} permeabilities but similar K^{+} permeabilities in diffusion dialysis. The difference in the Mg^{2+} permeabilities may arise from obvious defects, such as those in Figure A5, on the alumina supports from the new box. These membrane supports have a skin layer of 20 nm pores on top of a base with 200 nm pores. When there is a defect in the skin layer, the PEMs will not completely bridge the underlying large pores. These defects areas likely occupy less than 1% of the total area. Compared to the new box, coated nanoporous alumina membranes from the old box show both lower Mg^{2+} permeability and far fewer defects. In fact, defects were hard to find.

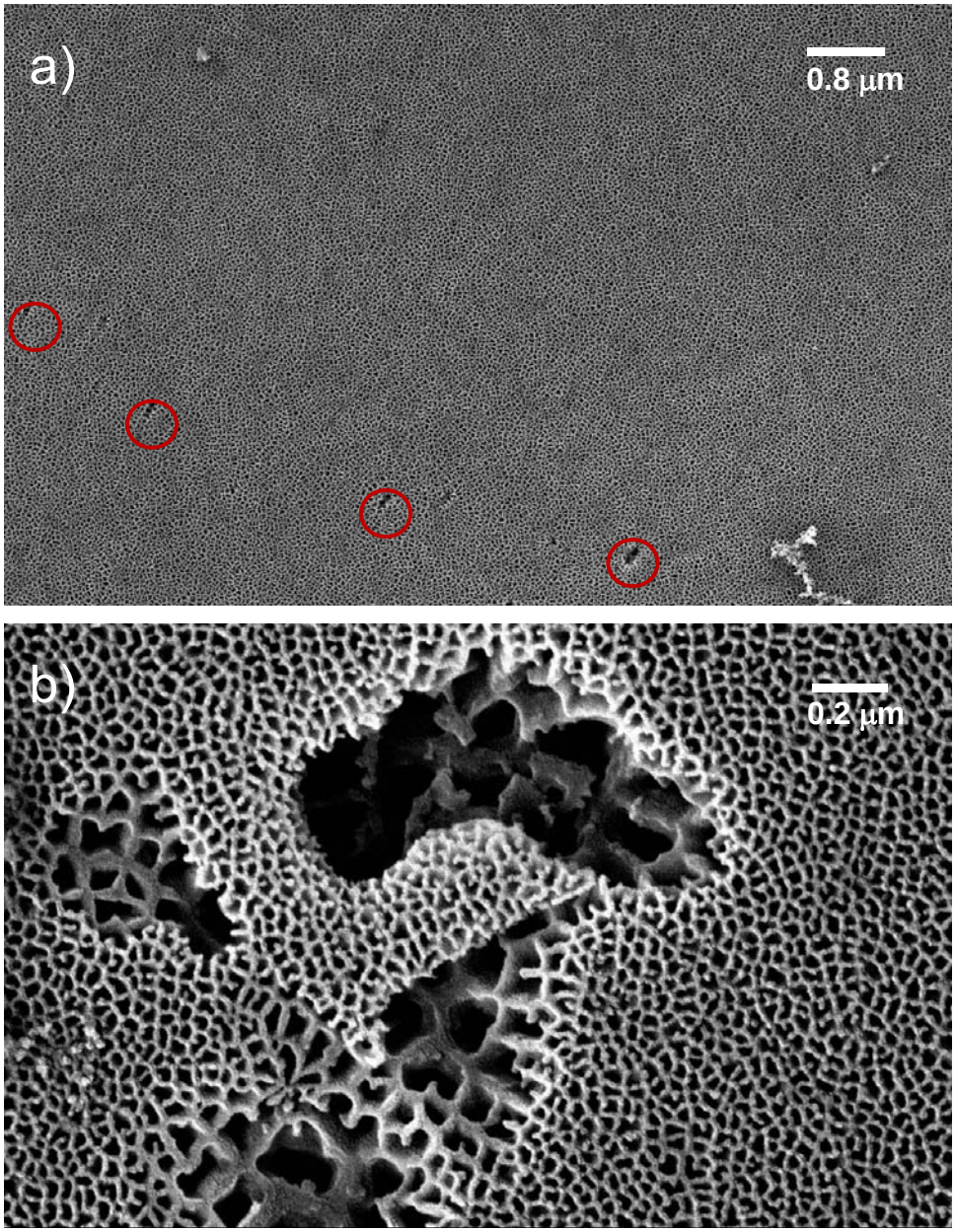

Figure A5. SEM images of bare alumina membranes from the new box. (a) low-magnification view showing several defects. (b) an enlarged membrane defect.

REFERENCES

REFERENCES

(1) Decher, G., *Science* **1997,** 277, 1232-1237.

(2) Decher, G.; Hong, J. D., *Berichte der Bunsengesellschaft-Phys. Chem. Chem. Phys.* **1991,** 95, 1430-1434.

(3) Tagliazucchi, M.; Calvo, E. J., *Chemphyschem* **2010,** 11, 2957-2968.

(4) Adusumilli, M.; Bruening, M. L., *Langmuir* **2009,** 25, 7478-85.

(5) Bason, S.; Oren, Y.; Freger, V., *J. Membr. Sci.* **2011,** 367, 119-126.

(6) Bason, S.; Freger, V., *J. Membr. Sci.* **2010,** 360, 389-396.

(7) Bason, S.; Kaufman, Y.; Freger, V., *J. Phys. Chem. B* **2010,** 114, 3510-3517.

(8) Bason, S.; Kedem, O.; Freger, V., *J. Membr. Sci.* **2009,** 326, 197-204.

(9) Bason, S.; Oren, Y.; Freger, V., *J. Membr. Sci.* **2007,** 302, 10-19.

(10) Toutianoush, A.; Schnepf, J.; El, H. A.; Tieke, B., *Adv. Funct. Mater.* **2005,** 15, 700-708.

(11) Harris, J. J.; Stair, J. L.; Bruening, M. L., *Chem. Mater.* **2000,** 12, 1941-1946.

(12) Kim, B. Y.; Bruening, M. L., *Langmuir* **2002,** 19, 94-99.

(13) Shiratori, S. S.; Rubner, M. F., *Macromolecules* **2000,** 33, 4213-4219.

(14) Krasemann, L.; Tieke, B., *Langmuir* **2000,** 16, 287-290.

(15) Krasemann, L.; Tieke, B., *Mater. Sci. Eng. C-Biomimetic Supramol. Syst.* **1999,** 8-9, 513-518.

(16) Krasemann, L.; Toutianoush, A.; Tieke, B., *J. Membr. Sci.* **2001,** 181, 221-228.

(17) Krasemann, L.; Tieke, B., *J. Membr. Sci.* **1998,** 150, 23-30.

(18) Meier-Haack, J.; Lenk, W.; Lehmann, D.; Lunkwitz, K., *J. Membr. Sci.* **2001,** 184, 233-243.

(19) Sullivan, D. M.; Bruening, M. L., *Chem. Mater.* **2003,** 15, 281-287.

(20) Leväsalmi, J. M.; McCarthy, T. J., *Macromolecules* **1997,** 30, 1752-1757.

(21) Ouyang, L.; Malaisamy, R.; Bruening, M. L., *J. Membr. Sci.* **2008,** 310, 76-84.

(22) Stanton, B. W.; Harris, J. J.; Miller, M. D.; Bruening, M. L., *Langmuir* **2003,** 19, 7038-7042.

(23) Malaisamy, R.; Bruening, M. L., *Langmuir* **2005,** 21, 10587-10592.

(24) Miller, M. D.; Bruening, M. L., *Langmuir* **2004,** 20, 11545-11551.

(25) Saren, Q.; Qiu, C. Q.; Tang, C. Y. Y., *Environ. Sci. Technol.* **2011,** 45, 5201-5208.

(26) Qiu, C. Q.; Qi, S. R.; Tang, C. Y. Y., *J. Membr. Sci.* **2011,** 381, 74-80.

(27) Setiawan, L.; Wang, R.; Li, K.; Fane, A. G., *J. Membr. Sci.* **2011,** 369, 196-205.

(28) Qiu, C.; Setiawan, L.; Wang, R.; Tang, C. Y.; Fane, A. G., *Desalination* **2012,** 287, 266-270.

(29) Wijmans, J. G.; Baker, R. W., *J. Membr. Sci.* **1995,** 107, 1-21.

(30) Baker, R. W., *Membrane technology and applications*. John Wiley & Sons, Ltd: West Sussex, England, 2004.

(31) Bhanushali, D.; Kloos, S.; Bhattacharyya, D., *J. Membr. Sci.* **2002,** 208, 343-359.

(32) Jin, W.; Toutianoush, A.; Tieke, B., *Langmuir* **2003,** 19, 2550-2553.

(33) Gilron, J.; Gara, N.; Kedem, O., *J. Membr. Sci.* **2001,** 185, 223-236.

(34) Zhu, A.; Long, F.; Wang, X.; Zhu, W.; Ma, J., *Chemosphere* **2007,** 67, 1558-1565.

(35) Yeo, S. J.; Kang, H.; Kim, Y. H.; Han, S.; Yoo, P. J., *ACS Applied Materials & Interfaces* **2012,** 4, 2107-2115.

(36) Liu, X.; Bruening, M. L., *Chem. Mater.* **2004,** 16, 351-357.

(37) Amado, G. E.; Blanco, L. H., *Fluid Phase Equilib.* **2004,** 226, 261-265.

(38) Pan, C. F., *Can. J. Chem.* **1980,** 58, 1386-7.

(39) Archer, D. G.; Wood, R. H., *J. Solution Chem.* **1985,** 14, 757-780.

(40) Rodil, E.; Vera, J. H., *Fluid Phase Equilib.* **2001,** 187-188, 15-27.

(41) Farhat, T. R.; Schlenoff, J. B., *J. Am. Chem. Soc.* **2003,** 125, 4627-36.

(42) Stoykovich, M. P.; Daoulas, K. C.; Müller, M.; Kang, H.; de Pablo, J. J.;

Nealey, P. F., *Macromolecules* **2010,** 43, 2334-2342.

(43) Kielland, J., *J. Am. Chem. Soc.* **1937,** 59, 1675-1678.

(44) Marcel, M., Basic principles of membrane technology. In Kluwer Academic Publishers: 1996; p 320.

(45) Bard, A. J.; Faulkner, L. R., *Electrochemical methods: fundamentals and applications*. John Wiley & Sons, Ltd: New York, NY, 2000.

(46) Egueh, A.-N. D.; Lakard, B.; Fievet, P.; Lakard, S.; Buron, C., *J. Colloid Interface Sci.* **2010,** 344, 221-227.

(47) Bard, A. J.; Faulkner, L. R., Electrochemical Methods: Fundamentals and Applications. In *Electrochemical Methods: Fundamentals and Applications*, John Wiley & Sons, Ltd: New York, NY, 2000; p 72.

(48) Harned, H. S.; Polestra, F. M., *J. Am. Chem. Soc.* **1954,** 76, 2064-2065.

Chapter 3 Cation Separations in Electrodialysis through Membranes Coated with Polyelectrolyte Multilayers

3.1 Introduction

Alternating adsorption of polycations and polyanions is a simple method for ultrathin film formation with fine control over film thickness.[1, 2] For polyelectrolytes with a high charge density and solutions that do not contain supporting electrolytes, each adsorption step increases film thickness only ~2 nm.[3] Such control over film thickness makes polyelectrolyte multilayers (PEMs) particularly attractive as the selective skins of separation membranes because the skin permeance is inversely proportional to its thickness.

A number of studies demonstrate that layer-by-layer adsorption of PEMs can yield thin, essentially defect free films on porous supports.[4-6] Tailoring of deposition conditions (polyelectrolyte structure and concentration, pH, and supporting electrolyte composition and concentration) leads to relatively dense PEMs with highly charged surfaces,[7] and such films can serve as the selective skins of membranes for nanofiltration (NF),[8-13] reverse osmosis,[13-15] pervaporation,[12, 16, 17] and forward osmosis.[18-20] Highly

charged PEMs are especially attractive for their high selectivity for monovalent- over multivalent-ion passage in diffusion dialysis and NF.[8, 9, 21]

We observed K^+/Mg^{2+} selectivities >350 during diffusion dialysis through porous alumina membranes modified with $(PSS/PAH)_4$ films.[8] However, the K^+ flux in diffusion dialysis was relatively low (2.4±0.5 nmol cm^{-2} s^{-1}), and NF, which provides higher throughput, showed selectivities >20-fold lower than diffusion dialysis when comparing the same membranes and feed solutions.[8] Ideally, we would like to combine the selectivity of diffusion dialysis with a technique that provides more throughput (flux). This work investigates whether application of an electric current through a PEM-coated membrane (electrodialysis) can increase ion transport while maintaining the high monovalent/divalent ion selectivity of diffusion dialysis.

Electrodialysis through anion- and cation-exchange membranes is a well-known technique for potential applications such as brackish water desalination,[22, 23] water softening,[24] and desalting or deacidifying certain foods.[25] Typically an electric current or potential applied across a feed chamber bracketed by an anion- and a cation-exchange membrane leads to passage of salt from the chamber, where cations migrate toward the cathode and anions migrate to the anode. Couples of anion- and cation-exchange membranes placed between two electrodes create multiple feed and

concentrate compartments. In contrast, this paper investigates electrodialysis with PEM-modified membranes to separate monovalent from multivalent cations because the membrane is highly selective among cations and not simply between cations and anions.

Two recent papers examined electrodialysis through membranes coated with PEMs. Mulyati and coworkers reported that after modification of an anion-exchange membrane with a $(PSS/PAH)_7PSS$ coating, the Cl^-/SO_4^{2-} selectivity reversed from 0.8 to 2.5.[26] They also explored the antifouling potential of PEM-modified membranes in electrodialysis, and found that a negatively charged, hydrophilic PEM decreases the rate of membrane fouling by an anionic surfactant, sodium dodecylbenzene sulfonate.[26, 27] In other work, adsorption of single layers of polyethyleneimine or poly(styrene sulfonate) lead to increased monovalent/multivalent ion selectivities in electrodialysis.[28, 29] However, the selectivities we describe herein are at least an order of magnitude higher than those mentioned in prior studies.

This study employs $(PSS/PAH)_5$ films as a selective barrier on porous alumina or commercial NF membranes to separate monovalent and multivalent cations in diffusion dialysis and electrodialysis. We compare selectivities and fluxes in diffusion dialysis and electrodialysis, examine film stability during electrodialysis, and study how K^+ and Mg^{2+} fluxes depend on

the anion in the solution. Remarkably, K^+/Mg^{2+} selectivities in electrodialysis are typically >100, and with a commercial NF membranes as a support, electrodialysis fluxes are more than an order of magnitude higher than diffusion dialysis fluxes.

3.2 Experimental Section

3.2.1 Materials

Poly(sodium 4-styrenesulfonate) (PSS, M_W=70,000 Da) and poly(allylamine hydrochloride) (PAH, M_W=15,000 Da) were purchased from Sigma-Aldrich. Salts were obtained from Columbus Chemical Industries, Sigma-Aldrich, Spectrum Chemical, and J.T.Baker. All chemicals were used as received without further purification. Alumina membranes were purchased from Whatman (surface pore size 0.02 μm), and NF270 membranes were a gift from the Dow Chemical Company.

3.2.2 Surface Modification

Porous alumina membranes were cleaned with UV-O_3 (Boekel UV-Clean Model 135500) for 15 min to remove organic contaminants on the membrane surface, and NF270 membranes were rinsed and immersed in deionized water

for 5 min prior to film deposition. The alternating adsorption of PSS and PAH occurred by exposing the feed side of the membrane (membrane skin) to the polyanion or polycation solution for 5 min followed by 1 min of rinsing with deionized water to remove excess polyelectrolyte. Adsorption began with the polyanion, which likely adsorbs to the NF270 surface via hydrophobic interactions. Both the polyelectrolyte solutions contained 0.02 M polymer repeating units and were adjusted to pH 2.3. The PSS solution also contained 0.5 M NaCl, whereas 1 M NaCl was added to the PAH solution to increase the film's positive surface charge to enhance monovalent/multivalent cation separations.[9] The use of five PSS/PAH bilayers to coat membranes minimizes cation permeation through defects without giving a thick film that has a low permeance.[5] The membranes were stored in deionized water. (Drying membranes leads to a decrease in their monovalent/multivalent ion selectivities).

3.2.3 Diffusion Dialysis

The diffusion dialysis apparatus was described previously.[30] The membrane was clamped between source and receiving cells with an O-ring on source-phase side. The modified surface faced the source-phase solution. The source phase contained K^+ and Mg^{2+} salts that permeated through the

membrane to the receiving cell, and the discussion section provides specific solution compositions for each experiment. Both source-phase and receiving-phase solutions (initially 90 mL each) were stirred vigorously during passage of ions from the source phase to the receiving phase through the membrane. The effective area of alumina membranes (2.1 cm^2) was defined by a polyethylene ring affixed to the top of the membrane by the manufacturer. For NF270 membranes, the O-ring on the source side of the dialysis apparatus exposed an area of 3.15 cm^2. Periodically 1-mL aliquots were taken from each cell to determine the moles of ions permeating through the membrane per unit area as a function of time. These aliquots were analyzed using inductively couple plasma-optical emission spectroscopy (Varian 710-ES). All the experiments were performed with at least three different membranes, and the uncertainties represent the standard deviation.

3.2.4 Electrodialysis

The electrodialysis experiments used the same cells and membranes employed for diffusion dialysis to facilitate comparison of these two techniques. Platinum wire electrodes were inserted in each cell to apply an electric current through the membrane. To obtain an approximately constant current of 8 mA, a constant electric potential (4.44 V) was applied across a resistor (555 Ω)

using a CH Instruments model 604 potentiostat. As Figure 3.1(a) shows, the lead for the working electrode was connected to one end of the resistor, and the lead for the reference electrode was connect to the other end of the resistor as well as the Pt electrode in the source-phase solution. The lead for the counter electrode was connected to the Pt electrode in the receiving phase. However, the current in this apparatus is sometimes limited by the potentiostat and less than 8 mA. To achieve higher currents, we employed a DC power supply (Protek, 3006B) to apply a potential between electrodes in the source and receiving phases. A multimeter (TEK DMM249) in series measured currents (Figure 3.1(b)). The results and discussion section describes the solution compositions in the source and receiving phases for electrodialysis. Notably, the electrodialysis receiving phase contained both a sodium salt to make the solution conductive and an acid to prevent precipitation of $Mg(OH)_2$. The anode and cathode were in the source phase and receiving phase, respectively, so the current moved cations from the source phase to the receiving phase and anions from the receiving phase to the source phase. The primary electrode reactions likely generated protons in the source phase and hydroxide in the receiving phase. Solution pH values were determined with a pH meter after 1.5 h of electrodialysis.

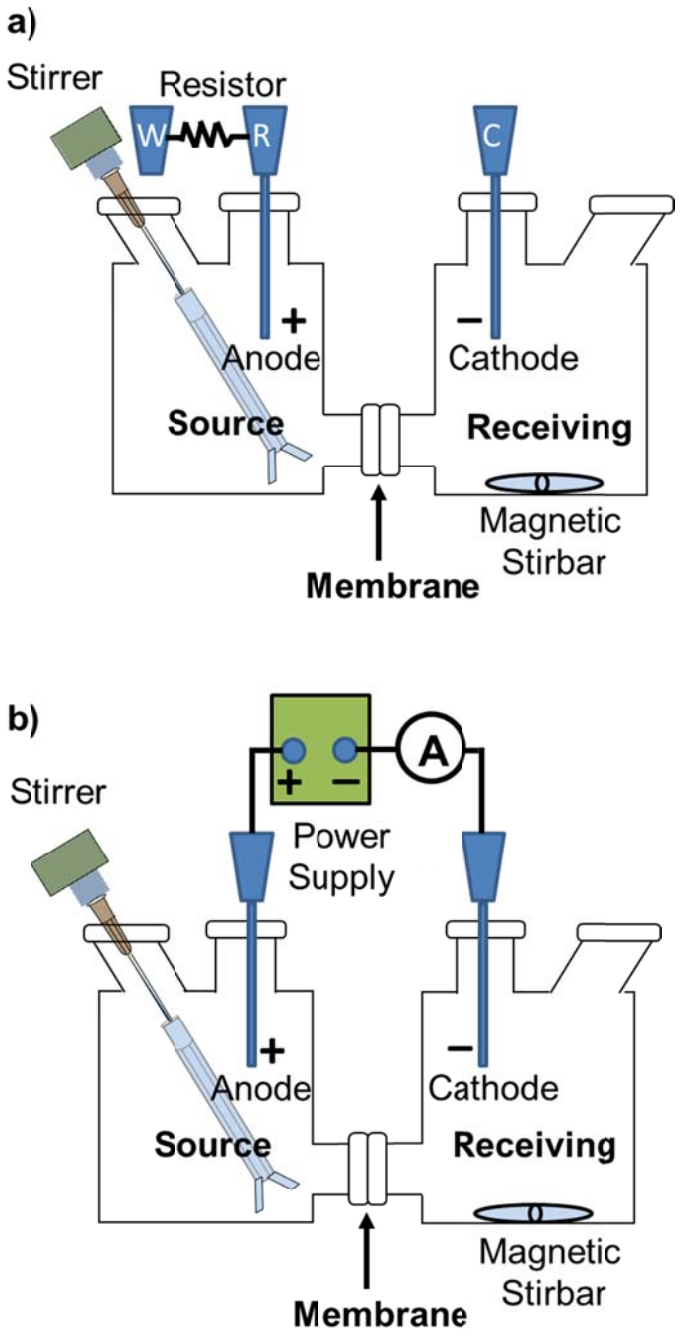

Figure 3.1 Home-built electrodialysis apparatuses consisting of two 100-mL glass cells filled with salt solutions connected by a 2.5 cm neck that contained the PEM-modified membrane. Both source and receiving phases were stirred vigorously to create homogeneous solutions. (a) By controlling the potential

Figure 3.1 (cont'd) across a resistor between the working and reference electrode terminals, a potentiostat controls the current through the working and counter electrodes. (b) An applied potential across the membrane generates a current that is determined with a multimeter.

3.2.5 Zeta potential

Streaming potentials were determined with a Brookhaven Instruments Electrokinetic Analyszer (Holtsville, NY) containing a clamping cell (Anton Paar, Graz, Austria). Polyethersulfone (PES) membranes (Pall Corp.,100 kDa, 30 mm × 50 mm) were used as substrates instead of alumina membranes due to the large surface area required by the clamping cell. The membranes were soaked in deionized water for 1 h before polyelectrolyte deposition, and the deposition procedure was the same as with the alumina membranes. The polyelectrolyte-modified, PES membranes were placed against a 10 mm x 20 mm piece of grooved poly(methyl methacrylate) (PMMA), and the streaming potential was measured between the two Ag/AgCl electrodes of the clamping cell during pumping of the test solutions (1 mM $MgCl_2$ or 1 mM $MgSO_4$) through the cell. As the PMMA spacer also contributes to the zeta potential, its zeta potential (ζ_{spacer}) must be subtracted from the sample zeta potential. Equation (1) shows the zeta potential for the test sample,

$$\zeta_{sample} = 2\zeta_{average} - \zeta_{spacer} \quad (3.1)$$

where ζ_{sample} is the zeta potential of the PEM-modified membrane, $\zeta_{average}$ is the effective zeta potential measured with the sample pressed against the PMMA spacer, and ζ_{spacer} is the zeta potential with a piece of PMMA pressed against the cell (-7.8 mV in $MgCl_2$ solution and 1.4 mV in $MgSO_4$ solution). The reported zeta potentials are the averages of values determined for three different pieces of PES membranes, and the uncertainties are the standard deviations of these values.

3.3 Results and Discussion

This work investigates whether the high diffusion-dialysis selectivities of PEM membranes translate to electrodialysis, and whether applied electric currents or potentials significantly increase ion flux compared to simple diffusion dialysis. Electrically driven transport adds several complications to a dialysis experiment, including electrode reactions that alter the compositions of source and receiving phases, generation of reactive species that may decrease membrane stability, and a need for a conductive receiving phase. Additionally, in electrodialysis several ions will carry current, but for energy-efficient separations the ion of interest should carry as high a fraction of the current as possible.

Below we compare diffusion dialysis and electrodialysis separations of K^+ and Mg^{2+} using PEM membranes deposited on either porous alumina or commercial NF membranes. We chose the K^+/Mg^{2+} separation because $(PSS/PAH)_4$-coated membranes show K^+/Mg^{2+} selectivities >350 in diffusion dialysis.[8] The next few subsections examine cation transport as a function of the accompanying anion during dialysis through $(PSS/PAH)_5$ films deposited on porous alumina. The anion affects flux, current efficiency, and membrane stability during separations. The final subsection examines electrodialysis through $(PSS/PAH)_5$ coatings on NF270 membranes. Relative to porous alumina, the NF270 support yields more convincing evidence that electrodialysis enhances ion flux while maintaining the high selectivities of diffusion dialysis.

3.3.1 Diffusion Dialysis and Electrodialysis with KCl and $MgCl_2$

In diffusion dialysis with a 0.01 M KCl, 0.01 M $MgCl_2$ source phase and an initial receiving phase of deionized water, a concentration gradient drives ions across the membrane. Moreover, because the concentration in the receiving phase is constant, the amount of K^+ in the receiving phase increases essentially linearly with time (Figure 3.2(a)). The amount of Mg^{2+} in the receiving also increases linearly, albeit very slowly, and in some cases the

increase is not detectable. Specifically, the KCl flux during diffusion dialysis through porous alumina membranes coated with a $(PSS/PAH)_5$ film is 3.5±0.6 nmol cm^{-2} s^{-1}, whereas $MgCl_2$ flux is 7.6±4.1 pmol cm^{-2} s^{-1}, and the K^+/Mg^{2+} selectivity is >290 (Table 3.1). [8]

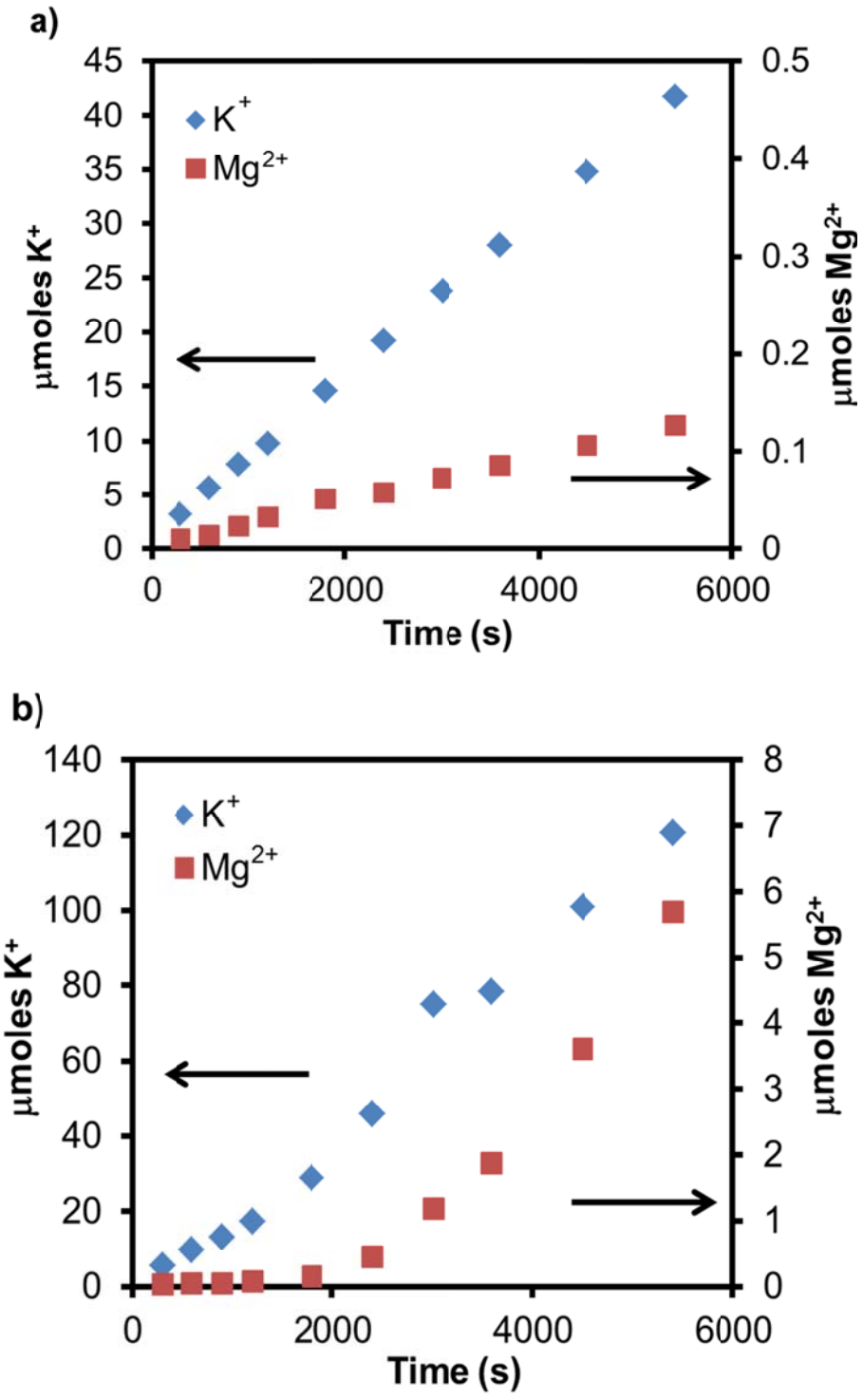

Figure 3.2 Moles of K^+ and Mg^{2+} in the receiving phase as a function of time during (a) diffusion dialysis with 0.01 M KCl, 0.01 M $MgCl_2$ in the source phase

Figure 3.2 (cont'd) and water in the receiving phase and (b) electrodialysis with 0.01 M KCl, 0.01 M $MgCl_2$ in the source phase and 0.04 M NaCl, 0.01 M HCl in the receiving phase. The membranes consisted of $(PSS/PAH)_5$ films on porous alumina, and the electrodialysis experiment employed 7.7 mA of current. Note the large differences in scales for K^+ and Mg^{2+}.

Table 3.1 Cation fluxes and K^+/Mg^{2+} selectivities in diffusion dialysis and electrodialysis with chloride or nitrate salts and $(PSS/PAH)_5$-modified alumina membranes.

	Diffusion Dialysis (Cl^- Salts)	Electrodialysis (Cl^- Salts)	Diffusion Dialysis (NO_3^- Salts)	Electrodialysis (NO_3^- Salts)
Source Phase	0.01 M KCl 0.01 M $MgCl_2$	0.01 M KCl 0.01 M $MgCl_2$	0.01 M KNO_3 0.01 M $Mg(NO_3)_2$	0.01 M KNO_3 0.01 M $Mg(NO_3)_2$
Receiving Phase	Deionized Water	0.04 M NaCl 0.01 M HCl	Deionized Water	0.04 M $NaNO_3$ 0.01 M HNO_3
K^+ Flux (nmol cm^{-2} s^{-1})	3.5±0.6	11.4±1.9	4.7±0.3	7.1±1.8
Mg^{2+} Flux (pmol cm^{-2} s^{-1})	7.6±4.1	16.2 ± 14.3 (initial 20 min) 1320±40 (last 45 min)	5.9±2.1	12.6±7.6
Selectivity	>290[a]	>390[a] (initial 20 min) 4.3±2.7 (last 45 min)	>540[a]	>340[a]
Current (mA)	-	~7.4	-	~7.6

[a]These values represent the lowest selectivity from at least 3 replicate experiments.

In electrodialysis experiments the receiving phase contained 0.04 M NaCl to decrease solution resistance and allow passage of significant currents, and 0.01 M HCl to prevent precipitation of $Mg(OH)_2$. As in diffusion dialysis, the source phase contained 0.01 M KCl and 0.01 M $MgCl_2$. During application of 7.7 mA of current across the membrane, the K^+ flux was 11.4±1.9 nmol cm^{-2} s^{-1}, or about 3 times the flux in diffusion dialysis (Table 3.1). For the first 20 min of electrodialysis, the Mg^{2+} flux was <30 pmol cm^{-2} s^{-1}, so the K^+/Mg^{2+} selectivity was >390, or similar to that in diffusion dialysis. Thus, the applied current initially increased K^+ flux compared to diffusion dialysis while maintaining selectivity. However, as Figure 3.2(b) shows, after the initial 30 min of electrodialysis the amount of Mg^{2+} in the receiving phase increased much more rapidly, and Mg^{2+} flux reached 1.3 nmol cm^{-2} s^{-1} over the last 30 min of the experiment. This enhanced Mg^{2+} flux gives a K^+/Mg^{2+} selectivity of only ~4. Subsequent diffusion dialysis through the same membranes also showed low K^+/Mg^{2+} selectivities, indicating that the membrane permeability changes during electrodialysis. This change in permeability likely stems from PEM damage due to Cl_2 generated during the electrodialysis. The standard electrode potential for chlorine generation is similar to that for water oxidation (Equations (3.2) and (3.3)). [31]

$$O_2 + 4H^+ + 4e^- \rightleftharpoons 2H_2O \quad E^o = 1.23\ V \tag{3.2}$$

$$Cl_2(g) + 2e^- \rightleftharpoons 2Cl^- \; E^o = 1.36\ V \tag{3.3}$$

We sensed a strong Cl_2 odor after long periods (4 h) of electrodialysis, and the membrane damage did not occur when using other anions in the source and receiving phases.

3.3.2 Diffusion dialysis and electrodialysis with KNO_3 and $Mg(NO_3)_2$

Nitrate has a similar mobility (see Table 3.2) and the same charge as chloride. Thus we thought that nitrate salts would give diffusion dialysis and electrodialysis cation fluxes similar to those with chloride salts while eliminating Cl_2 damage to the membrane. Table 3.1 shows that in diffusion dialysis (columns 2 and 4), K^+ and Mg^{2+} fluxes change by less than 35% when using nitrate rather than chloride.

Table 3.2 Electrophoretic mobilities (infinite dilution, 25 ºC) of ions relevant to this work.[31]

Cations	K^+	Na^+	H^+	Mg^{2+}
u_i (10^{-4} cm^2 s^{-1} V^{-1})	7.6	5.2	36.2	5.5
Anions	Cl^-	NO_3^-	OAc^-	SO_4^{2-}
u_i (10^{-4} cm^2 s^{-1} V^{-1})	7.9	7.4	4.2	8.3

Perhaps more importantly, K^+/Mg^{2+} selectivities are >340 in both diffusion dialysis and electrodialysis with nitrate salts, and these selectivities are stable over the course of the experiment (1.5 h). Thus, with nitrate salts electrodialysis does not damage the membrane. However, application of ~8 mA of current across the membranes only increases the K^+ flux from 4.7 to 7.1 nmol cm^{-2} s^{-1}. If K^+ were the only ion that carries current across the membrane we would expect an electromigration flux of 40 nmol cm^{-2} s^{-1} with 8 mA of current.[31] Equation (3.4) shows how the transference number for a given ion, t_i-the fraction of current carried by that ion, depends on the ion mobility, u_i, charge, z_i, and concentration, C_i, along with the product $|z_j|u_j C_j$ for all the ions in the solution.

$$t_i = \frac{|z_i| u_i C_i}{\sum_j |z_j| u_j C_j} \quad (3.4)$$

The small K^+ flux during electrodialysis implies a low K^+ transference number. However, the even lower Mg^{2+} flux across the membrane suggests that K^+ should be the primary current-carrying cation unless the proton concentration on the source-phase side of the membrane becomes significant. Unfortunately, due to proton generation at the cathode and diffusion of protons from the receiving phase to the source phase, the pH of the source phase decreases from ~5 to ~2 over 1.5 h of electrodialysis. Given that the mobility of protons is 5 times the mobility of K^+ ions (Table 3.2), the protons in the receiving phase may carry a large fraction of the current.

Nitrate electromigration from the receiving phase to the source phase will also carry current. Notably, the K^+ concentration in the source phase is 0.01 M whereas the NO_3^- concentration in the receiving phase is 0.05 M. The combination of proton and NO_3^- electromigration likely explain why the experimental K^+ flux increase is only 2.4 nmol cm^{-2} s^{-1} on going from diffusion to electrodialysis.[8] The increase might be even lower than this value if in diffusion dialysis the receiving phase contained the same salts as in electrodialysis (see below).

3.3.3 Diffusion Dialysis and Electrodialysis with K_2SO_4 and $MgSO_4$

Relative to salts containing monovalent anions, diffusion dialysis and electrodialysis using salts with multivalent anions may change fluxes and selectivities because of either a low anion permeability or divalent anion adsorption that changes the membrane charge or structure. In diffusion dialysis with a 0.01 M KCl, 0.01 M $MgCl_2$ source phase, the Mg^{2+} flux is ~8 pmol cm^{-2} s^{-1} and the K^+/Mg^{2+} selectivity is >290 (Table 3.1). In contrast, with the same membranes diffusion dialysis with a 0.005 M K_2SO_4, 0.01 M $MgSO_4$ source phase lead to a >10-fold increase in the Mg^{2+} flux and a K^+/Mg^{2+} selectivity of only ~30 (Table 3.3). A subsequent experiment with the same membranes showed a K^+/Mg^{2+} selectivity of >320 when the source-phase solution returned to 0.01 M KCl, 0.01 M $MgCl_2$. Thus, SO_4^{2-} does not damage the PEM, but it decrease selectivity when present. The large selectivity drop in the presence of SO_4^{2-} might result from a change in the PEM structure that enhances the membrane permeability. However, the K^+ flux with the sulfate salts does not increase dramatically compared to chloride salts, and a neutral molecule, nitrobenzene has a similar flux through the membrane with both chloride and nitrate salts (1.1±0.1 nmol cm^{-2} s^{-1} in a 0.01 M KCl, 0.01 M $MgCl_2$ solution and 1.4±0.1 nmol cm^{-2} s^{-1} in 0.005 M K_2SO_4, 0.01 M $MgSO_4$ solution).

Although the sulfate anion does not significantly alter K^+ or nitrobenzene flux, it decreases the PEM surface charge, which likely gives rise to the increase in Mg^{2+} flux. Measurements of streaming potentials show that $(PSS/PAH)_5$-modified PES membranes have a zeta potential of 27 ± 5 mV in 1 mM $MgCl_2$ and 8 ±1 mV in 1 mM $MgSO_4$, indicating that the polyelectrolyte film has less surface charge when exposed to a $MgSO_4$ solution rather than a $MgCl_2$ solution. Adsorption of sulfate presumably decreases the electrostatic exclusion of Mg^{2+} from the film.

Although sulfate salts give rise to lower selectivities than chloride salts in diffusion dialysis, electrodialysis with sulfate salts gives a K^+/Mg^{2+} selectivity of 46, which is similar to the diffusion dialysis selectivity. (In electrodialysis, the source phase was the same as in diffusion dialysis, but the receiving phase contained 0.018 M Na_2SO_4 and 0.005 M H_2SO_4, rather than deionized water.) Importantly, as Table 3.3 shows, the K^+ flux in electrodialysis with ~6.9 mA of current is 5 times the K^+ flux in diffusion dialysis with deionized water as the receiving phase. However, when diffusion dialysis employs the same receiving phase composition as in electrodialysis, the K^+ fluxes in diffusion dialysis and electrodialysis are very similar (Table 3.3). In diffusion dialysis with salt and acid in the receiving phase, diffusion of protons and Na^+ from the

receiving phase to the source phase should generate a transmembrane potential that accelerates K^+ transport. This diffusion potential should decrease during electrodialysis as protons generated in the source phase reduce the proton concentration gradient across the membrane. Thus, quantitating the increase in K^+ transport during electrodialysis is challenging because the composition of the source and receiving phases may change due to electrogenerated species. In any case, K^+ fluxes are much smaller than the expected value of 40 nmol cm^{-2} s^{-1} based on K^+ carrying all of the applied current.

Table 3.3 Cation fluxes and K^+/Mg^{2+} selectivities in diffusion dialysis and electrodialysis with sulfate salts and $(PSS/PAH)_5$-modified alumina membranes.

	Diffusion Dialysis	Diffusion Dialysis	Electrodialysis
Source Phase	0.005 M K_2SO_4 0.01 M $MgSO_4$	0.005 M K_2SO_4 0.01 M $MgSO_4$	0.005 M K_2SO_4 0.01 M $MgSO_4$
Receiving Phase	Deionized Water	0.018 M Na_2SO_4 0.005 M H_2SO_4	0.018 M Na_2SO_4 0.005 M H_2SO_4
K^+ Flux ($nmol/cm^{-2}\ s^{-1}$)	2.2±1.5	8.3±0.2	8.3±3.9
Mg^{2+} Flux ($pmol/cm^{-2}\ s^{-1}$)	86±6	243±103	181±87
Selectivity	30±12	38±13	46±0
Current (mA)	-	-	~6.9

3.3.4 Diffusion dialysis and electrodialysis with KOAc and $Mg(OAc)_2$

Acetate solutions might give rise to higher K^+ transference numbers in the membrane because acetate will buffer the source-phase solution to keep proton concentrations low. Moreover, the aqueous mobility of acetate is only 50% of that for Cl^- (Table 3.2), and a low acetate mobility in the membrane should also lead to higher cation transference numbers during transport

through the membrane. In diffusion dialysis with 0.01 M KOAc and 0.01 M $Mg(OAc)_2$ in the source phase and deionized water as the receiving phase, the K^+ flux is about 20-40% lower than the same experiments with chloride or nitrate salts (compare Tables 3.1 and 3.4). Presumably, this reflects a low membrane permeability to acetate salts in comparison with chloride and nitrate salts.

Table 3.4 Cation fluxes and K^+/Mg^{2+} selectivities in diffusion dialysis and electrodialysis with acetate or nitrate salts and $(PSS/PAH)_5$-modified alumina membranes.

	Diffusion Dialysis	Diffusion Dialysis	Electro-dialysis	Diffusion Dialysis	Electro-Dialysis	Electro-Dialysis[b]
Source Phase	0.01 M KOAc 0.01 M $Mg(OAc)_2$	0.01 M KOAc 0.01 M $Mg(OAc)_2$ 0.03 M HOAc	0.01 M KOAc 0.01 M $Mg(OAc)_2$ 0.03 M HOAc	0.01 M KOAc 0.01 M $Mg(OAc)_2$ 0.03 M HOAc	0.01 M KOAc 0.01 M $Mg(OAc)_2$ 0.03 M HOAc	0.01 M KOAc 0.01 M $Mg(OAc)_2$ 0.03 M HOAc
Receiving Phase	Deionized Water	0.01 M NaOAc 0.03 M HOAc	0.01 M NaOAc 0.03 M HOAc	0.01 M $NaNO_3$ 0.03 M HOAc	0.01 M $NaNO_3$ 0.03 M HOAc	0.01 M $NaNO_3$ 0.03 M HOAc
K^+ Flux ($nmol/cm^{-2}\ s^{-1}$)	2.8±0.1	1.1±0.1	1.3±0.3	1.2±0.1	3.0±0.2	4.8±0.5
Mg^{2+} Flux ($pmol/cm^{-2}\ s^{-1}$)	8.8±4.3	5.0±2.7	6.4±2.8	5.3±1.5	7.8±4.1	9.8±1.6
Selectivity[a]	>190	>125	>110	>180	>220	>450
Current (mA)	-	-	~4.2	-	~5.0	~16

[a]These values represent the lowest selectivity from at least 3 replicate experiments.

[b]Electrodialysis carried out with the apparatus in Figure 3.1(b) to obtain higher currents. Other electrodialyses were carried out with set up shown in Figure 3.1(a).

For electrodialysis with acetate salts, we employed a receiving phase that contained 0.01 M NaOAc to provide conductivity and 0.03 M HOAc to acidify the solution and prevent precipitation of $Mg(OH)_2$. We also performed diffusion dialysis with this receiving phase to facilitate comparisons of diffusion dialysis and electrodialysis. Unfortunately, application of an electric current (4 mA) increased flux only 20% relative to diffusion dialysis with the same receiving phase, again showing a very low transference number for K^+.

Unexpectedly, if KNO_3 instead of KOAc is the supporting salt in the receiving phase, K^+ flux is 2.5 times the flux in diffusion dialysis with the same receiving phase (Table 3.4). With 16 mA of current, the K^+ flux is 4 times that in diffusion dialysis. Thus this particular system shows the largest increase in flux on going from diffusion dialysis to electrodialysis through coated porous alumina membranes. Although we reproduced this result with 3 different membranes at each current level, the reason for the increased K^+ flux in electrodialysis when using KNO_3 rather than KOAc in the receiving phase is not clear to us. The lower pH of the receiving phase with KNO_3 or a higher permeability to NO_3^- than acetate should decrease the transference number for K^+, leading to a lower electrodialysis flux. Nevertheless, the high K^+/Mg^{2+} selectivity of 500±40 along with the high K^+ flux in electrodialysis (4-fold higher than in diffusion dialysis) provides strong evidence that the selectivity in

electrodialysis is the same as in diffusion dialysis. Moreover, we performed 1.5-h electrodialysis experiments 8 times with the same membrane without losing the high monovalent/multivalent ion selectivity or K^+ flux. Thus, in the absence of chloride, these membranes are stable during electrodialysis.

3.3.5 Electrodialysis and diffusion dialysis through PEMs deposited on NF270 membranes

Because alumina membranes are fragile and expensive, we also investigated diffusion dialysis and electrodialysis through $(PSS/PAH)_5$ films deposited on NF270 nanofiltration membranes. Figure 3.3 shows the amount of K^+ and Mg^{2+} in the receiving phase as a function of time during diffusion dialysis followed by electrodialysis with the same solutions and membranes. Interestingly, although the coated NF270 membranes allow only very low fluxes (170 ± 30 pmol cm^{-2} s^{-1}) during diffusion dialysis with sulfate salts, in electrodialysis the K^+ flux is 7.6 ± 0.9 nmol cm^{-2} s^{-1} and the K^+/Mg^{2+} selectivity is 95 ± 42 when the source and receiving phases contain sulfate ions. The dramatic increase in flux upon application of current shows that essentially all of the K^+ transport results from electromigration. Moreover, the selectivity is at least as high as with alumina supports, which show decreased K^+/Mg^{2+} selectivities when sulfate, rather than chloride or nitrate, is the

counterion. Electrodialysis with bare NF270 membranes showed K^+/Mg^{2+} selectivities of only 11.

Figure 3.3(b) shows that the flux of both ions during electrodialysis decreases with time, most likely due to a buildup of hydrogen ions on the feed side and a corresponding decrease in K^+ and Mg^{2+} transference numbers. (The flux values given above are average fluxes over the entire experiment.) Using the average flux values, the K^+ transference number is 0.34 for the 6.8 mA of current in this experiment. (A current of 6.8 mA should give a K^+ flux of 22.4 nmol cm^{-2} s^{-1} if the K^+ tranferrence number were 1.) This is the highest transference number that we saw, perhaps because of a low SO_4^{2-} permeability. The transference number decreases with time due to the decreased pH of the source phase. Low transference numbers are clearly a major challenge when not using anion-exchange or cation-exchange membranes for electrodialysis. With ion-exchange membranes, only cations or anions pass through the membrane so transference numbers may be high relative to corresponding transference numbers in PEMs that allow passage of both cations and anions. However, the high selectivities of PEMs may make them attractive for purifying specific ions.

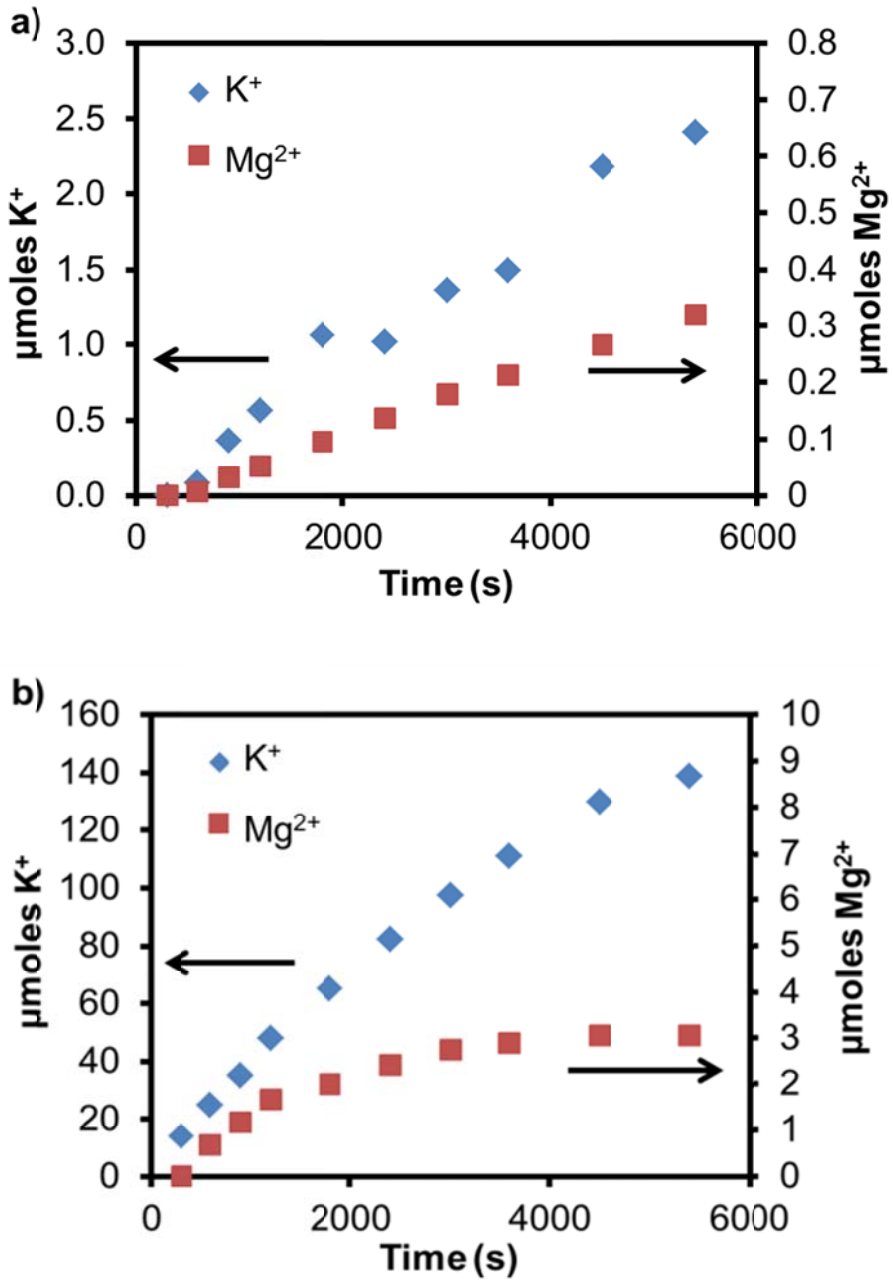

Figure 3.3 Moles of K^+ and Mg^{2+} in the receiving phase as a function of time during (a) diffusion dialysis with 0.005 M K_2SO_4, 0.01 M Mg SO_4 in the source phase and 0.018M Na_2SO_4, 0.005M H_2SO_4 in the receiving phase and (b) subsequent electrodialysis using the same membranes and source and

Figure 3.3 (cont'd) receiving phases. Dialysis occurred through $(PSS/PAH)_5$ films on NF270 membranes, and the electrodialysis experiment employed 6.8 mA of current. Note the large differences in scales for K^+ and Mg^{2+} and for diffusion dialysis and electrodialysis.

When using chloride solutions, electrodialysis with the coated NF270 membranes gives a K^+/Mg^{2+} selectivity of 62±13, and the K^+ flux is again much higher in electrodialysis (7.4 ± 0.5 nmol cm^{-2} s^{-1}) than diffusion dialysis (78 ± 20 pmol cm^{-2} s^{-1}). Similar to NF270 membranes with sulfate salts, the K^+ transference number decreases with time, likely due to a buildup of source-phase hydrogen ions. In some cases, the Mg^{2+} increases with time, suggesting that these membranes may also suffer from instability due to chlorine generation.

3.4 Conclusions

Application of a current through $(PSS/PAH)_5$-coated membranes can increase the K^+ flux relative to diffusion dialysis while maintaining K^+/Mg^{2+} selectivities >100 or more. However, selectivities depend on the anion of the salts as well as the membrane support. Sulfate anions decrease membrane

zeta potentials and reduce K^+/Mg^{2+} selectivities to ~30 for diffusion dialysis through $(PSS/PAH)_5$ films adsorbed on porous alumina. In the case of chloride salts, Cl_2 generation in electrochemical reactions appears to damage membranes coated with $(PSS/PAH)_5$ and greatly reduces selectivity. $(PSS/PAH)_5$-coated NF270 membranes show a 45-fold increase in flux upon application of an electric current, mostly because the diffusion dialysis flux through these membranes is low. One drawback to these separations is that the K^+ flux is at most ~35% of the flux that would occur if K^+ carried all the current. Protons and anions carry most of the current.

REFERENCES

REFERENCES

(1) Decher, G., *Science* **1997,** 277, 1232-1237.

(2) Decher, G.; Hong, J. D., *Ber. Bunsen-Ges. Phys. Chem. Chem. Phys.* **1991,** 95, 1430-1434.

(3) Harris, J. J.; Bruening, M. L., *Langmuir* **2000,** 16, 2006-2013.

(4) Zhang, G. J.; Song, X.; Ji, S. L.; Wang, N. X.; Liu, Z. Z., *J. Membr. Sci.* **2008,** 325, 109-116.

(5) Harris, J. J.; Stair, J. L.; Bruening, M. L., *Chem. Mat.* **2000,** 12, 1941-1946.

(6) Sullivan, D. M.; Bruening, M. L., *Chem. Mat.* **2003,** 15, 281-287.

(7) Dubas, S. T.; Schlenoff, J. B., *Macromolecules* **1999,** 32, 8153-8160.

(8) Cheng, C.; Yaroshchuk, A.; Bruening, M. L., *Langmuir* **2013,** 29, 1885-1892.

(9) Ouyang, L.; Malaisamy, R.; Bruening, M. L., *J. Membr. Sci.* **2008,** 310, 76-84.

(10) Su, B. W.; Wang, T. T.; Wang, Z. W.; Gao, X. L.; Gao, C. J., *J. Membr. Sci.* **2012,** 423, 324-331.

(11) Malaisamy, R.; Bruening, M. L., *Langmuir* **2005,** 21, 10587-10592.

(12) Zhao, Q.; An, Q. F. F.; Ji, Y. L.; Qian, J. W.; Gao, C. J., *J. Membr. Sci.* **2011,** 379, 19-45.

(13) Jin, W. Q.; Toutianoush, A.; Tieke, B., *Langmuir* **2003,** 19, 2550-2553.

(14) Fadhillah, F.; Zaidi, S. M. J.; Khan, Z.; Khaled, M. M.; Rahman, F.; Hammond, P. T., *Desalination* **2013,** 318, 19-24.

(15) Toutianoush, A.; Jin, W. Q.; Deligoz, H.; Tieke, B., *Appl. Surf. Sci.* **2005,** 246, 437-443.

(16) Zhu, Z.; Feng, X.; Penlidis, A., *Mater. Sci. Eng., C* **2007,** 27, 612-619.

(17) Yin, M. J.; Qian, J. W.; An, Q. F.; Zhao, Q. A.; Gui, Z. L.; Li, J., *J. Membr. Sci.* **2010,** 358, 43-50.

(18) Saren, Q.; Qiu, C. Q.; Tang, C. Y. Y., *Environ. Sci. Technol.* **2011,** 45, 5201-5208.

(19) Duong, P. H. H.; Zuo, J.; Chung, T. S., *J. Membr. Sci.* **2013,** 427, 411-421.

(20) Qi, S. R.; Li, W. Y.; Zhao, Y.; Ma, N.; Wei, J.; Chin, T. W.; Tang, C. Y. Y., *J. Membr. Sci.* **2012,** 423, 536-542.

(21) Hoffmann, K.; Friedrich, T.; Tieke, B., *Polym. Eng. Sci.* **2011,** 51, 1497-1506.

(22) Walha, K.; Ben Amar, R.; Firdaous, L.; Quemeneur, F.; Jaouen, P., *Desalination* **2007,** 207, 95-106.

(23) Strathmann, H., *Desalination* **2010,** 264, 268-288.

(24) Kabay, N.; Demircioglu, M.; Ersöz, E.; Kurucaovali, I., *Desalination* **2002,** 149, 343-349.

(25) Strathmann, H., *Sep. Purif. Technol.* **1985,** 14, 41-66.

(26) Mulyati, S.; Takagi, R.; Fujii, A.; Ohmukai, Y.; Matsuyama, H., *J. Membr. Sci.* **2013,** 431, 113-120.

(27) Mulyati, S.; Takagi, R.; Fujii, A.; Ohmukai, Y.; Maruyama, T.; Matsuyama, H., *J. Membr. Sci.* **2012,** 417, 137-143.

(28) Sata, T.; Yamaguchi, T.; Matsusaki, K., *J. Membr. Sci.* **1995,** 100, 229-238.

(29) Sata, T.; Izuo, R., *Colloid Polym. Sci.* **1978,** 256, 757-769.

(30) Liu, X. Y.; Bruening, M. L., *Chem. Mat.* **2004,** 16, 351-357.

(31) Vanýsek, P., Ionic Conductivity and Diffusion at Infinite Dilution. In *CRC Handbook of Chemistry and Physics, 94th Edition*, CRC Press: 2013.

Chapter 4. Towards Electrically Driven Ion Separations in Porous Membranes Modified with Conductive Polymer Films

4.1 Introduction

Nanofiltration (NF) and reverse osmosis (RO) are both pressure-driven membrane processes that require less energy than conventional water-treatment techniques such as distillation. Nevertheless, increases in permeability and selectivity will further enhance the efficiency of membrane processes. High charge densities at the membrane surface, in particular, may dramatically increase ion-transport selectivities in nanofiltration, diffusion dialysis and electrodialysis because charged surfaces exclude ions with the same charge, especially multivalent ions.[1, 2] A number of studies aimed to increase membrane surface charge to enhance monovalent/multivalent ion selectivities.[3, 4] We hypothesized that an electrical potential applied between a conducting, permeable membrane skin and the surrounding solution would further exclude anions or cations, particularly divalent ions, to increase rejections and ion-transport selectivities in NF or diffusion dialysis (Figure 4.1). In addition, application of an electrical potential will help elucidate how membrane surface charge affects ion rejections and ion-transport selectivities.

Polyaniline (PAN) was the first polymer reported to possess metallic conductivity.[5] When doped with acid, films of the half-oxidized form of PAN (emeraldine) show a conductivity of 70 S cm^{-1}.[6] In some cases, PAN membranes are highly selective in gas separations, which demonstrates that these materials have a relatively dense, defect-free structure.[7, 8] To fabricate a membrane with a high water permeability to examine ion separations, we deposited PAN nanofibers as a conductive and permeable skin layer on a porous support. The nanofibers align perpendicular to the support and should not provide a significant resistance to water flow. There are numerous approaches to the synthesis of PAN nanofibers including polymerization in the presence of hard templates,[9-12] electrospinning,[13, 14] interfacial polymerization,[10, 15] and seeding polymerization.[16-18] Chiou et al. developed dilute polymerization to synthesize aligned PAN fibers by exposing a substrate to monomer and oxidant solutions, which is particularly simple and inexpensive.[6, 19] This chapter describes modification of membranes with PAN nanofibers through dilute polymerization and early studies of whether potentials applied with these membranes affect ion transport.

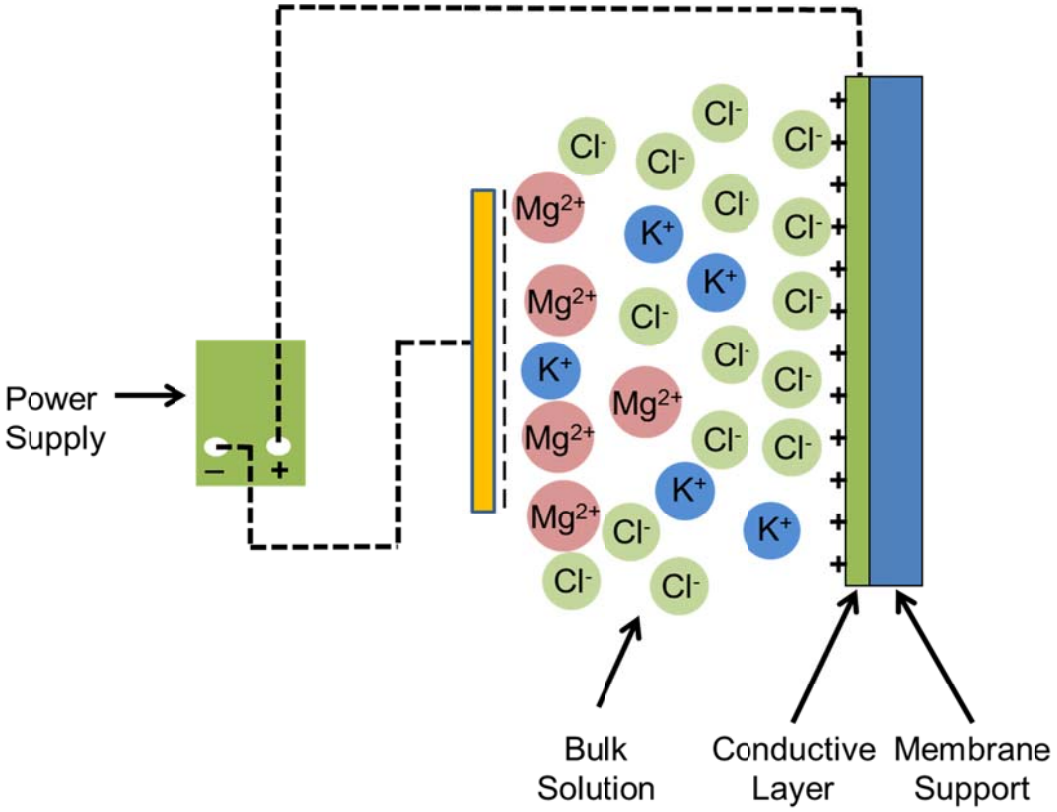

Figure 4.1 Illustration of an applied potential between a conductive membrane skin and an electrode in solution. The electrical double layer that develops at the membrane surface should exclude ions (cations in this case) to enhance ion rejections and monovalent/divalent ion selectivities.

4.2 Experimental Section

4.2.1 Materials

Aniline, ammonium persulfate, perchloric acid, poly(sodium 4-styrenesulfonate) (PSS, M_W=70 000 Da), poly(allylmine hydrochloride) (PAH, M_W=15 000 Da) and salts were purchased from Sigma-Aldrich and used without further purification. Polyvinylidene difluoride (PVDF) membranes (Durapore® Millipore, 0.45 μm, hydrophobic), Polyethersulfone (PES) membranes (Pall Corp., 100 kDa), and alumina membranes (Whatman 0.02 μm) were utilized as the porous substrate for conductive film deposition.

4.2.2 Dilute PAN polymerization on membranes

The alumina membranes were first modified with 2 bilayers of PSS/PAH to partially cover the pores and generate a relatively smooth surface for subsequent deposition of polyaniline nanofibers.[1] Specifically, alumina membranes were cleaned with UV/O_3 (Boekel UV-Clean Model 135500) for 15 min, and the top surface of the membrane was sequentially exposed to polyanion (0.02 M PSS, 0.5 M NaCl, pH 2.3) and polycation (0.02 M PAH, 1 M NaCl, pH 2.3) solutions for 5 min with a 1 min rinse with deionized water after exposure to each polyelectrolyte solution. PVDF and PES membranes were used as received. The $(PSS/PAH)_2$ modified alumina membranes and bare

PVDF or PES membranes were floated (with the membrane active layer down) on a solution which contained 0.02 M aniline, 0.01 M $(NH_4)S_2O_8$ and 1 M $HClO_4$. The solution was stirred for 24 h in an ice bath. PAN nanofibers were generated at the solution-air interface, on the membrane surface and in the solution as well.

4.2.3 Membrane Characterization

The membranes were cracked in liquid nitrogen, mounted on a glass slide with carbon glue and subsequently sputter coated (Pelco model SC-7 auto sputter coater) with 8 nm of gold. Scanning electron microscope (SEM) images were obtained with a Hitachi S-4700 II field-emission SEM. The PAN-modified PVDF membranes were etched with a focused ion beam to generate a tilted and smooth cross section to observe the film formation on the membrane surface by dual-column focused ion beam–secondary electron microscopy (FIBSEM, Carl Zeiss Auriga).

The membrane conductivity was measured using 4-probe measurements (Lucas Signatone Corp, 302 Resistivity Stand). Modified membranes were immersed in 1 M HCl or 0.02 M phosphate buffer solution (PBS) at pH 2, dried in air, and placed on a glass slide with the four probes pressing gently on the membrane. At least four measurements were carried out with in one area of the membrane and at least four areas were interrogated. A contact angle

analyzer (FTÅ200 (first ten angstroms)) was used at room temperature to evaluate the membrane hydrophobicity.

4.2.4 Ion Separations

NF with an applied electrical potential was performed with the home-built apparatus shown in Figure 4.2. The feed solution contained 0.01 M $MgCl_2$ and 0.01 M KCl, with 0.02 M phosphate buffer solution (PBS) at pH 2. We employed a low-pH solution because polyaniline exhibits poor conductivity in solutions with pH values higher than 3.[20] The feed solution was pressurized with N_2 and forced through a stainless prefilter (Mott Corp.), a flow meter, and across the PAN-modified PES membrane using a centrifugal pump. The NF cell exposed a membrane area of 2.4 cm^2, and the rententate was circulated back to the feed tank. Figure 4.3 shows the design of the membrane cell. The conductive membrane served as one electrode and the gold-coated portion of the upper piece of the cell served as a second electrode. The electrical potential drop was applied between the membrane surface (through the copper O-ring) and the upper electrode. Permeate aliquots (<10 mL) were collected without electrical potential applied and with 2 V applied at the membrane surface (the membrane was positive with respect to the upper electrode). The feed solution, which had an initial volume of 2 L, was sampled at the end of the experiment, and all solution concentrations were determined

using inductively couple plasma-optical emission spectroscopy (Varian 710-ES).

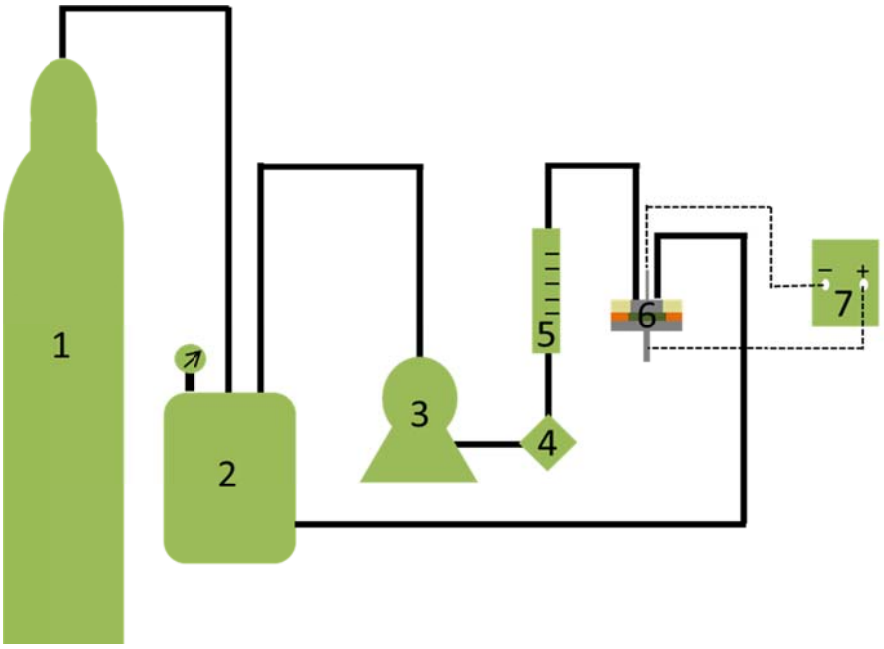

Figure 4.2 NF apparatus: (1) N_2 tank, (2) stainless steel feed tank, (3) centrifugal pump, (4) prefilter, (5) flowmeter, (6) membrane cell, and (7) power supply. All solid lines represent pressurized tubing, and dashed lines denote electrical wires.

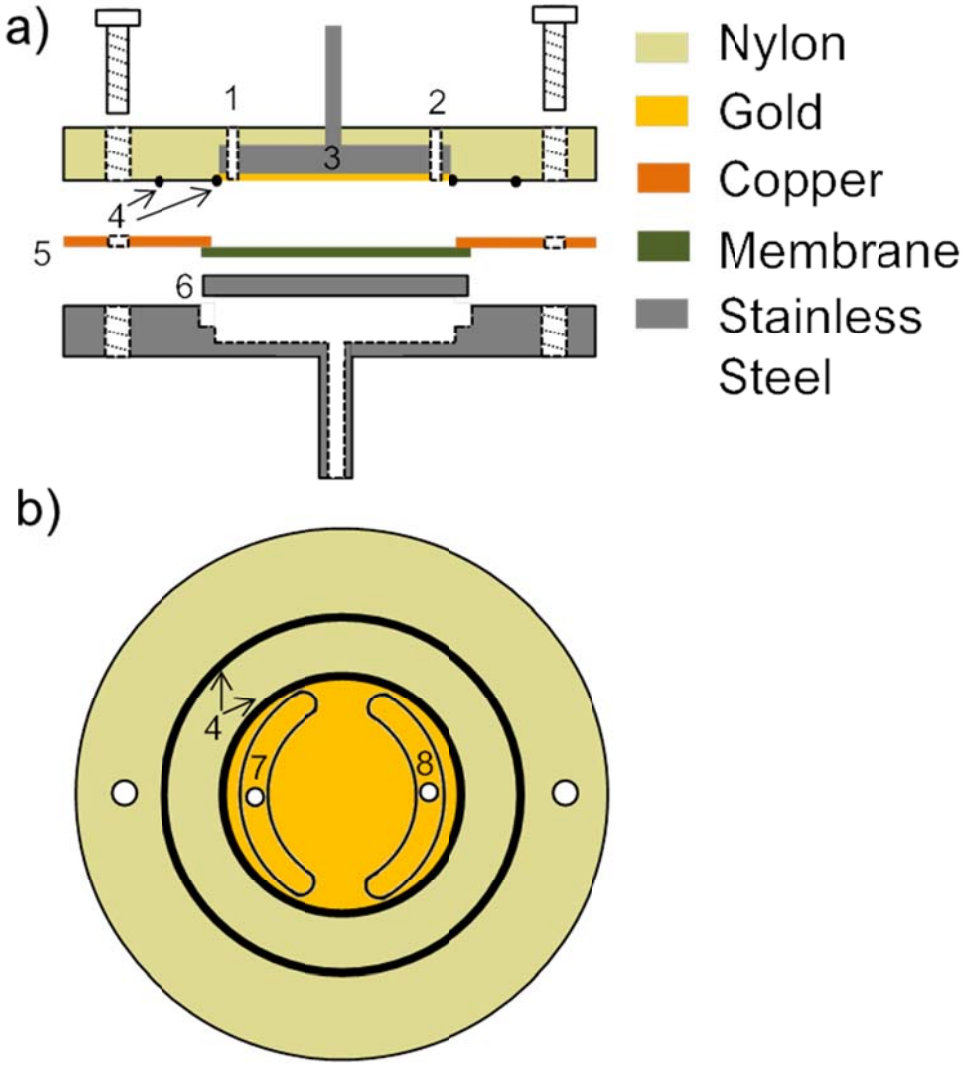

Figure 4.3 Diagram of the membrane cell for NF. a) side-view cross section: (1) and (2) inlet/outlet ports (threads not shown), (3) upper electrode coated with a thin layer of gold, (4) rubber O-rings, (5) membrane that functions as an electrode via copper foil connections attached to the membrane with silver epoxy, (6) porous stainless steel frit. b) a bottom view of the upper portion of the cell: (4) rubber O-rings, (7) and (8) inlet and outlet flow distribution channels.

Diffusion dialysis was performed as described previously.[21] A $(PSS/PAH)_2$/PAN-modified membrane with a copper foil ring attached to the top of the membrane with silver epoxy was sandwiched between the source and receiving cells, and the solutions in each cell (initially 90 mL each) were stirred vigorously. The cells exposed a membrane area of 2.1 cm^2. One-mL aliquots were withdrawn periodically from the receiving cell to monitor the analyte flux as a function of time, and similar aliquots were taken from the source phase to maintain equal volumes. The source phase contained 0.01 M $MgCl_2$ and 0.01 M KCl with 0.02 M PBS at pH 2, while the receiving phase initially contained only pH 2 PBS. To apply the electrical potential, the working electrode of the potentiostat was connected to the copper ring on the membrane. A Ag/AgCl reference electrode and a platinum counter electrode were placed in the source cell. A constant electric potential (-2 V) was applied between the membrane surface and the reference electrode using a CH Instruments model 604 potentiostat.

4.3 Results and Discussion

4.3.1 Membrane Characterization

The bare PVDF membrane has a static water contact angle of 113° at room temperature. After polyaniline modification, the water contact angle decreases to 25°, showing that the polyaniline nanofibers make the

membrane surface hydrophilic. The PAN modified membrane shows an average sheet resistance of 4000 ± 3000 Ω/sq after immersion in 1 M HCl, and 9000 ± 2000 Ω/sq after immersed in 0.02 M PBS at pH 2.

Figure 4.4 shows the top of an alumina membrane modified with a $(PSS/PAH)_2$ film and PAN nanofibers. The fibers are clearly visible on the membrane surface and completely cover the pores in the alumina support. Figure 4.5 shows SEM images of PVDF membranes before and after modification. The fibers are uniformly deposited on the spongy membrane surface, but they do not cover the relatively large pores in these membranes. Figure 4.6 presents images of cross sections of the membranes, and indicates that the nanofiber length is on the order of a tens of nanometers. The PAN nanofibers deposit only on the membrane surface and do not modify the inner pores. The PVDF membrane has a hydrophobic surface, which likely serves as a barrier to monomer diffusion from aqueous solution into the membrane inner pores.

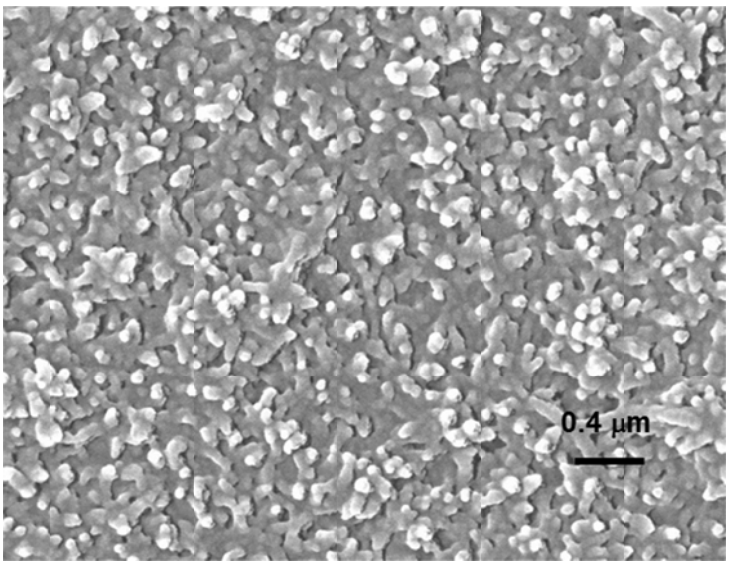

Figure 4.4 SEM image of the top of a $(PSS/PAH)_2$/PAN-coated alumina membrane.

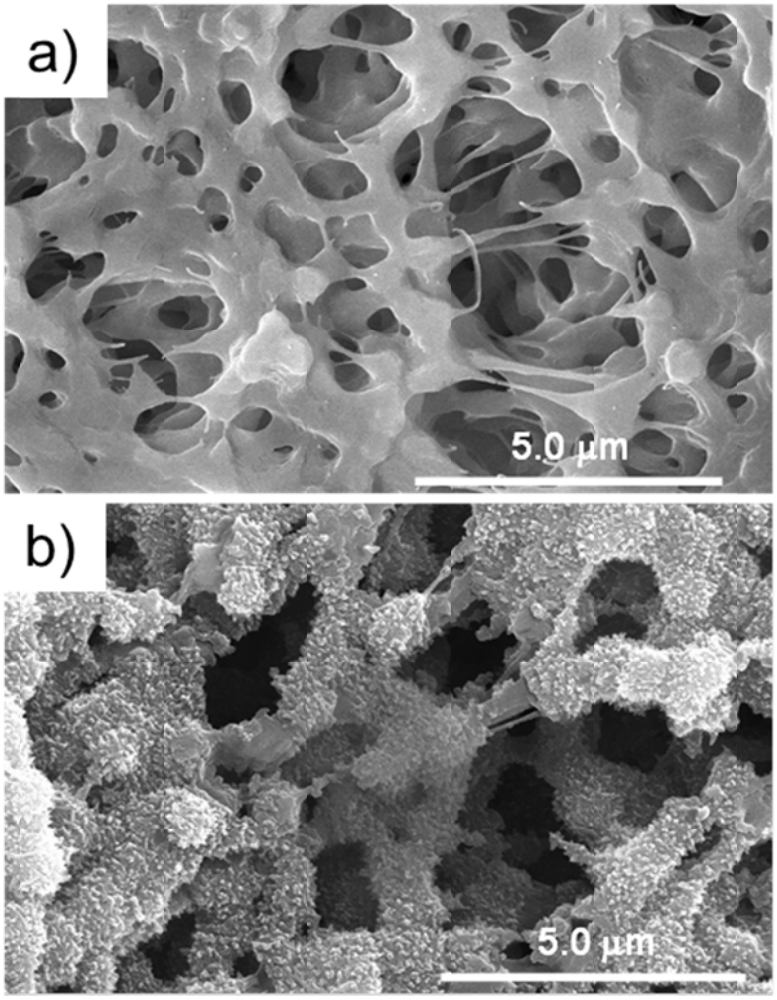

Figure 4.5 SEM images of the tops PVDF membranes (a) before and (b) after modification with PAN nanofibers.

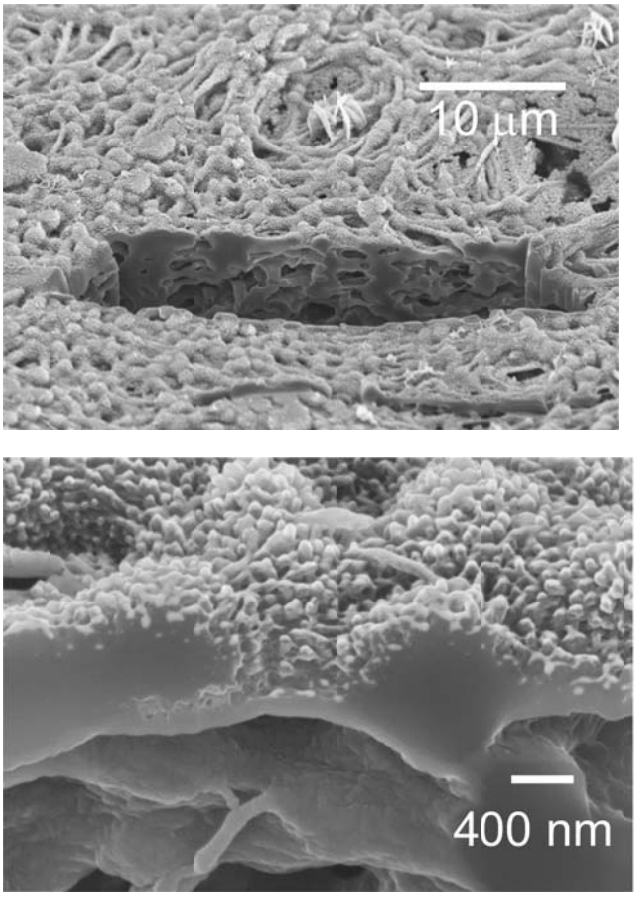

Figure 4.6 FIBSEM images of cross sections of PVDF membranes modified with PAN nanofibers. The two images show different magnifications.

4.3.2 Ion Separations

In one NF experiment without an applied potential, a PAN-modified PES membrane showed rejections of 71% and 50% for Mg^{2+} and K^{+}, respectively. Upon application of a 2 V potential between the membrane electrode and the upper gold-coated electrode (the membrane electrode is positive with respect to the gold-coated electrode), the Mg^{2+} and K^{+} rejections were 66% and 56%, respectively. Thus, the ion rejections and ion selecitivities did not change

substantially upon application of an electrical potential. However, poor electrical connections between the copper foil ring and the membrane may have affected this result. After the NF experiment (>20 h), the copper ring peeled off the membrane. In addition, the membrane surface conductivity may not be sufficient to apply a uniform potential across the membrane. The main electric potential drop may occur from the membrane edge to the membrane center instead of from the membrane surface to the solution, as the membrane sheet resistance is around 9000 Ω/sq after immersion in 0.02 M PBS at pH 2.

In diffusion dialysis without an applied electrical potential the $(PSS/PAH)_2$/PAN-modified alumina membrane allowed a K^+ flux of 2.1 nmol cm^{-2} s^{-1} and a Mg^{2+} flux of 0.3 nmol cm^{-2} s^{-1}. (The source phase contained 0.01 M $MgCl_2$, 0.01 M KCl in 0.02 M phosphate buffer solution (PBS) at pH 2, and the initial receiving phase contained deionized water.) Because the ion flux is on the order of nmol cm^{-2} s^{-1} and a positive potential applied on the membrane should further decrease the flux, ion analysis would be a challenge. Thus, with the same system, we applied -2 V between the membrane surface and a Ag/AgCl reference electrode in the source phase, and the K^+ flux was 2.8 nmol cm^{-2} s^{-1} and Mg^{2+} flux was 0.4 nmol cm^{-2} s^{-1}. This very small increase in flux with an applied potential suggests that anion exclusion from an electrochemical double layer does not significantly alter the flux in this case. However, more studies are in progress to provide a firmer conclusion as to

whether potentials applied with conductive membranes can alter ion fluxes in NF and diffusion dialysis. We also aim to test positive potentials.

4.4 Conclusion

Dilute polymerization yields a dense covering of PAN nanofibers on the surface of porous membranes. PVDF membrane surfaces become hydrophilic after modification with PAN nanofibers, and four-probe measurements show that membrane resistance across the membrane is less than a few MΩ. Initial experiments did not show significant effects of applied potentials (between the membrane and the source phase or feed) on ion transport, but further studies are needed to verify this conclusion.

REFERENCES

REFERENCES

(1) Cheng, C.; Yaroshchuk, A.; Bruening, M. L., *Langmuir* **2013,** 29, 1885-1892.

(2) Mulyati, S.; Takagi, R.; Fujii, A.; Ohmukai, Y.; Maruyama, T.; Matsuyama, H., *J. Membr. Sci.* **2012,** 417, 137-143.

(3) Ouyang, L.; Malaisamy, R.; Bruening, M. L., *J. Membr. Sci.* **2008,** 310, 76-84.

(4) Ng, L. Y.; Mohammad, A. W.; Ng, C. Y., *Adv. Colloid Interface Sci.* **2013,** 197–198, 85-107.

(5) Cao, Y.; Smith, P.; Heeger, A. J., *Synth. Met.* **1992,** 48, 91-97.

(6) Chiou, N. R.; Epstein, A. J., *Adv. Mater.* **2005,** 17, 1679-1683.

(7) Anderson, M. R.; Mattes, B. R.; Reiss, H.; Kaner, R. B., *Synth. Met.* **1991,** 41, 1151-1154.

(8) Hasbullah, H.; Kumbharkar, S.; Ismail, A. F.; Li, K., *J. Membr. Sci.* **2011,** 366, 116-124.

(9) Jackowska, K.; Biegunski, A. T.; Tagowska, M., *J. Solid State Electrochem.* **2008,** 12, 437-443.

(10) Zhang, X.; Chan-Yu-King, R.; Jose, A.; Manohar, S. K., *Synth. Met.* **2004,** 145, 23-29.

(11) Parthasarathy, R. V.; Martin, C. R., *Chem. Mat.* **1994,** 6, 1627-1632.

(12) Mazur, M.; Tagowska, M.; Palys, B.; Jackowska, K., *Electrochem. Commun.* **2003,** 5, 403-407.

(13) Attout, A.; Yunus, S.; Bertrand, P., *Polym. Eng. Sci.* **2008,** 48, 1661-1666.

(14) Hong, K. H.; Kang, T. J., *J. Appl. Polym. Sci.* **2006,** 99, 1277-1286.

(15) Li, R. Q.; Chen, Z.; Li, J. Q.; Zhang, C. H.; Guo, Q., *Synth. Met.* **2013,** 171, 39-44.

(16) Wang, D. H.; Ma, F. H.; Qi, S. H.; Song, B. Y., *Synth. Met.* **2010,** 160, 2077-2084.

(17) Zhang, X. Y.; Goux, W. J.; Manohar, S. K., *J. Am. Chem. Soc.* **2004,** 126, 4502-4503.

(18) Xing, S. X.; Zhao, C.; Jing, S. Y.; Wang, Z. C., *Polymer* **2006,** 47, 2305-2313.

(19) Chiou, N.-R.; Lui, C.; Guan, J.; Lee, L. J.; Epstein, A. J., *Nat. Nanotechnol.* **2007,** 2, 354-357.

(20) Chiang, J.-C.; MacDiarmid, A. G., *Synth. Met.* **1986,** 13, 193-205.

(21) Liu, X.; Bruening, M. L., *Chem. Mater.* **2004,** 16, 351-357.

Chapter 5. Conclusion and Future Work

This dissertation demonstrates remarkable monovalent/divalent ion-transport selectivities in diffusion dialysis and electrodialysis through membranes coated with PEMs. Mechanistic studies suggest that these high selectivities rely in part on highly charged surfaces, so we began preparing conductive membrane to investigate whether greater control over surface charge can further enhance selectivity. In this regard, chapter 1 reviews common methods for fabricating polymer coatings, discusses specific techniques for membrane-based ion separations, and provides a brief introduction to conductive polymers.

Chapter 2 demonstrates that the PSS/PAH coatings on porous support can provide K^+/Mg^{2+} selectivities higher than 350 in diffusion dialysis. The K^+/Mg^{2+} selectivity drops to 16 in NF with the same membranes, suggesting that small defects in the membrane coating lead to convective coupling of water and salt transport. Measurements of transmembranes potentials show that $(PSS/PAH)_4$ coatings are much more permeable to Cl^- than Mg^{2+}, and the resulting transmembrane potential gives rise to a -200% rejection of trace K^+ in nanofiltration (the concentration of K^+ in the permeate is three times the concentration in the feed solution). Knowledge of single-ion permeabilities is vital for predicting the performance of polyelectrolyte films in the separation

and purification of mixed salts.

Chapter 3 investigates whether the diffusion dialysis selectivities of PSS/PAH-modified membranes translate to electrodialysis. Remarkably, with coated commercial NF membranes the K^+ flux increases 45-fold when comparing diffusion dialysis and electrodialysis, while the membrane maintains a K^+/Mg^{2+} selectivity around 100 in electrodialysis. However, the K^+ transference number is <0.34 because protons and anions carry most of the current. The anions of K^+/Mg^{2+} salts dramatically affect ion fluxes and monovalent/multivalent ion selectivities. Adsorption of sulfate in PEMs on porous alumina reduces the membrane surface charge, to give a K^+/Mg^{2+} only around 40. With the same membranes, nitrate salts give K^+/Mg^{2+} selectivities >540. Chlorine generated in electrodialysis with chloride salts damages the $(PSS/PAH)_5$-coated membranes, and K^+/Mg^{2+} selectivities decline dramatically as a result. Future work should examine selectivities among more valuable ions and methods for increasing the transference numbers for the ions of interest.

Chapter 4 proposes of the use of conductive polymer-modified membrane for ion separation with an applied electric potential between the conductive polymer skin and solution. We modified several membrane substrates with conducting PAN nanofibers. However, preliminary results of ion separations with these membranes show no significant changes in ion fluxes or selectivities upon application of an electrical potential. This may due a low

conductivity in polymer film or large gaps between conducting regions..

Future work should examine more conductive materials for the membrane coating (e.g. poly(3,4-ethylenedioxythiophene), sulfonated polyaniline and carbon nanotube-polymer complexes).[1-3] Some improvements on experimental designs, such as a low-resistance connection between membrane surface and a copper foil ring are essential to help achieve significant ion separations with conductive membranes. In addition, application of a potential with conductive membranes provide a potential method to combat membrane biofouling.[4] Future work may well demonstrate significant improvements in fouling control and ion rejections when using conductive membranes and applied potentials.

REFERENCES

REFERENCES

(1) Jia, P.; Argun, A. A.; Xu, J.; Xiong, S.; Ma, J.; Hammond, P. T.; Lu, X., *Chem. Mat.* **2010,** 22, 6085-6091.

(2) DeLongchamp, D.; Hammond, P. T., *Adv. Mater.* **2001,** 13, 1455-1459.

(3) de Lannoy, C. F.; Jassby, D.; Davis, D. D.; Wiesner, M. R., *J. Membr. Sci.* **2012,** 415, 718-724.

(4) de Lannoy, C.-F.; Jassby, D.; Gloe, K.; Gordon, A. D.; Wiesner, M. R., *Environ. Sci. Technol.* **2013,** 47, 2760-2768.